AN ABSTRACT OF THE DISSERTATION OF

<u>Amanda L. Whitmire</u> for the degree of <u>Doctor of Philosophy</u> in <u>Oceanography</u>
presented on <u>June 5, 2008</u>.

Title: <u>The Spectral Backscattering Properties of Marine Particles</u>

Abstract approved:

_____

Timothy J. Cowles

The inherent and apparent optical properties of different ocean regimes are the
basis for all optical remote sensing of the ocean. Ecological information derived from
remote sensors therefore relies on having a detailed understanding of how particulate
backscattering and absorption contribute to the bulk optical signal. The absorption
characteristics of oceanic particles, e.g. phytoplankton and marine bacteria, organic
detritus, and minerogenic particles, have been well characterized, and there are several
ways to determine their contribution to bulk signals. In contrast, the backscattering
properties of marine particles are not well understood, and indeed there is still some
uncertainty regarding the dominant sources of backscattering in the ocean. Recent
advances in optical instrumentation now permit laboratory and *in situ* examination of
the spectral backscattering properties of marine particles, and we use these new tools to
improve the characterization of backscattering in the ocean.

We first investigated the ratio of backscattering to total scattering across a wide
range of oceanic environments and particle types. The spectral dependency of the
particulate backscattering ratio (backscattering/scattering in all directions) is relevant in
the fields of ocean color inversion, light field modeling, and inferring particle properties
from optical measurements. Aside from theoretical predictions for spherical,
homogeneous particles, we have had very limited data showing the actual *in situ*

spectral variability of the particulate backscattering ratio. Our analysis of five data sets from different ocean regimes revealed no spectral dependence of the particulate backscattering ratio within our measurement certainty. We did find however, that different particle populations demonstrated qualitative differences in the backscattering ratio.

In an effort to better understand the variability that we observed in *in situ* backscattering, we investigated the spectral backscattering properties of thirteen species of marine phytoplankton using laboratory cultures. Theoretical analysis has shown that the backscattering coefficient and backscattering ratio may be influenced by particle size, shape, composition, and internal structure. We found species-specific relationships between backscattering and photosynthetic pigment concentration, and distinct differences between species in the backscattering ratio. These differences were related to cell size and were likely influenced by internal cell structure and composition. Of particular importance is our finding that backscattering by phytoplankton cells is higher than predicted by model studies.

Finally, we used the backscattering coefficient and the backscattering ratio to aid in the discrimination of non-algal particle populations and major phytoplankton taxonomic groups in a complex coastal environment. We combined information from multiple *in situ* measurements, including chlorophyll concentration, hyperspectral absorption and attenuation, as well as backscattering, to discriminate and track phytoplankton groups and colored detrital matter in an optically complex, nearshore environment. We applied these approaches to interpret a time-series of hyperspectral optical observations from a coastal mooring.

The Spectral Backscattering Properties of Marine Particles

by
Amanda L. Whitmire

A DISSERTATION

submitted to

Oregon State University

in partial fulfillment of
the requirements for the
degree of

Doctor of Philosophy

Presented June 5 2008
Commencement June 2009

<u>Doctor of Philosophy</u> dissertation of <u>Amanda L. Whitmire</u> presented on <u>June 5, 2008</u>

APPROVED**:**

_____

Major Professor, representing Oceanography

_____

Dean of the College of Oceanic and Atmospheric Sciences

_____

Dean of the Graduate School

I understand that my dissertation will become part of the permanent collection of Oregon State University libraries. My signature below authorizes release of my dissertation to any reader upon request.

_____

Amanda L. Whitmire, Author

ACKNOWLEDGMENTS

"We don't accomplish anything in this world alone ... and whatever happens is the result of the whole tapestry of one's life and all the weavings of individual threads from one to another that creates something."   - Sandra Day O'Connor

I am not solely responsible for this work. I had the benefit of encouragement, instruction, and camaraderie during the whole length of my graduate school experience, all of which contributed to the successful completion of my degree. As such, there are many people to acknowledge in these next few pages.

Before I started graduate school at Oregon State University, I attended a five-week summer course in Optical Oceanography at the University of Maine. I am deeply indebted to the organizers and teachers of this course for giving me a fantastic head start on the basics of "light and water." I thank Mary-Jane Perry, Curt Mobley, Emmanuel Boss, Collin Roesler, and teaching assistant Sam Laney for graciously sharing their time and knowledge. It was an extremely valuable experience and I'll never forget it.

I'd like to acknowledge the hard and diligent work of my committee members: Timothy Cowles, Emmanuel Boss, W. Scott Pegau, Patricia Wheeler, and my graduate representative Skip Rochefort. My major adviser, Tim Cowles, has been a steadfast source of support and instruction through all of my graduate endeavors. He gave me the freedom to pursue my own interests, and never complained when I finally settled into a subject that was fairly far afield from his own research foci. Tim also gave me the leeway to work at my own pace (within reason), and to take some time to pursue an opportunity in applied research outside of the academic setting. I will always appreciate his confidence in my ability to balance graduate work and relevant non-academic work concurrently. Tim has been, and will continue to be, a wonderful and important mentor to me. I am very lucky to have had him as my major adviser, and I doubt that I have ever thanked him enough.

Emmanuel Boss – what would I have done without you?! Despite being across the country, Emmanuel was never difficult to reach. I already miss his frequent phone calls to check in and see how I am doing. Emmanuel has been an essential ally and

friend during the last seven years. He has helped me to figure out a seemingly endless string of problems and confusing results, and often gave me a different and enlightening perspective. I always appreciated his feedback, even when it led to more work for me. Emmanuel provided critical support during the writing of my first first-author paper (Chapter 2 of this manuscript), and certainly improved its quality. I am extremely grateful for Emmanuel's assistance over the years, and look forward to continuing to work together on future projects.

Like Emmanuel, Scott was another long-distance source of support and guidance. Scott is largely responsible for teaching me how to carefully and knowledgeably utilize optical instrumentation, a fundamental skill that will carry me all the way to the end of my career. I will never forget the sage advice that he gave me early on: "Never trust the manufacturer! Always test and calibrate your own instruments. Do it carefully, and do it often." In my field, these are words to live by. Scott allowed me to join in on his project, with co-PI Lee Karp-Boss, to study the spectral backscattering properties of phytoplankton. The work that we did in the lab was fun and extremely interesting. I thank Scott and Lee for generously allowing me to take the lead on the data analysis and write-up of this research.

Pat Wheeler provided much-needed constructive criticism on this work. She never let me get away with any shoddy or unsupported conclusions, and living up to her skepticism improved the strength of this work. Pat also provided an editor's perspective on my dissertation, and in doing so caught many errors that had slipped by me. I appreciate that immensely.

In addition to my committee members, there are numerous people who greatly contributed to the quality and enjoyment of my graduate experience. The Cowles research group is full of wonderful characters, and I am glad to have worked with all of them. Nathan Potter was a hilarious and understanding office mate. He specialized in rude noises and other base humors, which I thoroughly enjoyed, introduced me to BoingBoing, and helped me to get comfortable with the once-mysterious Unix machine. I am glad to call him a friend. Chris Wingard is my Matlab Sensei, and I owe him a huge debt of gratitude for introducing me to batch processing via the 'dir' command.

Were it not for Chris' sage advice and the scripts that I pirated from him, I would probably still not be finished. Chris and I also spent many long hours together on the fantails of various UNOLS vessels, calibrating what felt like every optical instrument known to man. These were hard hours, but were also fun because he kept us laughing all the while. While Chris and I were calibrating, Russ Desiderio was usually inside the ship on the other end of a two-way radio. His dry wit and good humor also got me through many long hours at sea. On land, Russ proved to be the go-to guy for questions in math and physics, as well as tips for making the perfect baguette. I look forward to more adventures in baking with Russ.

A job opportunity for my husband sent us on a three-year detour to Seattle from June 2004 to July 2007. During this time I had the good fortune of working part-time with the excellent people of Sequoia Scientific. Yogi Agrawal gave me the opportunity to put many of his ideas to the test in the laboratory, and I thoroughly enjoyed every new project. Yogi and I started many afternoons with a good conversation, and he was always willing to listen to my latest tribulations with a sympathetic ear. I thank him for his encouragement and confidence. Though I never had the chance to get involved in any of Curt Mobley's projects, he did get me out to do some kayaking and to enjoy some of the finer aspects of life in Seattle. Everyone at Sequoia was responsible for making it fun to go to work every day. I thank Yogi, Curt, Chuck, Greg, Doug, Jamie, Bonnie, Kurt, Khanh, and Kam.

I thank my friend and colleague Grace Chang Spada for her unyielding camaraderie over the years. I can honestly say that without Grace's support and encouragement I would not be where I am today. She took me under her wing at my first Ocean Optics Conference, and has introduced me to scads of wonderful and important people. Grace involved me in her research projects before I realized that I had anything to offer, and I thank her for helping me to realize my talents. She also helped me to write a successful bid for a Sea Grant fellowship that allowed me to travel down to Santa Barbara and tag along with her research program (Chapter 4 of this work). Those trips were as fun as they were productive, and Grace had everything to do with

that. I also thank Grace for being such an inspiring mentor. I was always proud to work with her, and will continue to be. Thanks GS!

I am not ashamed to admit that I was never willing to give up my personal life for the sake of school. Some weekends, yes; every weekend, no. To that end, my close friends have played an important role in keeping me balanced and sane during the last several years. To my friends and volleyball teammates in Seattle – thank you, I love you, and may Joy of Sets live forever! To Jen Burke, my fellow knitter – hey, we both finally finished! To Curt's MRM friends who welcomed me into the fold, Stacey and Chapell Miller, and Bridgette and Casey Lohrman – we are so lucky to have you as friends, and I think of you all as family. To Jen de-Vries, my fellow gardener – your strength of spirit and tenacity are an inspiration. And finally, to my classmates and earnest comrades from the very beginning, Russell Scranton and Angel White – there are no words. We started out as friends, but now you are family. I love you, and am so thankful to have found you both. What adventure can we go on next?

I'd like to finish this section by recognizing the support of my family. My Mom, Kathy Fulton, and her partner Brian Tinkler, and my brother Errin Briggs and his wife Hether, have all provided much-needed support, in many forms, over the course of my graduate studies. I am extremely lucky to have a familial support structure comprised of fantastic people who are family by birth, but friends by choice. My strength, stubbornness, and sense of humor are a direct result of the relationships that were nurtured and sustained by my family. I feel a great deal of gratitude that they are in my life.

Finally, my husband Curt deserves special recognition. He has supported me through frustrating and difficult times, and has celebrated with me during many joyous moments. He is my best friend, my true and perfect mate. He is my partner in all things, large and small, significant and trivial. He gets my jokes and more importantly, he really knows how to make me laugh. It is impossible to imagine a better match for me. He is my beloved, brehuvian companion. My life, my love, my dearest. I thank you for being you, and know that I am a better person with you than without you.

CONTRIBUTION OF AUTHORS

Timothy J. Cowles provided intellectual contributions and editing for all chapters of this manuscript. W. Scott Pegau and Emmanuel Boss provided valuable feedback on data analysis and interpretation for chapters two and three and are co-authors on these chapters. Lee Karp-Boss, Amanda Ashe, and Chad Waluk assisted in data collection for chapter three and are co-authors on that chapter. Grace Chang and Andrew Barnard provided assistance in experimental design and data collection for chapter four, and are co-authors, along with Tim Cowles, on that chapter.

TABLE OF CONTENTS

TABLE OF CONTENTS (continued)

LIST OF FIGURES

LIST OF FIGURES (continued)

LIST OF FIGURES (continued)

LIST OF TABLES

Chapter 1. General Introduction

It is well known that phytoplankton provide the foundation of the food web in marine ecosystems. While individual cells are small (generally less than 200 microns; Lalli and Parsons, 1997), and have generation times on the order of days, blooms of phytoplankton can persist for weeks and cover hundreds of horizontal kilometers in vast, productive upwelling regions (Mann and Lazier1996). Rates of primary production in marine systems develop from the spatial and temporal patterns of distribution of the phytoplankton in relation to light and nutrients. Planktonic ecological processes (phytoplankton growth and senescence, species succession, etc.) produce a wide and complex range of particle types and sizes (Stramski & Reynolds, 1993), which often dominate the optical properties of productive coastal regions (Oliver et al.*,* 2004).

Conventional *in situ* methods of monitoring phytoplankton generally treat the community in bulk, due mainly to an inability to effectively and efficiently isolate and monitor specific phytoplankton taxa *in situ*. Progress in hydrologic optics, coupled with new developments in optical instrumentation, now make it possible to address key questions in phytoplankton ecology and remote sensing. Optical instruments are now being used on a variety of platforms at time and space scales relevant to phytoplankton physiology and ecology (Figure 1.1; Dickey, 1991; Chang et al. 2001). For example, fine-scale vertical distributions in phytoplankton biomass can be detected on the order of centimeters with fast sampling rate fluorometers and absorption and attenuation sensors (Dekshenieks et al, 2001). Autonomous gliders equipped with chlorophyll fluorescence and backscattering sensors can resolve mesoscale patterns in phytoplankton distributions for several weeks. Autonomous profiling floats can do the same for several years and cover several thousand kilometers (Boss et al., 2008). Space-based satellites can produce global maps of surface chlorophyll concentrations daily (http://oceancolor.gsfc.nasa.gov/).

The spectral backscattering coefficient ($b_b(\lambda)$) is a crucial determinant of ocean color. To first order the remote sensing reflectance of the ocean is directly proportional to the ratio of backscattering to absorption ($b_b(\lambda)$ and a( ) respectively; Gordon et al., 1975; Gordon and Morel, 1983), which in turn depend upon the particulate and dissolved constituents of seawater. However, we possess limited knowledge about the linkage between marine particle characteristics and spectral backscattering. The absorption properties of marine substances have been well characterized through laboratory and field measurements, but major gaps exist in our understanding of the backscattering properties of marine substances (Stramski et al., 2004). For example, we do not know the consequences of taxonomic shifts in the phytoplankton assemblage on the ratio of backscattering to absorption, and thus on the remotely sensed reflectance.

Inversion methods for obtaining the particulate backscattering spectrum from remote sensing reflectance often assume that it is a smoothly varying hyperbolic function (Morel, 1973). However, we have limited knowledge of the actual magnitude, shape, and variability of the particulate backscattering spectrum *in situ*. Thus, it is crtitical that we have a thorough understanding of how the types and concentrations of various particles contribute to the bulk spectral backscattering coefficient. It is paramount to obtain insight into the spectral characteristics of the backscattering properties of marine particles because satellite remote sensors sample at one angle (or field of view) and depend solely on information derived from spectral relationships to estimate chlorophyll concentration and other products (primary productivity, CDOM concentration, etc.). A better understanding of how phytoplankton taxonomic groups contribute to the bulk backscattering coefficient is essential in order for satellite data interpretation to progress beyond bulk chlorophyll estimation into monitoring ecological processes.

The backscattering magnitude and spectrum of marine phytoplankton provide key information regarding particle size and index of refraction (Ulloa et al., 1994; Twardowski et al., 2001; Boss et al., 2004b), yet these properties (which vary widely with differences in size, shape, morphology and internal structure) have only recently been rigorously measured in the laboratory (Vallaincourt et al., 2004). These recent

observations reinforce the potential for remotely-sensed bio-optical measurements to reveal key ecological parameters, such as concentration, mean particle size and index of refraction, within the upper ocean. To realize that potential, we must have a better understanding of the sources of variability of the spectral backscattering *in situ*.

It is the uncertainty about the sources of variability in the spectral backscattering coefficient that motivated this research. The overarching objective of this project was to quantify the relationship between the physical and biological properties of marine particulate matter, especially phytoplankton, and the spectral backscattering characteristics of those particles.

To that end, we first examined the spectral variability of the particulate backscattering ratio (the ratio of backscattering-to-total scattering, b_{bp}/b_p) across a wide range of oceanic water types and particle populations in Chapter 2 of this dissertation. The product of the backscattering ratio and the scattering coefficient is often used in inversions of satellite remote sensing data in lieu of using the backscattering coefficient because it was assumed (from model results) that the backscattering ratio was spectrally flat, and that the scattering spectrum could be determined from attenuation and absorption, two well-constrained quantities (Roesler and Boss, 2003). However, *in situ* measurements of the backscattering ratio were sparse. We used a large *in situ* dataset to investigate the variability in the magnitude and spectral shape of the backscattering ratio. We found no spectral dependence in the ratio and that the magnitude varied with changes in the bulk particle population.

In an effort to better understand how specific phytoplankton taxa contribute to bulk backscattering measurements, we examined the spectral backscattering properties of thirteen marine phytoplankton species in Chapter 3. We measured the absorption and attenuation coefficients at nine wavelengths, chlorophyll concentration, particle size and concentration, and the volume scattering function at 140° and six wavelengths for fifteen strains of phytoplankton. We found significant spectral variation in the backscattering coefficient between species, but none in the spectral backscattering ratio. The backscattering ratio was highest for dinoflagellates and diatoms, and was positively

related with cell size. We found that phytoplankton have higher backscattering efficiencies than previous work, using models, has shown.

In the Chapter 4 of my dissertation, "Temporal changes in nearshore surface optical properties in relation to phytoplankton community structure in the Santa Barbara Channel," we used the backscattering coefficient and the backscattering ratio to aid in the discrimination of non-algal particle populations and phytoplankton taxonomic groups. We used information from backscattering in conjunction with other optical and hydrographic parameters to identify and track phytoplankton populations in an optically complex coastal environment.

Finally, in Chapter 5 of this work, I summarize my results and discuss some of the ecological questions that can be addressed as a result of this work. I speculate about the implications of some of my findings, and propose areas for future work.
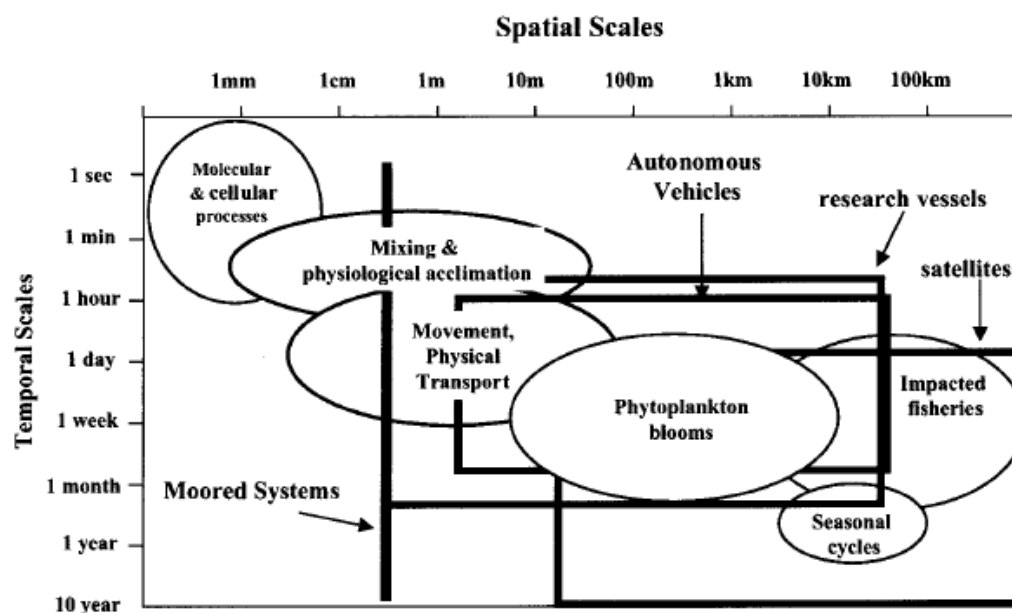
Spatial Scales

Figure 1.1. Temporal and spatial scales of processes important to phytoplankton ecology (ovals) and sampling scales of various platforms for optical instruments (boxes). From Schofield et al., 1999

Chapter 2. Spectral variability of the particulate backscattering ratio

A.L. Whitmire, E. Boss, T. J. Cowles, and W. S. Pegau

2.1 Abstract

The spectral dependency of the particulate backscattering ratio is relevant in the fields of ocean color inversion, light field modeling, and inferring particle properties from optical measurements. Aside from theoretical predictions for spherical, homogeneous particles, we have very limited knowledge of the actual *in situ* spectral variability of the particulate backscattering ratio. This work presents results from five research cruises that were conducted over a three-year period. Water column profiles of physical and optical properties were conducted across diverse aquatic environments that offered a wide range of particle populations. The main objective of this research was to examine the behavior of the spectral particulate backscattering ratio *in situ*, both in terms of its absolute magnitude and its variability across visible wavelengths, using over nine thousand 1-meter binned data points for each of five wavelengths of the spectral particulate backscattering ratio. Our analysis reveals no spectral dependence of the particulate backscattering ratio within our measurement certainty, and a geometric mean value of 0.013 for this dataset. This is lower than the commonly used value of 0.0183 from Petzold's integrated volume scattering data. Within the first optical depth of the water column, the mean particulate backscattering ratio was 0.010.

2.2 Introduction

The spectral particulate backscattering ratio, $\widetilde{b}_{bp}(\lambda)$, is the ratio of light scattered in the backward hemisphere to the total light scattered by a particle or group of particles. There are currently two primary applications for backscattering ratio data; inferring particle composition from *in situ* optical measurements, and modeling the *in situ* light field. In a study that used HYDROLIGHT to investigate the effects of the shape of the scattering phase function and the backscattering ratio on the underwater light field, Mobley et al. (2002) found that using the correct backscattering ratio was crucial in obtaining closure between model and field data. They obtained closure in observed and modeled reflectance when using empirical or analytical phase functions that had the

backscattering ratio observed in the field. Results were insensitive to the detailed volume scattering function [VSF] in the backward direction (90 – 180 degrees).

The spectral particulate backscattering ratio also has important applications in the interpretation of remote sensing data. To first order, the reflectance of the ocean, *R*, the ratio of upwelled radiance (or irradiance) to downwelled irradiance, is directly proportional to the ratio of backscattering to absorption ($b_b(\lambda)$ and a( ) respectively; Gordon and Morel, 1983), which in turn depend upon the particulate and dissolved constituents of seawater. The absorption properties of marine substances have been well characterized through laboratory and field measurements, but major gaps exist in our understanding of the backscattering properties of marine substances (Stramski et al., 2004). As a result, many remote sensing algorithms estimate the particulate backscattering coefficient as the product of the backscattering ratio and the scattering coefficient. Radiance models for Case I waters have long assumed a backscattering probability between 0.2% and 2% depending on the chlorophyll concentration (Gordon et al., 1988; Morel, 1988), but little *in situ* data has been available to test this assumption.

The backscattering ratio has also been used to infer particle properties *in situ*. The backscattering ratio, in concert with the slope of the particle size distribution, provides an estimate of the bulk refractive index of particles in the ocean, allowing discrimination between organically dominated particulate assemblages from those dominated by inorganic particles (Twardowski et al., 2001; Boss et al., 2004). This separation is a consequence of the larger water fraction in organic particles compared to inorganic particles, thus lowering their index of refraction (Aas, 1996). This characteristic has significant ecological consequences since particulate sinking depends linearly on the particles' excess density relative to water, which correlates well with index of refraction (Carder et al., 1974). When the spectral backscattering ratio is added to a suite of standard optical measurements (e.g. attenuation $c(\lambda)$, absorption $a(\lambda)$, and chlorophyll) more information is available to elucidate and track particle assemblages because the ratio often exhibits a different spatial distribution pattern than the other measurements (Boss et al., 2004; Sullivan et al., 2005). For example, unlike

measurements of c_p440 and a_p676, the ratio may not resolve a high chlorophyll concentration at the surface due to the low index of refraction of most phytoplankton relative to water. The ratio could, however, strongly define the bottom boundary layer even when beam attenuation is low [see Boss et al., 2004, Fig. 3]. This indicates that the distribution of the particulate backscattering ratio may offer information on the distribution of various particle populations in optically complex waters.

Due to the limited *in situ* data on the spectral dependence of the backscattering ratio for natural particles, it has been assumed to be spectrally flat as predicted by Mie theory (Ulloa et al, 1994). MacDonald et al. (2000) found less than 10% variability between wavelengths in their estimates of spectral particulate backscattering ratios. In a study conducted on a fixed platform in the Black Sea, Chami et al. (2005) found that the mean particulate backscattering ratio had less than 4% variability between three wavelengths, but that significant deviations from a flat $\tilde{b}_{bp}(\lambda)$ spectrum occurred under certain conditions. In a study conducted in the Irish and Celtic Seas, wavelength dependence was observed in the ratio between two wavelengths (470 and 676-nm) under certain circumstances (McKee and Cunningham, 2005). The discrepancies in the results of these studies illustrate the need for a more comprehensive investigation of the behavior of the spectral particulate backscattering ratio *in situ*. As yet, published results on the actual variability of *in situ* spectral particulate backscattering ratios do not cover a sufficiently wide range of water types and particle populations to justify the assumption of a flat backscattering ratio spectrum, and assumptions inherent in the Mie model (spherical, homogeneous particles that obey a Junge-type size distribution), limit its applicability in characterizing the scattering properties of marine particles. In addition, some of the above-mentioned works suffer from limitations; the 676-nm channel used in McKee and Cunningham (2005) is known to be sensitive to chlorophyll fluorescence at high chlorophyll concentrations as discussed in (Boss et al., 2007). The sensor used in Chami et al., (2005) is a prototype that has not benefited from review by a community of users.

In an effort to clarify this issue, we have analyzed five *in situ* data sets to explore the spectral dependence of the backscattering ratio using a commercially available sensor. We focused our analysis on describing the magnitude range of the backscattering ratio across many environments, and on differences in the ratio across visible wavelengths. We also investigated the effect of different biogeochemical domains on $\tilde{b}_{bp}(\lambda)$. We present over nine thousand 1-meter binned data points for each of five wavelengths of the spectral particulate backscattering ratio.

2.3 Methods

The data used in this paper were compiled from pre-existing datasets that had been collected and archived by the Optical Oceanography Group at Oregon State University (Twardowski et al., 2001; Boss et al., 2004; Boss et al., 2007). The measurements were taken over a three-year period and cover diverse aquatic environments, offering a wide range of particle populations. Sampling sites included the region from the southern California coast to the Gulf of California, the mid-Atlantic Bight off the south coast of New Jersey, and Crater Lake, Oregon, USA. A summary of the dates and locations of these cruises is given in Table 1. Data were collected in various Case-1 and Case-2 waters ranging from near-shore coastal stations to oligotrophic and fresh-water environments. The variety of geographical locations and water types sampled offered a broad range of particle types and populations that spanned the expected range of the backscattering ratio. Note that the backscattering ratio depends on the properties of the particle assemblage, so the entire dynamic range of the particulate backscattering ratio may be observed in a single profile. The dataset does not cover all types of plankton assemblages (e.g. large, monospecific blooms), but does provide a very good representation of a broad range of mixed plankton populations, detritus composition, and lithogenic particles. We therefore believe that the results shown here are representative of the global oceans.

2.3.1 Field methods

In all cases except for the Crater Lake cruise, water column profiles of physical and optical properties were collected with a Slow Descent Rate Optical Profiler (SlowDROP; Barnard et al., 1998), a multi-instrument profiling system designed to freefall through the water column in order to isolate the profiler from ship motion. A SlowDROP package was unnecessary in the calm waters of Crater Lake, so standard winched profiles were conducted. The descent rate was on the order of 10's of centimeters per second, which enabled the capture of optical and hydrographic data on sub-meter scales ((O) 10cm). A typical instrument configuration on the profiler included a CTD, a chlorophyll fluorometer, a six-wavelength backscattering sensor, and two nine-wavelength dual path absorption and attenuation meters, one of which had a 0.2μm pre-filter to measure the dissolved signal (operationally defined as the fraction smaller than 0.2μm).

2.3.2 Data correction and processing

In situ total and dissolved spectral absorption and attenuation were measured with two WET Labs *ac*-9's at nine wavelengths; 412, 440, 488, 510, 532, 555, 650, 676, and 715-nm. Particulate absorption and attenuation were determined by the difference between the total and dissolved signals. To account for drift over the course of the cruises, daily field measurements of pure water were collected. Corrections for the temperature and salinity dependence of absorption and attenuation were also applied (Pegau et al., 1997), as well as a correction for scattering losses in the absorption tube (proportional method) (Zaneveld et al., 1994). The scattering coefficient, $b(\lambda)$, was calculated as the difference between attenuation and absorption.

Chlorophyll concentration was estimated using the chlorophyll absorption line height technique (Davis et al., 1997; Boss et al., 2007]. In this method the absorption due to chlorophyll-*a*, a_{chl}, is calculated using *ac*-9 particulate absorption data at 650, 676, and 715-nm as follows: $a_{chl} = a_p(676) - [39/65 \cdot a_p(650) + 26/65 \cdot a_p(715)]$. The

chlorophyll concentration is then estimated by normalizing a_{chl} by the chlorophyll-specific absorption coefficient, $a^*(676)$. We used an $a^*(676)$ of 0.014 m^2 g chl^{-1}, which is appropriate for oceanic waters dominated by phytoplankton (Sosik and Mitchell, 1995). This approach was utilized instead of estimating chlorophyll from fluorescence data to avoid the problem of non-photochemical quenching of fluorescence that occurs in surface waters under high light conditions. Previous work has shown this to be a robust technique, with an uncertainty in the chlorophyll estimate of ±0.2 μgL^{-1} (Boss et al., 2007; Sullivan et al., 2005).

The HOBI Labs Hydroscat-6 (HS-6) instrument measures the total volume scattering function, β, at 140 degrees and six wavelengths (Maffione and Dana, 1997). The wavelengths used in our study were 442, 488, 532, 555, 620, and 676-nm. An extra correction step before the conversion to the backscattering coefficient was necessary for these data. HOBI Labs released a revised estimate of the reflectivity of the Spectralon target used during the Hydroscat calibration procedure after the data were collected, and volume scattering data were corrected by a factor of 1.12 to account for the revised reflectivity (D. Dana, personal communication, 2004). Derived parameters for the HS-6 include volume scattering by particles, and the total and particulate backscattering coefficients ($\beta_p(\lambda)$, $b_b(\lambda)$ and $b_{bp}(\lambda)$ respectively) at six wavelengths. All of the backscattering data were processed according to the procedures for conversion from $\beta(\lambda, 140°)$ to $b_b(\lambda)$ that are discussed in Boss and Pegau (2001), using a conversion factor, χ, of 1.18.

Five out of six wavelengths in the HS-6 overlap with those of the ac-9, so particulate backscattering ratios were calculated directly as $b_{bp}(\lambda)/b_p(\lambda)$ for those wavelengths. The ac-9 does not have a 620-nm waveband, so $b_p(620)$ was estimated by linear interpolation between $b_p(555)$ and $b_p(650)$, and then the backscattering ratio was estimated using the result. We found that the data from the HS-6 676-nm waveband was significantly correlated with the chlorophyll concentration, which is likely the result of chlorophyll-a fluorescence excited at 676-nm and emitted at 681-nm (Boss et al., 2007). The HS-6 676-nm waveband detector has a FWHM of 20 nm, which is sufficiently

wide to detect chlorophyll-*a* fluorescence emission. Backscattering data from the 676-nm channel was therefore omitted from this analysis.

We used median values within 1-m depth bins for all variables, yielding a database of 10,513 data points for each IOP and hydrographic variable. The median was used instead of the mean because averages are sensitive to the presence of spikes caused by rare, large particles that may be observed by one instrument but not the other. Since rare particles are not normally distributed in time or space, excluding them through a median binning procedure minimizes their contribution to bias in the final data.

2.3.3 Uncertainties in the ratio

The particulate backscattering ratio, ($\tilde{b}_{bp}(\lambda)$), was calculated as the quotient of the particulate backscattering coefficient ($b_{bp}(\lambda)$ from the HS-6) and the particulate scattering coefficient ($b_p(\lambda)$ from the *ac*-9). Propagation of error in each processing step for each instrument resulted in uncertainties of 0.0007 m^{-1} and 0.006 m^{-1} for the particulate backscattering coefficient and the particulate scattering coefficient respectively. Data less than or equal to the detection limit was excluded from our analysis. This reduced the dataset by 1,359 data points, or 13%, to a final size of 9,154 data points for each variable.

In addition to the above uncertainties, there is also an uncertainty associated with estimating the backscattering coefficient from a single angle measurement in the backward direction, which is estimated to be approximately 10% (Boss and Pegau, 2001; Oishi, 1990; Chami et al., 2006; Sullivan et al., 2005). Another possible source of uncertainty in the ratio is related to the acceptance angle of the *ac*-9's beam transmission detector (Pegau et al., 1995). Instruments that measure beam attenuation have to make a compromise between reducing the acceptance angle to exclude forward scattered light and enlarging the pinhole to maintain enough signal for a robust measurement. Up to 30% of the total volume scattering coefficient can occur in the range from 0 to 1 degree in natural waters (Pegau et al., 1995). The acceptance angle of

the *ac*-9, 0.93 degrees, is large enough to accept some forward scattered light, especially when large particles are present. This would lead to an underestimate of the beam attenuation, and subsequently, the scattering coefficient. The end result in our application of *ac*-9 data would be an overestimate of the backscattering ratio.

The effect of the acceptance angle on the beam-*c* measurement has not been well characterized in the field. Based on Petzold's phase functions and the acceptance angle of the *ac*-9, we estimate a possible bias of 5-25% related to the uncertainty in the attenuation measurement when compared to theoretical calculations that do not take acceptance angle issue into account. The range in this estimate is due to the effect of particle size on the proportion of near-forward scattering. When more large particles are present the proportion of near-forward scattering relative to total scattering increases, and more scattered light is erroneously collected in the beam-*c* measurement. However, when compared to theoretical calculations where the acceptance angle is taken into account this bias is irrelevant (Boss et al, 2004). Due to the uncertainty of the effect of the *ac*-9 acceptance angle on the attenuation measurement in out data, we do not include this possible bias in our estimates of error at this time.

Despite the different instruments and techniques that are used to estimate the backscattering ratio, prior work has demonstrated consistency between approaches (see Boss et al. (2004) for a review of instruments and methods). Intercalibration experiments to compare estimates of $\tilde{b}_{bp}$ from different instruments and some of the data used here (Boss et al, 2004; Sullivan et al., 2005; Boss et al., 2007; Davis et al., 1997) reveal that the ratio is a robust parameter with differences between instruments and methods on the order of 10%. Given that the instruments used for these comparisons measure the VSF at different angles, have very different calibration methods, and different methods of computing the backscattering ratio, an uncertainty of only 10% between them is remarkable. Using propagation of errors from the scattering and backscattering measurements, we set a conservative estimate of the likely maximum error of the particulate backscattering ratio presented here to be 20%. This conservative estimate of error is greater than the estimate derived from the empirical

studies mentioned above because we erred on the side of caution at each propagation step. Relative to the 4 to 10-fold variability of the backscattering ratio observed, a 20% maximum uncertainty in the estimate is not significant for most likely applications of the data (e.g. using it as a proxy for bulk particle composition). This is especially true given that the sources of error in the ratio (e.g. choice of χ, acceptance angle of *ac*-9, measurement uncertainty) are not assumed to be spectrally dependent. Errors in our estimate of the ratio would affect all wavelengths similarly, and analyses of differences between the backscattering ratio at various wavelengths are therefore minimally influenced by even large uncertainties ((O) 20%).

2.4 Results

The frequency distributions of the particulate backscattering ratio for the combined dataset (all cruises pooled) at five wavelengths are shown in Figure 2.1A–E, and some parametric and non-parametric statistical descriptors are provided in Table 1. The ratios are clustered near zero and produce a distribution that is skewed to the right, with a skewness of 1.65. The geometric mean value of the ratio is 0.013, and the median is 0.012. This result is lower than the integration of the backward fraction of the Petzold phase function, 0.0183 (Petzold, 1972). Positively skewed and lognormal distributions are commonly observed in histograms of bio-optical variables (Campbell, 1995). We used a natural log transformation on the data to perform a parametric statistical analysis (assuming a normal distribution). Statistical descriptors such as the mean and standard deviation were estimated on the transformed data, and then back-transformed to obtain numbers that are on the same scale as the data. Transforming the backscattering ratios did not produce a normal distribution (e.g. it failed the Jarque-Bera test), but it did reduce the amount of skewness to 0.64.

Spectral relationships were examined using Model-II linear regression (Sokal and Rohlf, 1995). We derived regressions of particulate backscattering ratios between wavelengths to establish whether or not the ratio varies spectrally. A significant deviation from a slope of one would indicate that there is spectral variation in the ratio.

We chose 488-nm as the reference wavelength for plots to match previous work on global spectral IOP relationships (Barnard et al., 1998). We used the "least squares bisector" approach for the Model-II regressions (Peltzer, 2006). In this method a Model-I robust linear least squares model is fit to both *x*-on-*y* and *y*-on-*x,* e.g. $\widetilde{b}_{bp}$ (488) vs. $\widetilde{b}_{bp}$ (442) and vice-versa. The slope of the Model-II regression is determined by bisecting the minor angle between the two Model-I regression slopes (Figure 2.2). A robust model, which weights points close to the regression line more heavily than more distant points, was utilized to minimize the effect of outliers. We also centered the data by removing the mean value from all data points before performing the regression (Laws, 1997). The *y*-intercepts retrieved from the Model-II regressions were all well below the magnitude of our measurement certainty (<0.0001), and are therefore indistinguishable from zero. The slopes of the regressions varied between 0.97 and 1.04. The 90% confidence intervals for the regressions show that the slopes are not significantly different from one (Figure 2.2).

The particulate backscattering ratio has a wide dynamic range (0.005 – 0.06), often varying by an order of magnitude in a single profile. This is reflected in the large standard deviations around the mean $\widetilde{b}_{bp}$ (λ) spectra shown in Figure 2.3. Although plots of $\widetilde{b}_{bp}$ (λ) spectra for individual cruises show apparent spectral variation in their mean values, the variability between wavelengths is lower than the uncertainty in the estimate. Likewise, the variability between wavelengths in the combined data set is also much lower than the uncertainty in the estimation of the ratio. The results of the regressions, the level of uncertainty in the ratio, and the high standard deviations all point to the conclusion that there is no measurable difference between particulate backscattering ratios at the five wavelengths sampled, and we therefore find no statistically significant spectral dependence to the ratio.

2.5 Discussion

The absence of spectral differences in the particulate backscattering ratio has been predicted by Mie theory (Ulloa et al., 1994) for populations of spherical, homogeneous particles that follow a Junge-type size distribution and have a constant refractive index, similar to that of phytoplankton, across all wavelengths. Previous work found between 4% and 10% variability between wavelengths in the backscattering ratio (Chami et al., 2005 and Macdonald et al., 2000, respectively). Our findings, using a much larger data set than previous analyses, exhibit the same result with regard to spectral variability. This is illustrated by slopes not significantly different from one for linear regressions between five wavelengths of the ratio (Figure 2.2).

An exception to this linear relationship occurred in the regression of backscattering ratios at 488- and 620-nm for backscattering ratios larger than 0.025. Data points where ratios fell below the regression line had $c_p(\lambda)$-slopes near zero. This can occur when the particle population does not follow the hyperbolic size distribution model, and is usually the result of a phytoplankton bloom (Sullivan et al. 2005). Interestingly, the low $c_p(\lambda)$-slopes in these data are not coincident with high chlorophyll. Chami et al. (2005) observed that the particulate backscattering ratio occasionally exhibited spectral variability between three wavelengths when there was high non-algal particle absorption, but the relationship was not systematic enough to describe mathematically. These exceptions illustrate that important deviations from flat $\widetilde{b}_{bp}(\lambda)$ spectra can occur under specific circumstances. However, data points divergent from the regressions were very rare in our data set, and removing them from the database did not significantly affect the slope of the regression.

The particulate backscattering ratio is, by construction, a concentration independent quantity, as it is the ratio of two optical parameters that to first degree co-vary with concentration. Instead, this ratio provides information about characteristics of the bulk particle population (e.g. particle composition, mean size, shape etc.). In previous studies it was found (based on theory and observations) that the backscattering ratio is sensitive to composition (organic content and particle size distribution;

Twardowski et al., 2001; Boss et al., 2004). In this regard, we examined the magnitude and variability of $\widetilde{b}_{bp}(\lambda)$ across various biogeochemical provinces. We did not have ancillary information from discrete water samples to determine the dominant particle types for all of the stations in the database. Instead, backscattering ratios were partitioned into groups according to chlorophyll concentration, beam attenuation, and combinations of the two parameters. $\widetilde{b}_{bp}(\lambda)$ values were also examined in the first optical depth of the water column to determine if mean surface values differ from generalized whole water-column values.

Since most phytoplankton groups exhibit a low backscattering efficiency (Twardowski et al., 2001; Ahn et al., 1992; Bricaud et al., 1983), we expect to find low backscattering ratios in areas of high chlorophyll (and low proportions of mineral particles). To examine the relationship between chlorophyll and the particulate backscattering ratio we placed data into two groups, one with chlorophyll values between 0.02 and 2.0 μgL^{-1}, and the other with chlorophyll greater than 2 μgL^{-1}. We found that regions with low chlorophyll concentration exhibit higher backscattering ratios than areas with high chlorophyll (Figure 2.4A, black and green lines respectively). This result supports the approach taken in previous studies in which the magnitude of the backscattering ratio is approximated to first order by the chlorophyll concentration (Morel and Maritorena, 2001).

There was a weak relationship between chlorophyll concentration and the backscattering ratio in our data (Figure 2.5, solid red line). The relationship is similar to those found in several previous studies (Twardowski et al., 2001; Sullivan et al., 2005; Ulloa et al., 1994; Morel and Maritorena, 2001), despite the fact that these studies cover different ranges of chlorophyll concentration. For example, the chlorophyll concentration in our study ranged from undetectable to just over 12 μgL^{-1}. Sullivan et al. (2005) found a similar relationship between the particulate backscattering ratio and chlorophyll in a dataset the included a large set of high chlorophyll data points reaching up to 100 μgL^{-1}. The relationship found here is described by the equation:

$$\widetilde{b}_{bp}(555) = 0.0121[\text{chlorophyll}]^{-0.125}; r^2 = 0.36. \qquad\qquad \text{Eq.1}$$

However, below chlorophyll values of approximately 2 μgL^{-1} the particulate backscattering ratio is extremely variable, ranging from 0.004 to 0.05, and chlorophyll concentration is no longer a good predictor of the ratio in our data. Twardowski et al. (2001) found the same result, with large amounts of scatter in backscattering ratios at low chlorophyll values. Since phytoplankton exhibit relatively weak backscattering compared to lithogenic and non-algal material, we expect that other particles will contribute strongly to the magnitude of the backscattering ratio at low chlorophyll concentrations. The wide range of values observed reflects pervasive differences in bulk particle composition with changes in depth, water mass, and sampling location. The relationship between chlorophyll and the particulate backscattering ratio is slightly more robust within the first optical depth of the water column (Figure 2.5, red dashed line). The relationship is described by the power-law model in Eq. 2:

$$\tilde{b}_{bp}(555) = 0.0074[\text{chlorophyll}]^{-0.042}; \ r^2 = 0.47. \qquad \text{Eq. 2}$$

The lower value of the exponent in the model compared to Eq. 1 is the result of lower backscattering ratio values at the surface, which are presumably dominated by phytoplankton with a low refractive index.

It is interesting to note that backscattering ratios often exceeded values predicted by models with 'typical' phytoplankton input parameters, even when chlorophyll was high. For values of the real refractive index typical of phytoplankton (1.04 – 1.06 relative to water), and typical size distributions observed in the ocean, the Mie model predicts backscattering ratios between approximately 0.5 – 1% (Ulloa et al., 1994). We observed values as high as 0.02, or 2%, at chlorophyll concentrations as large as 6 μgL^{-1}, and ratios still as high a 1.5% at chlorophyll concentrations reaching 12 μgL^{-1}. This indicates that the ways in which phytoplankton deviate from the assumptions inherent in the Mie model may significantly increase their backscattering. For example, complex morphology (Gordon, 2006) and internal structure (Kitchen and Zaneveld, 1992) have been shown to increase the proportion of backscattering relative to homogeneous particles with an equivalent spherical diameter.

Samples with low beam attenuation and no chlorophyll generally occur below the chlorophyll maximum and above the bottom boundary layer, somewhere in the middle of the water column. Under these circumstances the inherent optical properties are presumably dominated by non-algal material. We classify samples with a beam attenuation of less than $0.5m^{-1}$ and no chlorophyll present to be 'non-algal' in nature. Previous work has hypothesized that very small non-algal particles are responsible for a large fraction of total backscattering in the ocean (Stramski et al. 2001, and references therein). We found that water masses dominated by such particles do exhibit high backscattering ratios, around 0.016 (Figure 2.4B, blue line). This result agrees well with previous work, which shows an increase in the backscattering ratio with depth as non-algal material becomes the dominant particle type in the water column (Bricaud et al., 1995). Previous work has shown that spectral dependence occurs in the backscattering ratio when absorption by non-algal particles dominates the absorption signal (Chami et al., 2005). We did not find the same result in our data, but it may be due to the different approach we took in categorizing non-algal particle populations (i.e. based on $c_p(650)$ and chlorophyll instead of absorption-based techniques).

Lithogenic materials have a very high backscattering efficiency (Twardowski et al., 2001). High values of both the particulate backscattering coefficient and the backscattering ratio are often seen in bottom boundary layers. Since our database of 234 profiles had a maximum depth range from 10 to 300 meters, using depth or depth from bottom was not a reasonable approach to deciphering which samples may be influenced by resuspended sediment. Profiles did not always reach proximity to the bottom, and even where the SlowDROP did reach the bottom a nepheloid layer was not always present. Instead, we classified 'lithogenic' samples according to chlorophyll (less than $0.5\mu gL^{-1}$) and beam attenuation ($c_p(650)$; greater than $1m^{-1}$). Using these criteria we found that results agreed well with previous studies (Figure 2.4B, black line). Samples that were categorized as being influenced by lithogenic particles had high backscattering ratios across all wavelengths, around 0.021, and represented the highest values in the dataset.

The backscattering ratio is an important parameter for remote sensing inversion algorithms (Roesler and Boss, 2003). To determine if surface values of the ratio differ significantly from mean water column values, we grouped data that was within the range of the first optical depth in all of our profiles. Figure 2.1F–J shows frequency distributions of $\widetilde{b}_{bp}(\lambda)$ at five wavelengths for these surface data. Compared to the entire data set, the surface values of $\widetilde{b}_{bp}(\lambda)$ are lower in magnitude, around 0.01 (see Table 2.2). This result has important implications when the backscattering ratio is employed in remote sensing algorithms, such as diver visibility algorithms designed to estimate the beam attenuation from inverted backscattering estimates (Roesler and Boss, 2003).

2.6 Conclusion

The main objective of this research was to examine the distribution of the spectral particulate backscattering ratio *in situ* across several oceanic domains, both in terms of its absolute magnitude and its variability across visible wavelengths. We analyzed over nine thousand 1-meter binned data points for each of five wavelengths of the spectral particulate backscattering ratio. We found the maximum uncertainty in the backscattering ratio to be 15-20%. This result is largely due to the assumptions inherent in the conversion factor, χ, from a single angle VSF measurement to the backscattering coefficient, and the propagation of uncertainties associated with using two instruments to compute the ratio. Within this measurement capability we found that there was no significant spectral dependence of the ratio. We observed rare instances of significant spectral deviation that were caused by particle populations that differ strongly from theoretical assumptions about their shape, composition, or size distribution. Spectral deviations in the particulate backscattering ratio have also been observed by others (Chami et al., 2005; McKee and Cunningham, 2005), and merit further investigation. Different vertical biogeochemical provinces demonstrated qualitative differences in the backscattering ratio that agreed well with previous work. Mid-water regions with low chlorophyll exhibited higher backscattering ratios than surface regions with relatively

higher chlorophyll. A power-law least-squares model was fit to the relationship between chlorophyll and the backscattering ratio. Though it was a weak relationship, it was similar to previous models. The relationship between chlorophyll and the ratio was more robust within the first optical depth of the water column, and had a lower slope exponent than the fit to the entire data set. Areas with a strong non-algal or lithogenic influence also showed elevated backscattering ratios compared with mean values. The highest ratios were associated with lithogenic material. Within one optical depth of the surface, the backscattering ratio averages 0.010, which is slightly lower than the mean of the data set as a whole. The lower backscattering ratio is associated with increased chlorophyll concentration near the surface.

2.7 Acknowledgements

Table 1. Global Data Set Description

Location	Data Set	Dates	Latitude, °N	Longitude, °W	Number of Profiles	Number of Samples
Gulf of California	GOC99A	April – May 1999	24.4 – 31.1	114.6 – 108.8	36	2808
San Diego, CA to the Gulf of California	MOCE-5	October 1999	21.8 – 32.5	117.4 – 105.7	25	1854
Mid-Atlantic Bight	HY00	July – Aug. 2000	39.3 - 39.6	74.0 - 74.4	95	1054
Crater Lake	CL01	June and Sept.	42.93	122.1	4	766
Mid-Atlantic Bight	HY01	July – Aug. 2001	39.15 – 40.7	71.4 – 74.2	74	2672

Experiment abbreviations are as follows: GOC99A, Gulf of California, 1999; MOCE-5, Marine Optical Characterization Experiment, west coast of Baja, California and Gulf of California, 1999; HY00, Hyperspectral Coastal Ocean Dynamics Experiments (HyCODE), south New Jersey coast, 2000; CL01, Crater Lake, OR, 2001; HY01, HyCODE, south New Jersey coast, 2001. Total numbers of profiles and samples for the data set are 234 and 9,154, respectively.
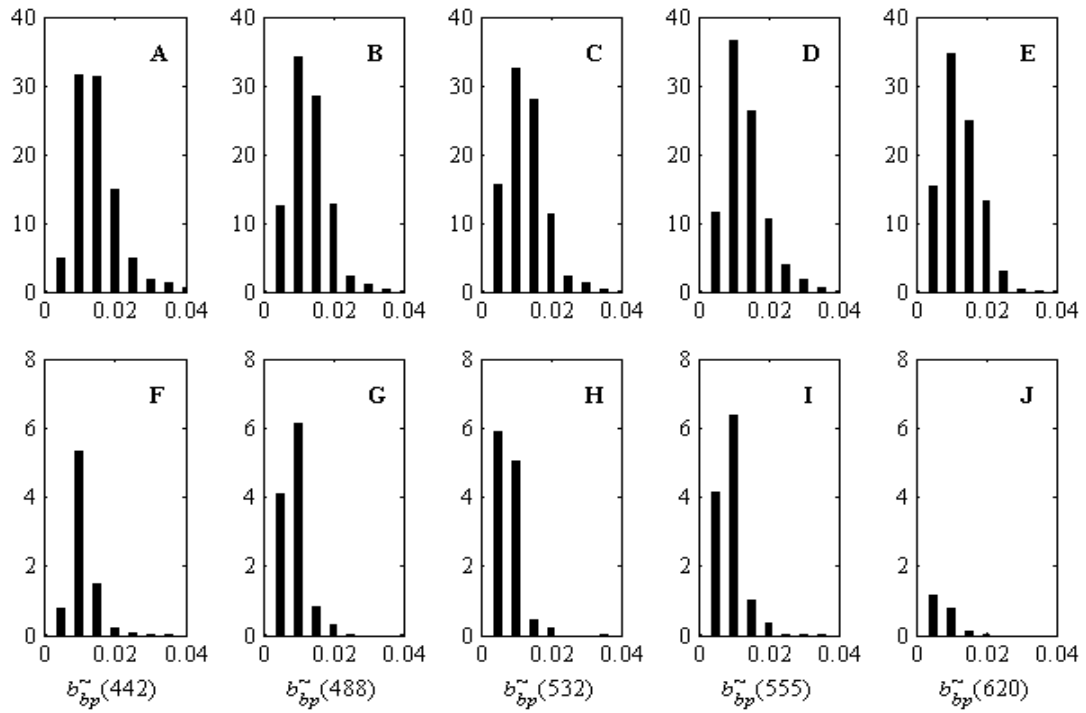
Figure 2.1. (A – E) Histograms of particulate backscattering ratio measurements for the entire data set are plotted for each wavelength. Frequency values shown on the *y*-axes have been divided by 100. N = 9,154 for each plot. (F – J) Particulate backscattering ratios that occur at or above one optical depth are plotted. (F) 442 nm, N = 797. (G) 488 nm, N = 1,149. (H) 532 nm, N= 1,154. (I) 555 nm, N= 1,193. (J) 620 nm, N= 212.

Table 2. Descriptive statistics of $\tilde{b}_{bp}(\lambda)$ for the individual data sets

Data Set		442 nm	488 nm	532 nm	555 nm	620 nm	442 nm	488 nm	532 nm	555 nm	620 nm
GOC99A	Mean	0.0130	0.0126	0.0121	0.0114	0.0113	0.0100	0.0095	0.0087	0.0090	0.0086
	10th percentile	0.0089	0.0081	0.0077	0.0077	0.0072	0.0074	0.0068	0.0063	0.0065	0.0061
	90th percentile	0.0179	0.0185	0.0179	0.0167	0.0172	0.0139	0.0134	0.0118	0.0127	0.0130
MOCE-5	Mean	0.0153	0.0125	0.0133	0.0123	0.0129	0.0104	0.0080	0.0079	0.0083	0.0074
	10th percentile	0.0100	0.0084	0.0086	0.0083	0.0083	0.0066	0.0051	0.0050	0.0053	0.0054
	90th percentile	0.0250	0.0183	0.0213	0.0176	0.0201	0.0155	0.0119	0.0121	0.0132	0.0121
HY00	Mean	0.0131	0.0113	0.0103	0.0097	0.0096	0.0113	0.0091	0.0080	0.0077	0.0075
	10th percentile	0.0094	0.0079	0.0067	0.0065	0.0061	0.0094	0.0066	0.0059	0.0056	0.0054
	90th percentile	0.0213	0.0189	0.0172	0.0162	0.0161	0.0204	0.0190	0.0115	0.0104	0.0169
CL01	Mean	0.0184	0.0144	0.0139	0.0166	0.0145	0.0156	0.0111	0.0131	0.0187	0.0136
	10th percentile	0.0098	0.0067	0.0068	0.0087	0.0081	0.0101	0.0054	0.0093	0.0150	0.0126
	90th percentile	0.0360	0.0309	0.0298	0.0296	0.0234	0.0264	0.0209	0.0191	0.0236	0.0150
HY01	Mean	0.0129	0.0108	0.0102	0.0126	0.0110	0.0103	0.0076	0.0064	0.0085	0.0069
	10th percentile	0.0074	0.0059	0.0056	0.0065	0.0061	0.0081	0.0054	0.0046	0.0051	0.0052
	90th percentile	0.0224	0.0200	0.0194	0.0237	0.0208	0.0131	0.0108	0.0088	0.0124	0.0097

Statistics for the entire data set are shown on the left. Statistics for data within the first optical depth are shown on the right. The geometric mean is shown.
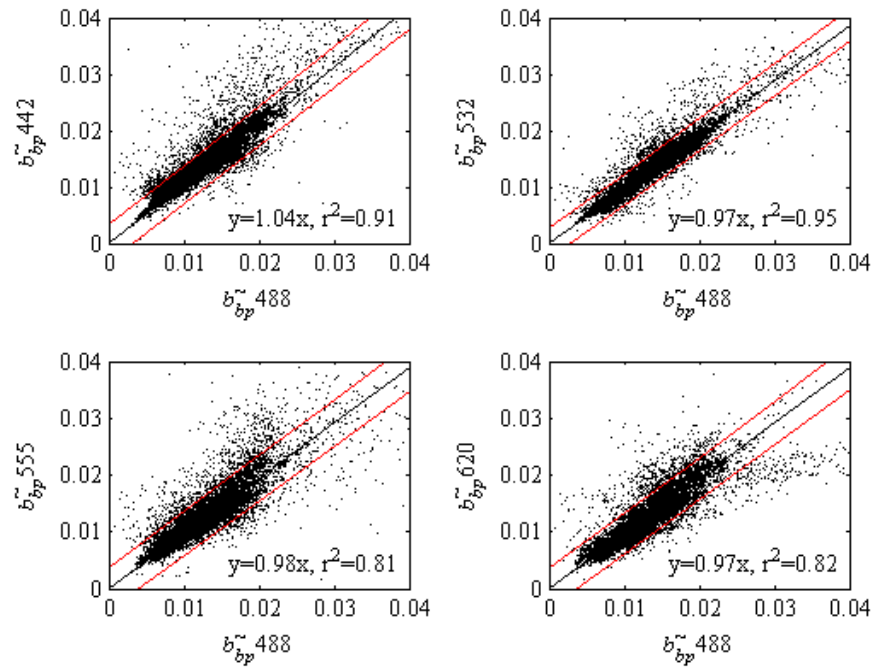
Figure 2.2. Particulate backscattering ratio at 488 nm plotted versus the particulate backscattering ratio measured at four other wavelengths for the entire global data set. The Model II regression fits at each wavelength are shown with 90% confidence limits (red). The number of data points for each regression is 9,154.
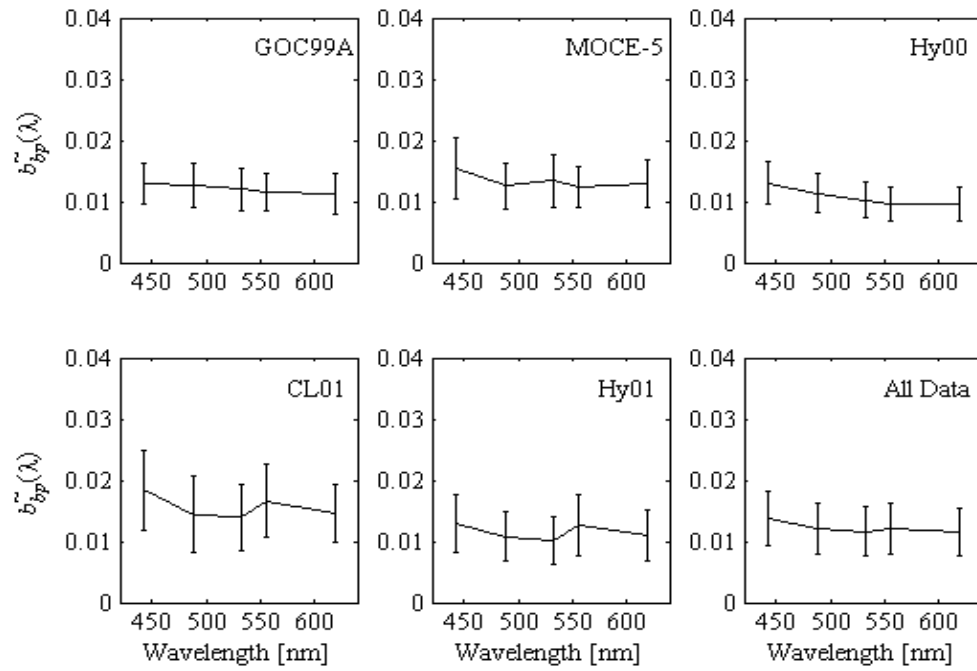
Figure 2.3. Mean particulate backscattering ratio spectra for individual data sets, with one standard deviation shown for each data point. The spectra are as follows: GOC99A (top, left), MOCE-5 (top, middle), HyCODE 2000 (top, right), Crater Lake 2001 (bottom, left), HyCODE 2001 (bottom, middle), and the mean of all of the data sets (bottom, right).
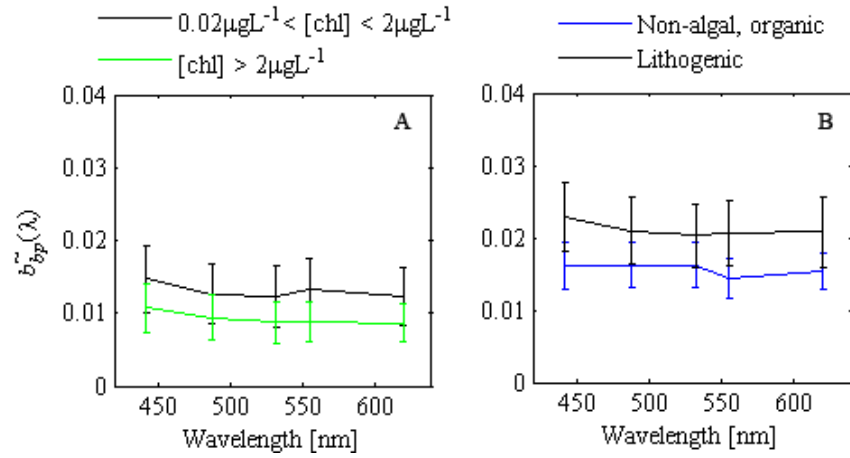
Figure 2.4. Mean particulate backscattering ratio spectra for different biogeochemical provinces. One standard deviation is plotted on each mean. (A) $b_{bp}(\lambda)$ ratios where chlorophyll concentration lies between 0.02 and $2\mu gL^{-1}$(black, N = 6,049) and $b_{bp}(\lambda)$ ratios where chlorophyll concentration is above $2\mu gL^{-1}$(green, N = 2,242). (B) $b_{bp}(\lambda)$ ratios where chlorophyll concentration is zero and where the particulate beam attenuation at 650 nm is <= $0.5m^{-1}$(blue, N = 772) and $b_{bp}(\lambda)$ ratios where chlorophyll concentration lies between 0 and $0.5\mu gL^{-1}$ and where the particulate beam attenuation at 650 nm is above $1m^{-1}$(black, N = 18).
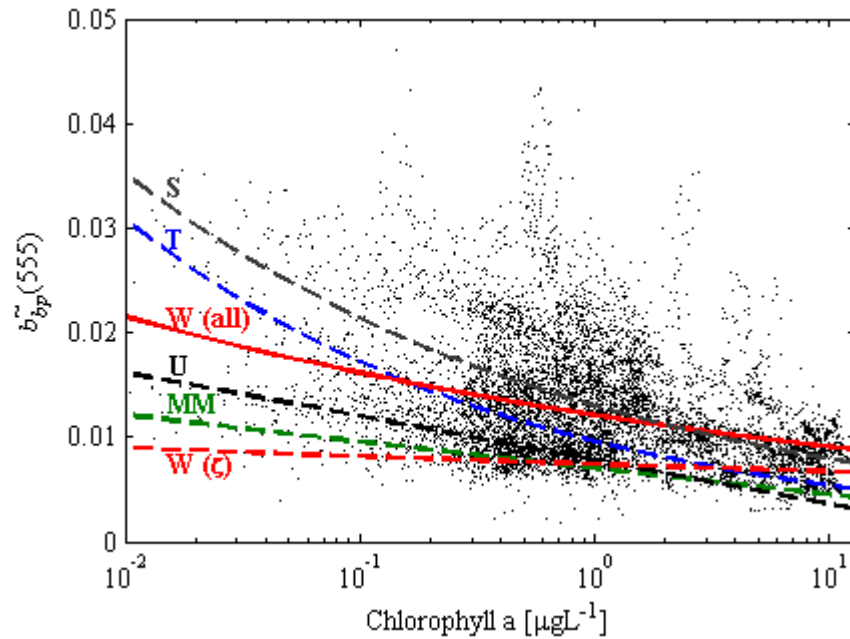
Figure 2.5. The particulate backscattering ratio at 555-nm as a function of chlorophyll-a concentration (W(all)). Curves showing the relationship based on models by Sullivan et al. [2006], Twardowski et al. [2001], Ulloa [1994], and Morel and Maritorena [2001] are identified as S, T, U, and MM respectively. The solid red line (W(all)) is the least-squares power-law fit to data in this study. The dashed red line (W(ζ)) is the least-squares power-law fit to the data above one optical depth.

Chapter 3. Spectral backscattering properties of marine phytoplankton cultures

A.L. Whitmire, W.S. Pegau, L. Karp-Boss, E. Boss, A. Ashe, and C. Waluk

3.1 Introduction

The structure and function of marine ecosystems are largely dictated by the composition of the phytoplankton community. Likewise, the bulk inherent optical properties of a water mass are determined by the sum of it's constituents (water, particles, and dissolved substances; Gordon et al. 1975; Mobley, 1994). Historical methods of monitoring phytoplankton abundance generally treat the community in bulk, due mainly to an inability to effectively and efficiently isolate and monitor specific phytoplankton taxa. Optical instruments are now being used on a variety of platforms at time and space scales relevant to phytoplankton physiology and ecology (Dickey et al., 2006). However, our understanding of how diverse phytoplankton taxa contribute to bulk optical measurements remains limited. This is especially true of the backscattering properties of marine phytoplankton, due to a paucity of measurements of this parameter on laboratory cultures (Stramski et al., 2004). A thorough understanding of how marine phytoplankton contribute to the bulk backscattering signal in the ocean is critical for accurate interpretation of remote sensing data because the ocean reflectance is determined by the ratio of backscattering to absorption (Gordon et al., 1975).

Historically, the backscattering properties of phytoplankton cells were investigated through the use of theoretical models because the instrumentation required to measure backward scattering was not commercially available. Early work that employed scattering theory for coated spheres (i.e., representing a cell as having a cell membrane or cell wall and a homogeneous interior) indicated that it was essential to account for a cell membrane when using models to represent biological cells because models that assumed homogeneous spheres (no cell wall or cell membrane) underestimated backward scattering (Meyer, 1979). Likewise, several modeling studies that incorporated layered or coated spheres (Quinby-Hunt et al., 1989; Kitchen and Zaneveld, 1992; Quirantes and Bernard, 2004) or non-spherical particles (Quirantes and Bernard, 2004; Clavano et al., 2007) also concluded that assuming sphericity and homogeneity resulted in underestimates of the backscattering coefficient by up to an order of magnitude.

Despite these cautionary findings, a majority of the studies that used models to obtain backscattering by phytoplankton and other marine microbial cells have relied upon the Mie model for light absorption and scattering and assumed spherical, homogenous cells (Morel and Bricaud, 1981; Bricaud et al., 1983; Bricaud and Morel, 1986; Morel and Bricaud, 1986; Morel and Ahn, 1990; Morel and Ahn, 1991; Stramski and Kiefer, 1991; Ahn et al., 1992; Stramski and Mobley, 1997; Stramski et al., 2001). These studies concluded that backscattering by phytoplankton, marine bacteria, ciliates and/or flagellates was weak compared to other marine particles such as detritus or lithogenic materials. The supposition that phytoplankton cells are weak backscatterers has strong ramifications in how they are modeled as a portion of the diverse oceanic particle population in radiative transfer simulations and remote sensing applications.

The backscattering properties of marine phytoplankton have only recently been rigorously measured in the laboratory on a limited basis (Volten et al., 1998; Vaillancourt et al., 2004). Volten et al. (1998) made detailed measurements of the volume scattering function for several phytoplankton species at a single wavelength, 633 nm. They found that morphology influenced the scattering distribution, but not in ways that were predictable. For example, two species with a similar shape produced different scattering signals, while two cultures with very different shapes, a cylinder and a sphere, produced similar scattering patterns. Volten et al. (1998) also found that internal structures, like gas vacuoles, had a significant impact on the scattering distribution. In comparing their measurements with Mie model simulations of the phytoplankton cells in their study, Volten et al. (1998) concluded that the Mie model, with its assumptions of sphericity and homogeneity, did not produce good approximations of scattering by phytoplankton. Vaillancourt et al. (2004) also found that the Mie model was unable to reproduce the magnitude of backscattering that they observed for phytoplankton cultures when "typical phytoplankton" values of the refractive index were used as inputs to the model ($n = 1.06 – 1.08$).

An analysis of the spectral backscattering properties of marine phytoplankton cultures at four wavelengths did not find any significant spectral variation between cultures (Vaillancourt et al., 2004). The spectral backscattering coefficients for all of the

cultures studied were normalized to cell concentration to obtain backscattering efficiencies, and then fit to power law functions. Relationships between backscattering efficiency and chlorophyll-a, particulate organic carbon, and cell size were all analyzed at a single wavelength. Measurements of complementary inherent optical properties, the absorption, attenuation, and scattering coefficients, were not collected in this study, which makes it difficult to place the backscattering measurements into context and compare them with the optical properties of other important marine particle types.

The shortage of direct measurements of the spectral backscattering properties of marine phytoplankton and the divisive results of various modeling studies highlight the need for additional empirical studies on this topic. This work presents results from laboratory analysis of the backscattering properties of fifteen phytoplankton species from five major taxa (diatoms, dinoflagellates, chlorophytes, cryptophytes, and prymnesiophytes). Optical measurements include portions of the volume scattering function (VSF) at six wavelengths, total absorption and attenuation at nine wavelengths, and stimulated fluorescence. The VSF is used to obtain the backscattering coefficient for each species, and we focus on intra- and interspecific variability in spectral backscattering in this work. We also investigate the spectral and angular variability in the conversion factor for single-angle VSF measurements to the backscattering coefficient for phytoplankton cultures. Ancillary measurements include chlorophyll and cell size, shape and morphology via Coulter counter and/or light microscopy. The goal of this work is to elucidate how and the extent to which diversity in size, shape, and morphology contribute to variability in backscattering within and between taxa.

3.2 Methods

3.2.1 Phytoplankton cultures

Most cultures were obtained from the Provasoli-Guillard Center for Culture of Marine Phytoplankton (CCMP) or the Canadian Center for the Cultivation of Microorganisms (CCCM; see Table 1). The species used in this experiment included centric diatoms, a pinnate diatom, a chain-forming diatom with spines, chain-forming

diatoms without spines, spheroid dinoflagellates that were armored and unarmored*,* single-celled, spherical and spheroid chlorophytes, and a prymnesiophyte. See Table 1 for information regarding the species and their general characteristics. All were grown in L1-enriched seawater media that was autoclaved and then filter sterilized using a 0.22 μm filter (Millipore, Steritop). Cultures were incubated at 17 degrees Celcius with an illumination of approximately 100 μmol photons m^{-2} s^{-1} under a 14:10 dark:light cycle. Cells were maintained in exponential growth by diluting them as needed with fresh media. The rate of dilution varied between species, depending on their growth rate determined via *in vivo* fluorometry.

3.2.2 Optical measurements

Measurements of the volume scattering function (VSF) were conducted in a custom 12½ inch (inner dimension) plexi-glass box that was built to replicate the manufacturers standard calibration chamber (HOBI Labs, Inc.). The chamber was filled with approximately 25 liters of 0.2μm-filtered seawater (FSW) and a Hydroscat-6 (HS6) was suspended with the instrument face one inch below the surface. The box was covered in opaque black cloth to exclude ambient light during measurements. An ac-9 (WET Labs, Inc.) was attached in-line with the calibration chamber and sample medium was circulated through the system with a small pump. After collecting a filtered seawater measurement sequentially with each instrument, 500 mL of culture was added to the sample chamber. The culture suspension was gently but thoroughly mixed again, and measurements were taken immediately. Sequential additions of culture were made until the entire volume had been added, generally between two and two and a half liters total. After each round of optical measurements was complete, aliquots of FSW and then culture suspension were collected for chlorophyll, Coulter counter, and microscopic analysis. When available, an ECO-VSF instrument (WET Labs, Inc.) was also used in the plexi-glass chamber to collect multi-angle, single wavelength VSF measurements. The same instrument orientation was used in each experiment. The sample box was thoroughly rinsed with deionized water (DIW) between cultures.

Measurements of DIW were taken daily as a means to calibrate the instruments and to ensure that the chamber was clean after each sample.

3.2.3 Ancillary measurements

Coulter counter measurements were conducted on the FSW media and on each addition of culture immediately following each experiment. We used a 100 μm aperture with a one milliliter sample volume. This provided a reliable particle size distribution and concentration range from 2 to 60 microns in equivalent spherical diameter. Removing the FSW counts from the cultures had a negligible impact on particle size distributions and particle counts, so we did not remove a 'blank' from our results. The mean size of a culture was determined by fitting a Gaussian function to the Coulter counter frequency distribution (raw particle counts normalized to each bin width). Cell concentration was estimated by summing all of the raw particle counts within two standard deviations of the mean particle size determined by the Gaussian fit. When cells were too large for the Coulter counter (*Ceratium longpipes*, e.g.), cell dimensions and concentration were obtained from preserved samples via light microscopy, and mean values were used to calculate a cross-sectional area for each culture. Chlorophyll measurements were collected using the acetone extraction technique (Yentsch and Menzel, 1963).

3.2.4 Instruments & Data Processing

Absorption and attenuation were measured at nine wavelengths with a WET Labs ac-9. DIW measurements were collected daily for calibrations. DIW data were temperature corrected and then subtracted from raw FSW and culture measurements. The data were then corrected for temperature and salinity (Pegau et al., 1997), and the absorption coefficient was corrected for scattering using the proportional method (Zaneveld et al., 1994). The mean value of the absorption, scattering, and attenuation

coefficients were calculated at each wavelength to obtain a single parameter value for each culture.

The volume scattering function, β, was measured at 140 degrees and six wavelengths (442, 488, 532, 555, 620, and 676 nm) with the HOBI Labs Hydroscat-6 (HS6) instrument (Maffione and Dana, 1997). We did not use the processing software provided with the instrument; instead, all processing was accomplished with our own routines via MATLAB. We obtained raw values of β from the HS6 and corrected for attenuation along the path length of the instrument using data obtained with an ac-9 (the "σ-correction"; Maffione and Dana, 1997). We then removed pure water volume scattering, β_w, from β to obtain β_p (Boss and Pegau, 2001). We used estimates for pure seawater volume scattering from Buiteveld et al. (1994) instead of Morel (1974). In brief, Buiteveld used more recent empirical data to define the depolarization ratio of water molecules, δ, which resulted in a more accurate parameterization of scattering by water molecules than earlier studies (see Twardowski et al. 2007 for a thorough discussion of this issue). These β_p values were then converted to the backscattering coefficient (see section 3.2.5). Derived parameters for the HS6 include volume scattering by particles, and the total and particulate backscattering coefficients (b_b and b_{bp} respectively). To account for any possible tank effects or filtered media effects, we subtracted $b_{bp}(\lambda)$ for FSW from $b_{bp}(\lambda)$ for each culture suspension.

Mie theory shows that for angles near 120 degrees the VSF for particles does not vary significantly between a wide range in particle properties and sizes (Oishi, 1990). This theoretical relationship facilitates the use of a single-angle scattering meter to estimate the backscattering coefficient. Empirical data continue to demonstrate that measuring scattering at one backward angle is a robust approach to estimating the backscattering coefficient in oceanic waters (Boss et al., 2004; Chami et al., 2006; Twardowski et al, 2007; Berthon et al., 2007; Stramski et al., 2007). However, there is some uncertainty in how much the VSF varies for phytoplankton, and whether or not previous values of the conversion factor, χ_p, can be applied to derive the backscattering coefficient from a single-angle measurement for phytoplankton (Chami et al., 2006).

We discuss our methods for determining the appropriate conversion factor in the next section.

3.2.5 Angular and spectral variation in the conversion factor, χ_p, for phytoplankton cultures

There are presently three approaches for the estimation of the backscattering coefficient from volume scattering measurements. The approach that most resembles the theoretical definition of the backscattering coefficient is to integrate the VSF over the entire backward hemisphere as:

$$b_b = 2\pi \int_{\pi/2}^{\pi} \beta(\theta)\sin\theta d\theta$$

Eq. 1

This approach is rarely used because it requires detailed scattering information over a wide angular range, and instrumentation is not yet commercially available to carry out such a measurement (though various prototype *in situ* instruments have been used on a limited basis for several decades, e.g. Petzold, 1972). An alternative method was developed by Moore et al. (2000) and refined by Sullivan et al. (2005). This approach uses scattering measurements at three angles in the backward direction (100, 125, and 150 degrees), and a fourth value for scattering flux at 180 degrees ($2\pi\sin\theta = 0$). A third-order polynomial is then fit to scattering flux at these four angles, and is integrated from $\pi/2$ to π to estimate b_b. A third method for estimating the backscattering coefficient is to measure scattering at one backward angle and convert it to b_b using a theoretically derived conversion factor (Oishi, 1990; Maffione and Dana, 1997). We used this approach because at the time of our sampling, the Hydroscat-6, which measures the VSF at a single angle, was the only commercially available backscattering sensor with multiple wavelengths.

Using this approach, volume scattering is converted to the backscattering coefficient in the following manner:

$$b_{bp}(\lambda) = 2\pi\chi_p(\theta)\beta_p(\lambda,\theta)$$

Eq. 2

where β_p is the particulate VSF at a given wavelength (λ) and scattering angle (θ). χ_p is a conversion factor to account for the relationship between scattering at one angle and the integral of the VSF from 90 to 180 degrees. χ_p varies with angle as a function of the shape (or slope) of the particle size distribution in the sampling volume, and the real and imaginary refractive index of the bulk particle population (Oishi, 1990).

While earlier studies found no spectral dependence in χ_p for oceanic particles (Boss and Pegau, 2001) or phytoplankton monocultures (Vaillancourt et al., 2004), Chami et al. (2006) recently showed significant spectral variation in χ_p for phytoplankton cultures at 140 degrees. As described earlier, our laboratory measurements of β were obtained with a Hydroscat-6 instrument at the single scattering angle of 140 degrees. It was therefore necessary to address these conflicting results before proceeding with our analyses.

We can apply the results obtained at a community 'scattering workshop' (http://www.opl.ucsb.edu/ScatteringWorkshop; Prentice et al., 2002) to evaluate the wavelength dependence of χ_p at various angles. During the workshop, a newly developed multi-spectral volume scattering meter (VSM) was tested alongside several other scattering sensors for measurements of polystyrene beads, Maalox solution, local river water, and several phytoplankton monocultures. We use the VSM data to examine the variability in the conversion factor, $\chi_p(\lambda,\theta)$, for thirteen phytoplankton cultures at 6 wavelengths (443, 490, 510, 555, 590, and 620 nm). This prototype VSM was the same type of instrument used in the field component of Chami et al. (2006). For a description of the operating principle of the VSM, see Lee and Lewis (2003).

The VSM measures the volume scattering function with 0.3 degree angular resolution from 0.4 – 178.5 degrees. We assumed that the volume scattering function was flat from 178.5 to 180 degrees, and then used a cubic interpolating spline to produce a VSF with 1-degree angular resolution from 0 to 180 degrees. We removed the volume scattering contribution by salt water according to Buiteveld et al. (1994), and then estimated b_{bp} according to Equation 1 above. The resulting volume scattering functions for phytoplankton cultures can be seen in Figure 3.1. After obtaining the

particulate backscattering coefficient and volume scattering function from the VSM, we estimated $\chi_p(\lambda,\theta)$ by rearranging Equation 2 as follows:

$$\chi_p(\lambda,\theta) = \frac{b_{bp}(\lambda)}{2\pi\beta_p(\lambda,\theta)}$$

Eq. 3

We calculated $\chi_p(\lambda,\theta)$ at the six wavelengths of the VSM at one degree angular resolution from 90 to 180 degrees (Figure 3.2, Table 3.2). We observed some minor spectral variability in the conversion factor between six wavelengths, but a one-way analysis of variance (ANOVA) conducted on the means of all six wavelengths between 100 and 150 degrees found no significant difference between them ($P = 0.623$; Figure 3). It is interesting to note that the highest standard deviations were observed for the average $\chi_p(\lambda,\theta)$ spectra that included data from more species, not fewer (e.g. 443, 555, 590 and 620 nm; see Table 3.2). This indicates that the width of the 95% confidence intervals shown in Figure 2 are more indicative of the natural variability between species, not measurement uncertainty. $\chi_p(\lambda,\theta)$ shows the most variability at angles greater than 155 degrees, which may be the result of high variability in the near-backward scattering for various species, or reflections inside the sample chamber.

Our results closely followed the angular dependence observed in previous studies, showing a broad maximum around 130 to 140 degrees (Figure 3.4; Boss and Pegau, 2001; Chami et al., 2006). Our results were higher than Sullivan et al. (2005; coastal waters) and Vaillancourt et al. (2004; cultures) at angles of 125 and 140 degrees respectively, but were generally consistent with estimates of χ_p at 555 nm for cultures published by Chami et al. (2006) from 90 to 120 degrees. We did not observe significantly higher values in χ_p for cultures from 130 to 160 degrees, which contradicts the findings of Chami et al. (2006) in that angular range. Interestingly, our average estimates of χ_p for cultures most closely resembled those of Boss and Pegau (2001) that were derived from the Mie model and from data collected in the coastal waters of the Eastern United States with an earlier generation of the VSM.

Contrary to Chami et al. (2006), we found that χ_p was independent of wavelength at several angles within the uncertainty of our measurements. We therefore

used the average χ_p from all cultures at all wavelengths sampled in our study at 140 degrees, 1.21, for all cultures at all wavelengths when estimating the particulate backscattering coefficient with data from the Hydroscat-6 instrument.

3.2.6 Optical cross-sections

To facilitate comparisons of spectral shape and the efficiency of backscattering between cultures in a way that is independent of concentration, it is useful to normalize the backscattering measurements by some other variable. In the case of phytoplankton cultures, chlorophyll, cell concentration, and particulate organic carbon content are commonly used in this regard (e.g. Vaillancourt et al., 2004). We normalized the particulate backscattering coefficient, and the other IOPs measured in this study, by cell concentration to produce IOP cross-sections for each culture. Single particle cross-sections, σ_x (where x is 'a' for absorption, 'b' for scattering, and 'bb' for backscattering), were calculated as the ratio of the bulk coefficient to particle concentration, *N/V* (in particles per cubic meter), measured with the Coulter counter. For example, the backscattering cross-section, σ_{bb}, was estimated as follows:

$$\sigma_{bb} = \frac{b_{bp}(\lambda)}{N/V} \qquad \text{Eq. 4}$$

Particle optical cross-sections describe the two-dimensional area of the particle that interacts with source light, and may or may not be directly related to the actual size or volume of the particle. For example, in the case of phytoplankton cells, pigment packaging may affect the absorption cross-section in a manner that is not linearly related to the cell size or volume (Bricaud et al., 1988). Also, the scattering cross-section of a non-spherical cell may vary depending on the orientation of the cell relative to the source and detector.

3.2.7 Uncertainties in optical parameters

We estimated the standard deviations of the absorption, attenuation, and backscattering coefficients for all of the dilution series of all cultures, and converted the data to the coefficient of variation (CV) to facilitate comparison between measurements at various concentrations. We found that for measurements of cultures, the absorption had an average (across all wavelengths) CV of approximately 1% of the signal. The attenuation measurement had an average CV of 0.5%. The backscattering coefficient had an average CV of 3% for the HS-6, and 3.5% for the ECO-VSF. By propagation of error, the uncertainty in the scattering coefficient is 1.5%. Based on the average CV for χ_p at 140 degrees for all cultures, the uncertainty in χ_p is 10%, and we estimate the uncertainty in the backscattering ratio to be approximately 15%. We did not collect replicate measurements of the particle counts from the Coulter counter, but we estimate the error in the mean particle size and concentration to be approximately 5%. We estimate the error in the absorption, scattering, and backscattering cross-sections as 6%, 5.5%, and 8% respectively.

3.3 Results

3.3.1 Spectral backscattering coefficients

We applied $\chi_p(140°)$ using Equation 2 to obtain $b_{bp}(\lambda)$ for each experimental culture (Figure 3.5). The shape of the particulate backscattering coefficient spectra for phytoplankton cultures showed distinct features within and between taxonomic groups. Backscattering generally decreased from blue to red with the exception of backscattering at 442 nm, where pigment absorption has been shown to influence backscattering intensity (Ahn et al., 1992; Stramski et al., 2001). We investigated the influence of absorption on the backscattering signal at 442 nm to determine if strong chlorophyll absorption diminished backscattering (Bricaud and Morel, 1983; Ahn et al., 1992). We estimated the slope of the backscattering spectrum between 442 nm and 488 nm, and compared these slopes to the absorption line height at 442 nm (e.g. Davis et al.,

1997; Boss et al., 2007). We did not find any significant relationship between the absorption line height and the slope of the backscattering spectrum between 442 nm and 488 nm when all cultures were combined. However, when we considered each taxonomic group individually, the slope of the backscattering spectrum in the blue for flagellates and dinoflagellates showed a strong relationship with absorption when the data were fit with linear least squares regressions ($R^2 = 0.93$ and 0.99 respectively; Figure 3.6). Flagellates exhibited a positive slope at high absorption, i.e. $b_{bp}(442)$ was lower than $b_{bp}(488)$. The dinoflagellates demonstrated the opposite trend, with high, positive backscattering slopes at low values of the absorption line height, and a negative slope at higher relative absorption. The slopes of the backscattering spectra between 442 nm and 488 nm for the diatoms had a weaker, positive linear relationship with the relative absorption ($R^2 = 0.25$).

Previous research has shown that measurements of backscattering at 676 nm can be artificially elevated due to fluorescence emission that is detected at this wavelength (Ahn et al., 1992; Boss et al., 2007; Whitmire et al., 2007; Dall'Olmo et al., in review). Our data corroborate these results and showed enhanced backscattering at 676 nm for all cultures. We therefore exclude $b_{bp}(676)$ from our plots and our analyses.

For non-absorbing particles, theory predicts that particles with a high scattering cross section (large particles) will have similar backscattering at all wavelengths, whereas smaller particles will have relatively higher backscattering at shorter wavelengths (Morel, 1973; Bohren and Huffman, 1984). As a result, smaller cells would produce a sloped spectrum, and larger cells a relatively flat spectrum. Recent work has shown that there is a relationship between the slope of the backscattering spectrum and the slope of the beam attenuation coefficient *in situ* (Slade and Boss, 2008), which implies that there is an empirical relationship between the particle size distribution and the slope of the spectral backscattering coefficient. We calculated the ratio of backscattering at 488 nm to 620 nm as a general indicator of the slope of the backscattering spectrum. We did not find any relationship between the equivalent spherical diameter of phytoplankton cells and ratios of the backscattering coefficient in our dataset (Figure 3.7).

3.3.3 Spectral backscattering ratios

The particulate backscattering ratios of the marine phytoplankton cultures that we sampled ranged from 0.0035 – 0.0290 at 442 nm (see Table 1). Although there is some apparent spectral variability, the differences between wavelengths for individual taxa were mostly within the 15% error in our estimates (Figure 3.8). Cultures with the lowest backscattering ratios, from 0.0035 to 0.0131, include *C. profunda, Chlorella*, *D. tertiolecta*, the prymnesiophyte *I. Galbana*, small centric diatoms (both strains of *T. pseudonana*, and *T. weissflogii*), a large centric diatom (*D. brightwellii*), and the pennate diatom *P. tricornutum* (Figure 3.8). The highest backscattering ratios, from 0.0195 to 0.0290, were observed in large centric diatoms (both strains of *C. radiatus*, and *T. rotula*) and all of the dinoflagellates sampled (*C. longpipes, G. simplex*, and *H. triquetra*). This result illustrates that the backscattering ratios in marine phytoplankton cultures are not simply the result of plasma membrane or cell wall material (i.e. silica vs. cellulose thecal plates), but are instead the result of complex interactions with size, shape, and the internal structures of the cells.

Except for the cryptophyte *C. profunda*, the remaining flagellates sampled, *I. galbana*, *Chlorella*, and *D. tertiolecta*, all had backscattering ratios of 0.0079 or less. Based on modeling studies that assumed homogeneous spherical particles, Morel and Ahn (1991) concluded that heterotrophic flagellates and ciliates had almost no effect on backscattering. Our measurements support their results to the extent that the autotrophic flagellates sampled in this work produced weak, but not insignificant, backscattering. The weak backscattering in these groups can be attributed to their relatively high water content (Morel and Ahn, 1991).

3.3.4 Backscattering and chlorophyll

When data from all cultures was grouped together, high backscattering values were observed at low, intermediate, and high chlorophyll concentrations, indicating that chlorophyll concentration was not a good predictor of backscattering, and vice versa,

for phytoplankton cultures *in toto* (Figure 3.9A). However, for each species in our study, backscattering was highly linearly correlated with the chlorophyll concentration when examined individually (Figure 3.9B,C). The slope of the relationship was species-specific. For example, *T. pseudonana* (CCMP1010) had a chlorophyll-*a* concentration of nearly 25 mg m^{-3} with a concurrent backscattering coefficient of 0.011 m^{-1}, whereas *C. longpipes* had a chlorophyll-*a* concentration of only 0.75 mg m^{-3} at a $b_{bp}(555)$ of 0.008 m^{-1}. This observation explains the range of variability we observe between Chl and backscattering *in situ*, where individual members of the phytoplankton community variously contribute to the bulk signals. This result provides some explanation as to why the magnitude of *in situ* backscattering would not always follow a single-order relationship with chlorophyll, even in high chlorophyll waters.

3.4 Discussion

3.4.1 Variability in the spectral particulate backscattering coefficient between cultures

We observed spectral variability in the backscattering coefficients of marine phytoplankton cultures that we could not attribute to cell size or absorption effects. Likewise, there were no obvious correlations between features in the attenuation, scattering, or absorption spectra and spectral variability in the backscattering coefficients of the cultures (Figures 3.10-12). It is possible that the limited number of wavelengths available (six) and wide spectral bands (10 nm FWHM) of the Hydroscat-6 instrument were insufficient for examining the spectral features seen in previous work (Bricaud and Morel, 1983; Ahn et al., 1992; Stramski et al., 2001). However, given the lack of published direct measurements of the backscattering properties of marine phytoplankton cultures, more general information on the backscattering properties of marine phytoplankton cultures is still needed. Despite the lack of strong spectral features in the backscattering coefficients, we did not fit a power law function to the spectra in an effort to produce 'representative' phytoplankton spectra like previous studies (Vaillancourt et al., 2004). There is no evidence to support the idea that individual phytoplankton cells or monodispersed cultures would adhere to such a

generalized spectral shape, especially given the extremely variable nature of phytoplankton size, morphology, and composition. Stramski et al. (2001), who presented the collected results of eight published papers on phytoplankton optical properties (though backscattering results were all derived from models), demonstrated that there was extreme spectral variation in the modeled particulate backscattering coefficients between species and phytoplankton groups that our measurements could not replicate. While our observations with the HS6 indicate that spectral backscattering differences were not influenced by particle size or shape, the backscattering ratio, in contrast, was quite sensitive to particle composition. We discuss these results in the next section.

3.4.2 Variability in the spectral particulate backscattering ratio between cultures, and comparison with previous models

Backscattering ratios for the diatoms that we sampled were highly variable, spanning nearly an order of magnitude from the highest observed $\widetilde{b}_{bp}$ (λ) to the lowest (0.0290 to 0.0035; Table 1). Given the range in size and variety of shapes for the eight diatoms that we sampled, the backscattering ratio appears to be largely a function of size for this group. In general the larger diatoms exhibited higher backscattering ratios and larger backscattering cross-sections than smaller diatoms. The presence of spines (*D. brightwellii*) does not appear to have a significant effect on the backscattering ratio in these cultures.

The dinoflagellates, which range in size from just under 12 μm to over 150 μm in our cultures, all had very high backscattering ratios (Table 1). This was consistent for both thecate (having cellulose thecal plates embedded in the cell membrane, *H. triquetra*) and non-thecate (lacking thecal plates, *G. simplex*) dinoflagellates. This supports the idea that cell composition and internal structure play a large role in backscattering (Kitchen and Zaneveld, 1992; Bricaud, 1992; Volten et al., 1998; Witkowski et al., 1998). Vaillancourt et al. (2004) also found that dinoflagellates had

the highest backscattering efficiency out of 12 classes of phytoplankton, which they attributed to the high carbon content of the group.

In addition to their high carbon content, dinoflagellates also have some unique internal structures that may contribute to increased backscattering. First, they have an organelle called a pusule, which is described as "an array of highly branched membranous sacs or tubules derived by invagination of the cell membrane" (Graham and Wilcox, 2000). These organelles are generally found in association with the flagella, and may be 2 to 10 microns in diameter (with much higher surface area due to their complex structure). The cell membrane of an algal cell is primarily lipids and proteins, and can have a refractive index as high as 1.10-1.16 relative to water (Meyer, 1979). If we assume the pusules maintain the same index of refraction as the cell membrane, they could significantly influence the backscattering properties of the cells by increasing the structural complexity and surface area of highly refractive material within the cells. Theoretically, this would result in high backscattering cross-sections (σ_{bb}) relative to other phytoplankton groups with cells of the same size. While our sample size is small, *G. simplex* and *H. triquetra* do have higher σ_{bb} than comparably sized diatoms *T. pseudonana* (CCMP1010) and *T. weissflogii* (Table 1).

Dinoflagellates also have very unusual chromosome morphology that is unique among eukaryotes (Bhaud et al., 2000). The chromatin of dinoflagellate deoxyribonucleic acid (DNA) lacks histones and nucleosomes, which results in chromosomes that remain permanently compressed except during DNA replication (Graham and Wilcox, 2000). Their chromosomes stay in very dense clusters in the nucleus, and contain large amounts of DNA. Their protein:DNA mass ratio is 1:10, whereas normal eukaryotes have a 1:1 ratio (Bhaud et al., 2000). The refractive index of DNA is 1.54 (or 1.16 relative to water) at 632 nm (Samoc et al. 2007), which is significantly higher than reported values for surrounding cytoplasm. Kitchen and Zaneveld (1992) showed that the backscattering from a three-layered-sphere model of a phytoplankton cell was more than an order of magnitude higher than for the same size homogeneous sphere. However, Kitchen and Zaneveld (1992) used an index of refraction of only 1.02 for the inner layer of the model sphere. A model representing the

dense aggregation of high refractive index DNA within the dinoflagellate nucleus would produce backscattering coefficients that were even higher than the ten-fold increase observed in Kitchen and Zaneveled's hypothetical phytoplankton cell. It is possible that the unique nucleus of the dinoflagellates could alone explain the high backscattering ratios that we observed, not even considering the possible contribution of the pusules.

The sole cryptophyte in our study, *C. profunda*, exhibited a relatively high backscattering ratio of 0.0131 at 442 nm. We hypothesize that the ratio was influenced by the unique plated periplast found in cryptomonads (Faust, 1974; Santore, 1984). The periplast is a three-layer cell membrane that is composed of an internal plasma membrane, an inner layer proteinaceous plates, and an outer fibrous layer. We speculate that the protein content of the periplast acts as a high refractive index outer shell, the effect of which has been shown to significantly increase backscattering in several studies (Meyer, 1979; Quinby-Hunt et al., 1989; Kitchen and Zaneveld, 1992; Bricaud, 1992; and Stramski and Piskozub, 2003). The backscattering ratio for *C. profunda* was even higher than that of a comparably sized diatom, *T. weissflogii*, which has a cell wall composed of silica, a high refractive index material.

We also found that the backscattering ratio was influenced by cell size (Figure 3.13). We fit a power law function to the backscattering ratio at 555 nm and the equivalent spherical diameter (ESD) and found that the relationship was described by the following function:

$$b_{bp}/b_p(555) = 4.390 \times 10^{-3} \times ESD^{0.432} \; ; R^2 = 0.56 \qquad \text{Eq. 4}$$

A similar relationship was observed between the backscattering cross-section at 555 nm and the ESD:

$$\sigma_{bb}(555) = 4.269 \times 10^{-14} \times ESD^{2.028} \; ; R^2 = 0.84 \qquad \text{Eq. 5}$$

These results are somewhat counter-intuitive because, all else being equal, a larger homogeneous particle has a lower backscattering efficiency than a smaller homogeneous particle. This is because larger particles scatter more light in the forward direction than smaller particles, which reduces their backscattering ratio. However, Vaillancourt et al. (2004) also found a strong positive relationship between

backscattering efficiency and cell diameter. One possible explanation of the positive relationship between ESD and the backscattering ratio and cross-section in our data is that the larger cells that we sampled were biased toward taxa with high-index outer coverings that increased their backscattering efficiencies. We did not sample any large flagellates, and it would be interesting to see how well they would fall in line with this relationship.

Another possible explanation is that the cultures of larger cells had high concentrations of detrital material or bacterial contamination, and that these small, non-algal particles elevated the backscattering magnitudes of the larger cells. However, given the difficulty of differentiating the potential effects of these non-algal particles from the signals originating from the cells of interest, we were unable to quantify their possible influence on our results (see Appendix A for a thorough examination of this issue). The argument could also be made that detrital matter, including small particles sloughed off from living cells, flocs of extracellular polymers, and broken bits of dead cells, are as much a part of the backscattering signal of phytoplankton *in situ* as in cultures, and that trying to remove the signal of these particles from measurements of cultures would produce results that were less applicable to interpretations of *in situ* data.

A final explanation for the positive relationship between cell size and backscattering ratio may be that the complex composition and internal structure of phytoplankton cells trump simplistic model interpretations of the way that light interacts with these particles. Our *a priori* assumption that "all else is equal" between two phytoplankton cells, aside from their size, may not apply to interpretations of their backscattering properties.

3.4.3 Comparison to other measured and modeled values and spectral shapes of phytoplankton IOPs

Optical cross-sections are a useful parameter for comparing the spectral optical properties of phytoplankton cells because the effect of concentration is removed and spectral shape can be examined. We found that the backscattering cross section ranged

from 1.16×10^{-12} m^2 cell^{-1} to 1.23×10^{-9} m^2 cell^{-1} at 442 nm (Table 1). We compared our results with the most recently published review on the inherent optical properties of phytoplankton cells (Stramski et al., 2001), and found agreement between absorption and scattering cross-sections (Figure 3.14A,B). In contrast, for the backscattering cross-section and backscattering ratio, we observed values up to one and two orders of magnitude higher, respectively, than previous work (Stramski et al. 2001) (Figure 3.14 C, D). However, these discrepancies between the backscattering magnitudes were not unexpected. The backscattering data from Stramski et al. (2001) were model results, and as discussed previously, the Mie model severely underestimates backscattering for non-spherical particles (Quirantes and Bernard, 2004; Clavano et al., 2007). It is also likely that the inhomogeneity of phytoplankton cells (i.e. the presence of cell walls and organelles) increases backscattering more than can be explained by the most commonly used models (Meyer, 1979; Hunt et al., 1989; Kitchen and Zaneveld, 1992; Volten et al. 1998). The same rationale can be used to explain the higher backscattering ratios in our results compared to previous model results (Figure 3.13D).

There is a longstanding, unresolved mystery among bio-optical oceanographers referred to as the "backscattering enigma" (Stramski et al., 2004). In making budgets for light scattering in the open ocean in non-bloom conditions, previous estimates were unable to account for a large portion of backscattered light. I.e., more light was backscattered from the ocean surface up to remote sensors than could be accounted for in theoretical models (Morel and Ahn, 1991; Stramski and Kiefer, 1991). Many researchers invoked the presence of small detrital particles that could not be physically discriminated from other oceanic particles as the source of the "missing backscattering" (Morel and Ahn, 1991; Stramski and Kiefer, 1991; Hout et al., 2008). Model efforts using non-spherical particles (Clavano et. al., 2007) or layered spheres (Kitchen and Zaneveld, 1992) have provided some basis for the argument that phytoplankton cells could realistically be a source of higher backscattering than previously thought, but the paucity of measurements of phytoplankton backscattering had left the "enigma" as an open question. Our results, some of the first of their kind, demonstrate that phytoplankton cells have significant backscattering efficiencies, likely owing to their

complex cellular compositions and morphologies. This finding suggests that we no longer have to make the assumption that very small (O. <1μm) particles, that we can't detect or measure specifically, must be present in order to close a backscattering budget for particles in the ocean.

3.5 Conclusions

The objective of this study was to examine the contribution of phytoplankton size, shape, and morphology to variability in backscattering. To this end we measured the VSF and the absorption and attenuation coefficients at several wavelengths for thirteen phytoplankton species (a total of fifteen strains). We also collected samples for chlorophyll concentration, and for cell counts and sizing via microscopy. Despite the fact that we took measurements at just six wavelengths, we were able to detect differences in the backscattering properties of the cultures, and relate these properties to differences in cellular structure and composition. We found that the spectral backscattering properties of phytoplankton deviate from theory at wavelengths where pigment absorption is significant. However, we were not able to detect the effect of cell size on the spectral shape of backscattering for cultures. Results also indicated that while particulate backscattering at 555 nm was well correlated to chlorophyll for any given species, the relationship was highly variable between species. This helps to explain why chlorophyll concentration is not a universal predictor of the magnitude of backscattering *in situ*.

The most significant finding in this work was that phytoplankton cells are a source of significant backscattering, in contrast to model predictions that are unable to account for the complex internal structure and morphology of phytoplankton cells, or their various cell coverings.

Table 1. Summary of phytoplankton characteristics. Optical data are shown at 442 nm.

Culture	Strain #	Algal Class	ESD [μm]	b_{bp}/b_p (HS6)	b_{bp}/b_p (ECO)	$\sigma_{bb\text{-}HS6}$	ξ	Shape
Ceratium longpipes~	*1170*	Dinophyceae	160*+, 55*-	0.0264	0.0281	1.23 x 10-09	4.20	
Chlorella #	*n/a*	Trebouxiophyceae	4.13	0.0079	0.0079	1.67 x 10-13	3.51	
Coscinodiscus radiatus~	*312*	Coscinodiscophyceae	94.06*	0.0290	0.0264	4.02 x 10-10	4.52	
Coscinodiscus radiatus~	*310*	Coscinodiscophyceae	33.48	0.0240	0.0035	2.35 x 10-10	3.88	
Cryptomonas profunda #	*n/a*	Cryptophyceae	9.08	0.0131	0.0057	1.78 x 10-12	3.12	
Ditylum brightwelii~	*2227*	Coscinodiscophyceae	61*+, 52*-	0.0116	0.0135	1.75 x 10-11	3.80	
Dunaliella tertiolecta #	*n/a*	Chlorophyceae	6.88	0.0061	n/a	4.81 x 10-13	-2.95	
Gymnodinium simplex~	*419*	Dinophyceae	11.69	0.0210	0.0268	1.93 x 10-11	3.90	
Heterocapsa triquetra~	*440*	Dinophyceae	13.33	0.0195	0.0438	7.56 x 10-12	3.95	
Isochrysis galbana~	*1323*	Prymnesiophyceae	3.9	0.0047	0.0034	1.31 x 10-13	3.45	
Phaeodactylum tricornatum #	*n/a*	Bacillariophyceae	4.14	0.0035	n/a	8.60 x 10-14	3.35	
Thalassiosira pseudonana^	*709*	Coscinodiscophyceae	4.2	0.0055	n/a	1.49 x 10-13	3.49	
Thalassiosira psuedonana~	*1010*	Coscinodiscophyceae	13.93	0.0096	0.0128	1.95 x 10-12	-1.35	
Thalassiosira rotula~	*1018*	Coscinodiscophyceae	16.65	0.0246	0.0274	1.53 x 10-11	3.97	
Thalassiosira weissflogii #	*n/a*	Coscinodiscophyceae	10.64	0.0105	0.0014	1.16 x 10-12	-6.04	

~CCMP - Center for Culturing of Marine Phytoplankton, Bigelow Laboratory, West Boothbay Harbor, ME

^NEPCC - North East Pacific Culture Collection from the Canadian Center for the Culture of Microorganisms

#Source unknown

*Size measured using light microscopy. +Size includes spines. -Size excludes spines.
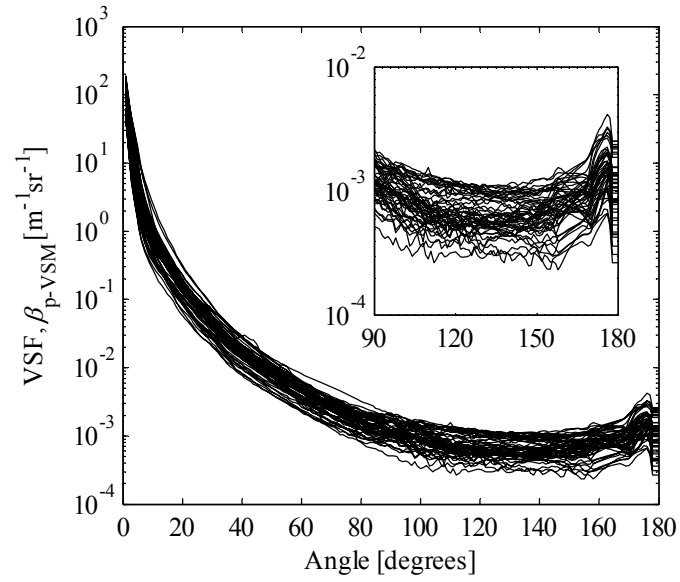
Figure 3.1. Volume scattering functions for thirteen phytoplankton monocultures at six wavelengths. The inset shows the backward portion of the VSF only.
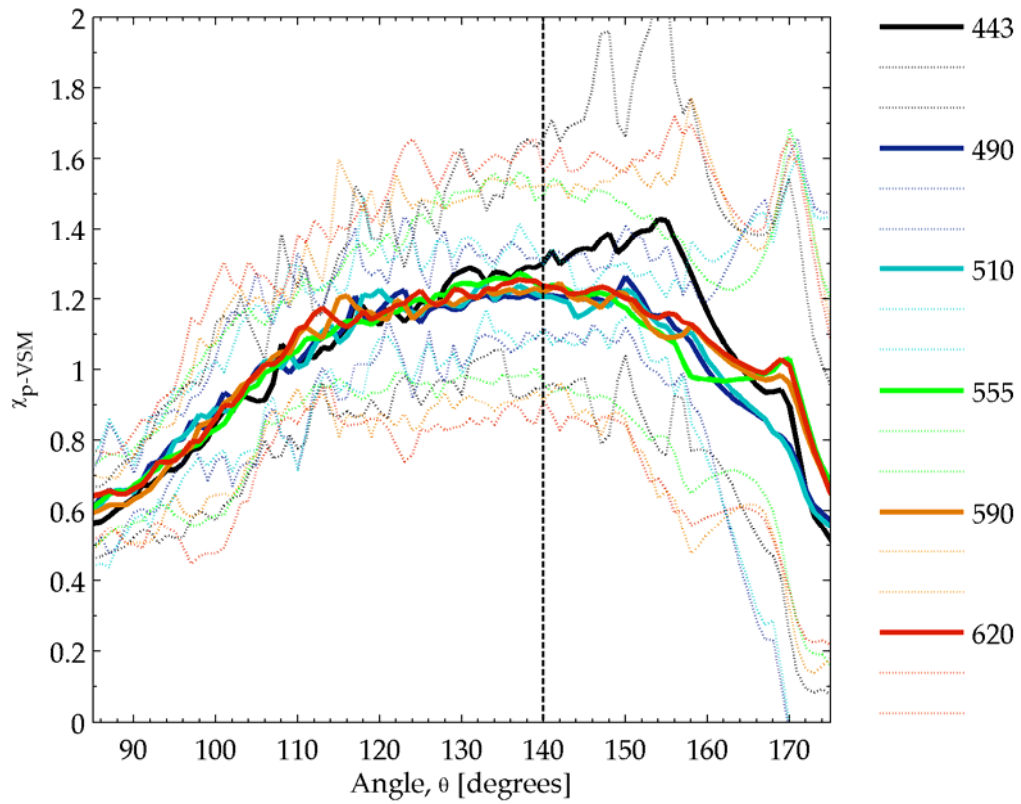
Figure 3.2. Angular variation in mean χ_p for phytoplankton cultures. Six wavelengths are shown for this study. The mean value for all species sampled is shown for each wavelength (bold lines), along with 95% confidence intervals (dotted lines). Not all wavelengths were available for all species. N=11 at 443nm, N=5 at 490 nm, N=5 at 510 nm, N=15 at 555 nm, N=9 at 590 nm, and N=11 at 620 nm. Dashed vertical line indicates the measurement angle of the Hydroscat-6 instrument.

Table 2. Average value and relative standard deviation of χ_p for thirteen phytoplankton species from 90 to 170 degrees at six wavelegnths. N is the number of cultures available to calculate the mean and standard deviation.

	N	θ								
		90	100	110	120	130	140	150	160	170
χ_p (442nm)	11	0.64	0.85	1.01	1.13	1.28	1.30	1.35	1.16	0.90
σ (442nm), %		9.11	16.71	11.60	11.06	14.01	14.00	11.76	17.18	36.77
χ_p (490nm)	5	0.65	0.89	1.02	1.17	1.17	1.21	1.26	1.00	0.79
σ (490nm), %		4.36	8.37	15.39	5.12	7.22	3.83	5.87	9.91	53.54
χ_p (510nm)	5	0.65	0.89	1.01	1.23	1.18	1.21	1.23	1.03	0.77
σ (510nm), %		5.84	7.72	14.72	5.69	8.26	3.89	3.23	13.97	51.93
χ_p (555nm)	15	0.67	0.83	1.05	1.14	1.24	1.23	1.17	0.97	1.03
σ (555nm), %		7.90	14.89	7.81	9.42	10.64	11.12	12.87	14.77	32.38
χ_p (590nm)	9	0.63	0.86	1.10	1.14	1.20	1.22	1.22	1.08	0.96
σ (590nm), %		10.11	12.78	7.04	11.81	12.07	12.77	14.93	25.81	34.10
χ_p (620nm)	11	0.66	0.86	1.11	1.16	1.22	1.24	1.20	1.08	1.01
σ (620nm), %		12.32	22.86	12.31	13.13	15.98	13.39	15.20	23.59	32.55
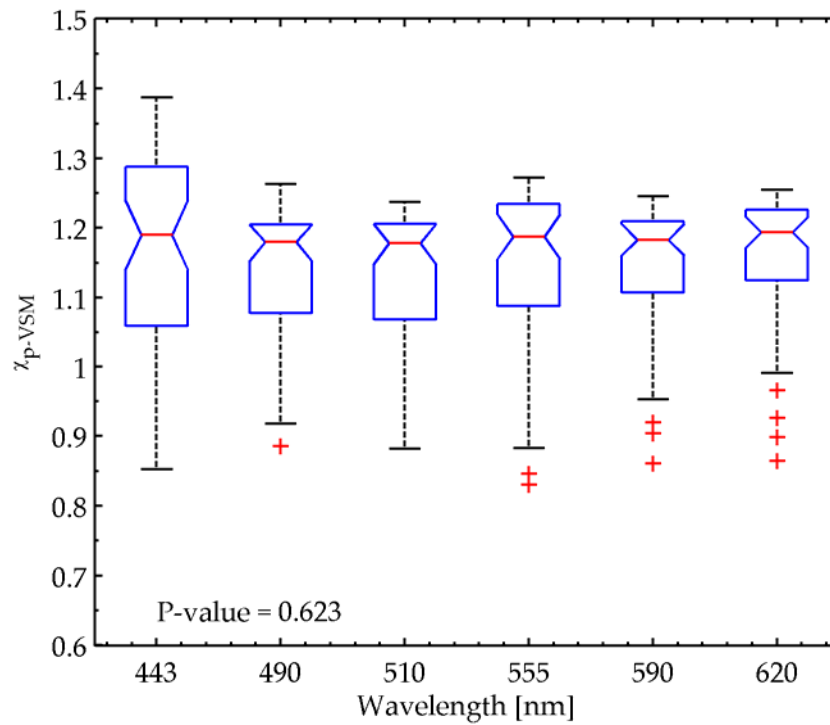
Figure 3.3. Box plot of results from a one-way analysis of variance between the means of χ_p at six wavelengths. The p-value above 0.05 indicates that the medians are not significantly different. The red lines are the medians at each wavelength. The notches indicate the 95% confidence limits. The dashed black lines indicate the range of χ_p at each wavelength, and the red plus symbols are outliers.
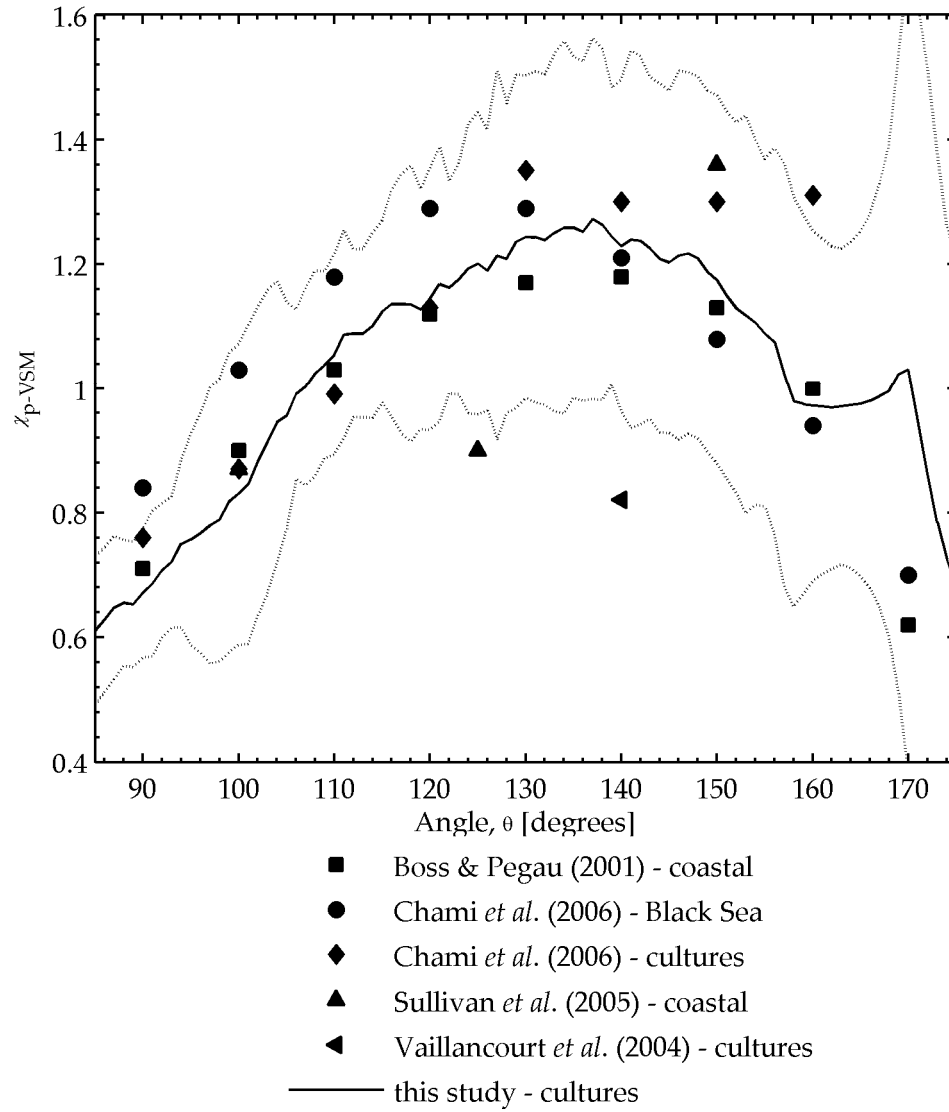
Figure 3.4. Angular variation in mean χ_p for coastal ocean particles and phytoplankton cultures (see legend). χ_p at 555 nm is shown for this study (bold line) with 95% confidence intervals (dashed lines). The other wavelengths used were 532 nm for Boss and Pegau (2001), 550 nm for Chami et al. (2006), 532 nm for Sullivan et al. (2005), and 514 nm for Vaillancourt et al. (2004).
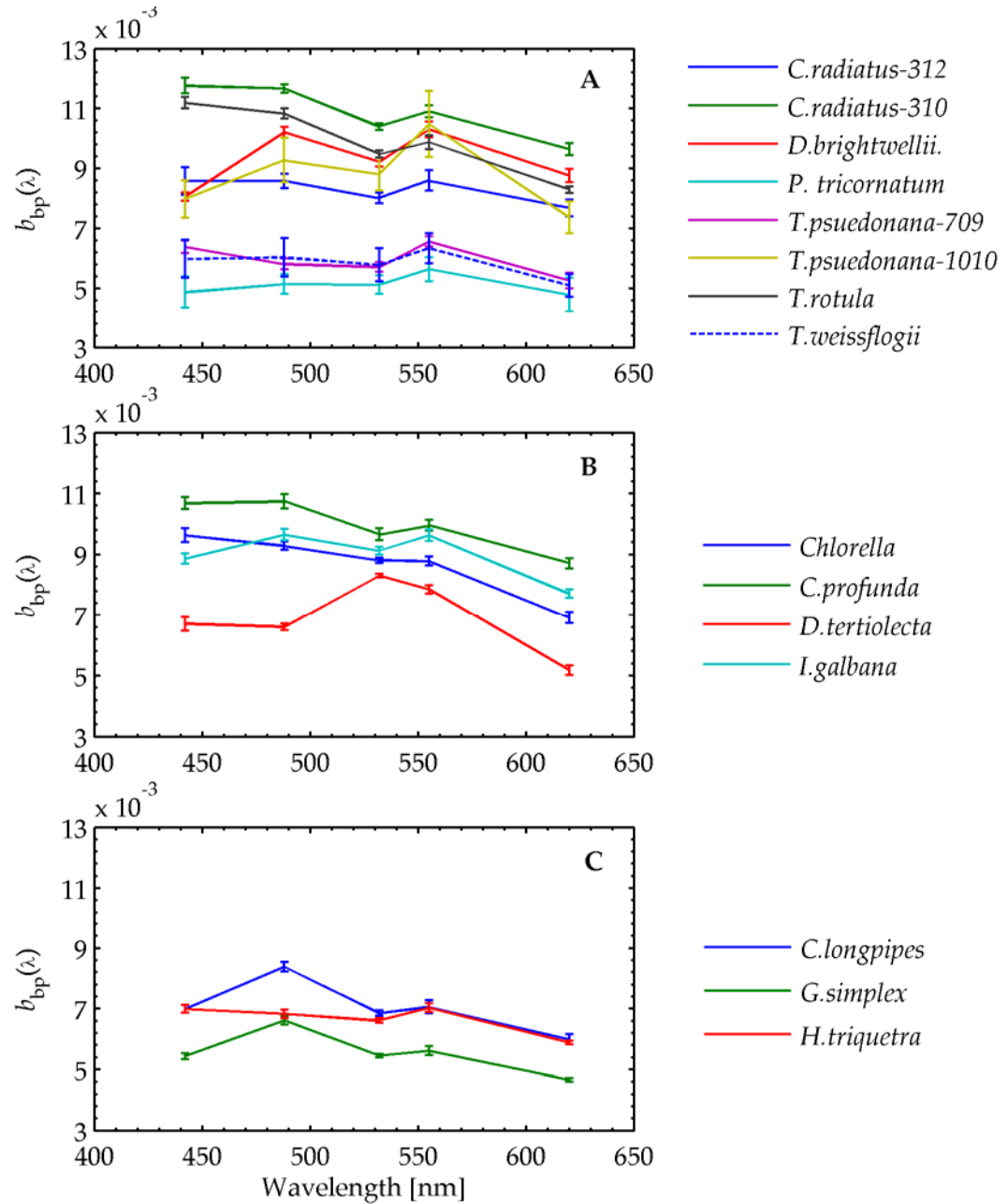
Figure 3.5. Spectral backscattering coefficients for fifteen phytoplankton species. Error bars represent one standard deviation. A) Diatom species sampled. Where more than one strain was sampled, the strain number is shown. B) Flagellates. C) Dinoflagellates.
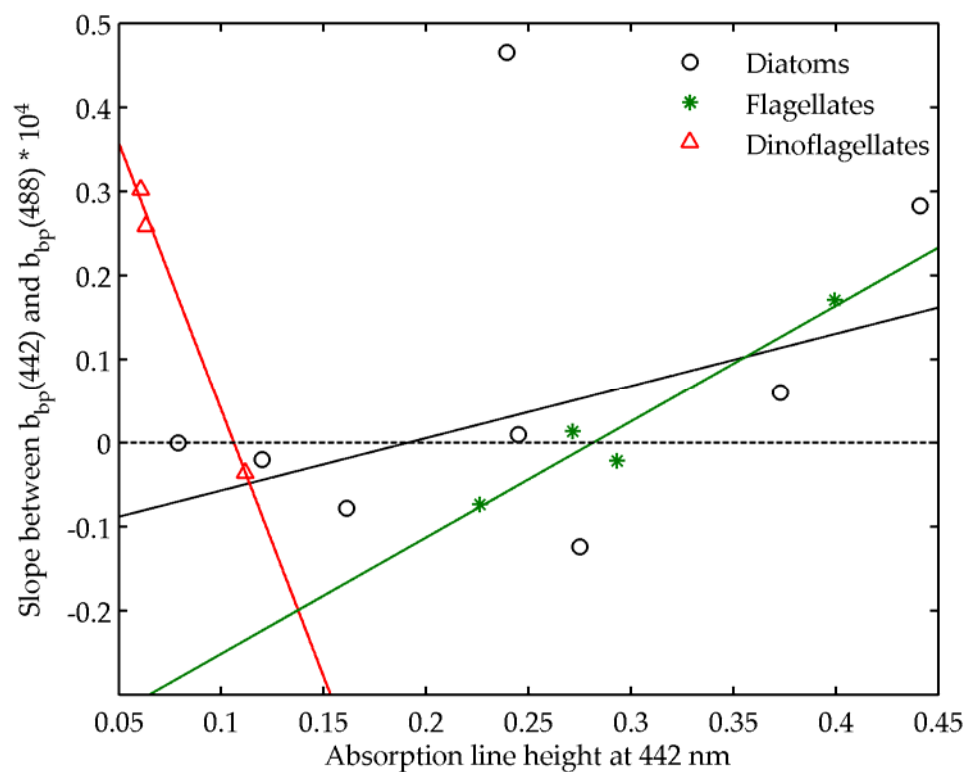
Figure 3.6. The slope of the backscattering spectrum between 442 and 488 nm (multiplied by 10,000) versus the absorption line height at 442 nm. Cultures are differentiated by taxonomic group, with diatoms ('o'), flagellates ('*'), and dinoflagellates ('Δ') identified. The linear least squares regressions for each taxonomic group are shown. The regression equations are: diatoms (black): $y = 0.62x - 0.12$, $R^2 = 0.25$; dinoflagellates (red): $y = -6.36x + 0.68$, $R^2 = 0.99$; flagellates (green): $y = 1.38x - 0.39$, $R^2 = 0.93$.
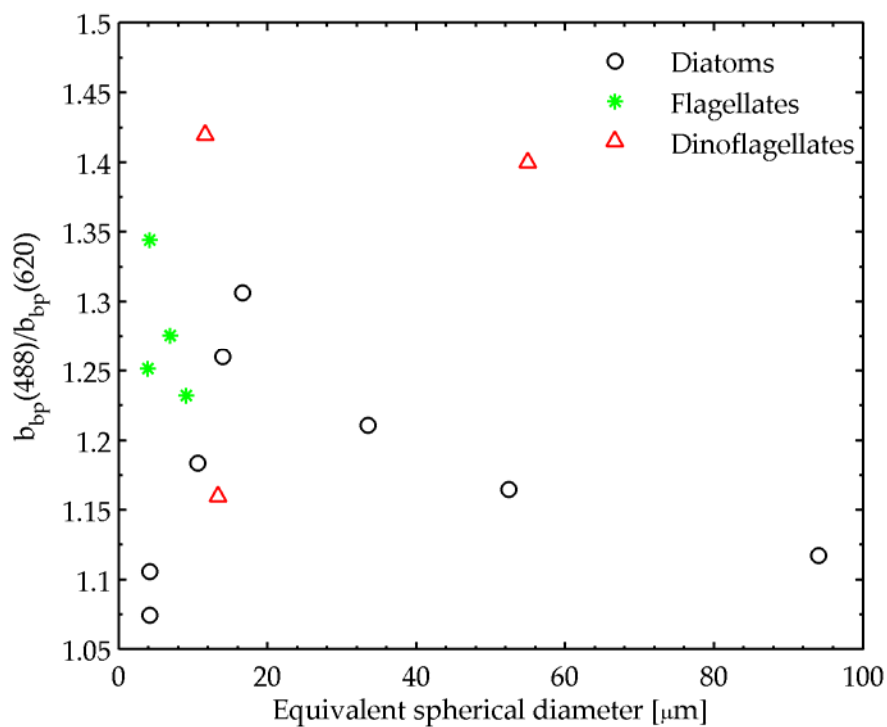
Figure 3.7. The ratio of backscattering at 448 nm and 620 nm versus equivalent spherical diameter of cultures as determined with a Coulter counter or microscopic analysis (see Table 1). Cultures are differentiated by taxonomic group, with diatoms ('o'), flagellates ('*'), and dinoflagellates ('Δ') identified.
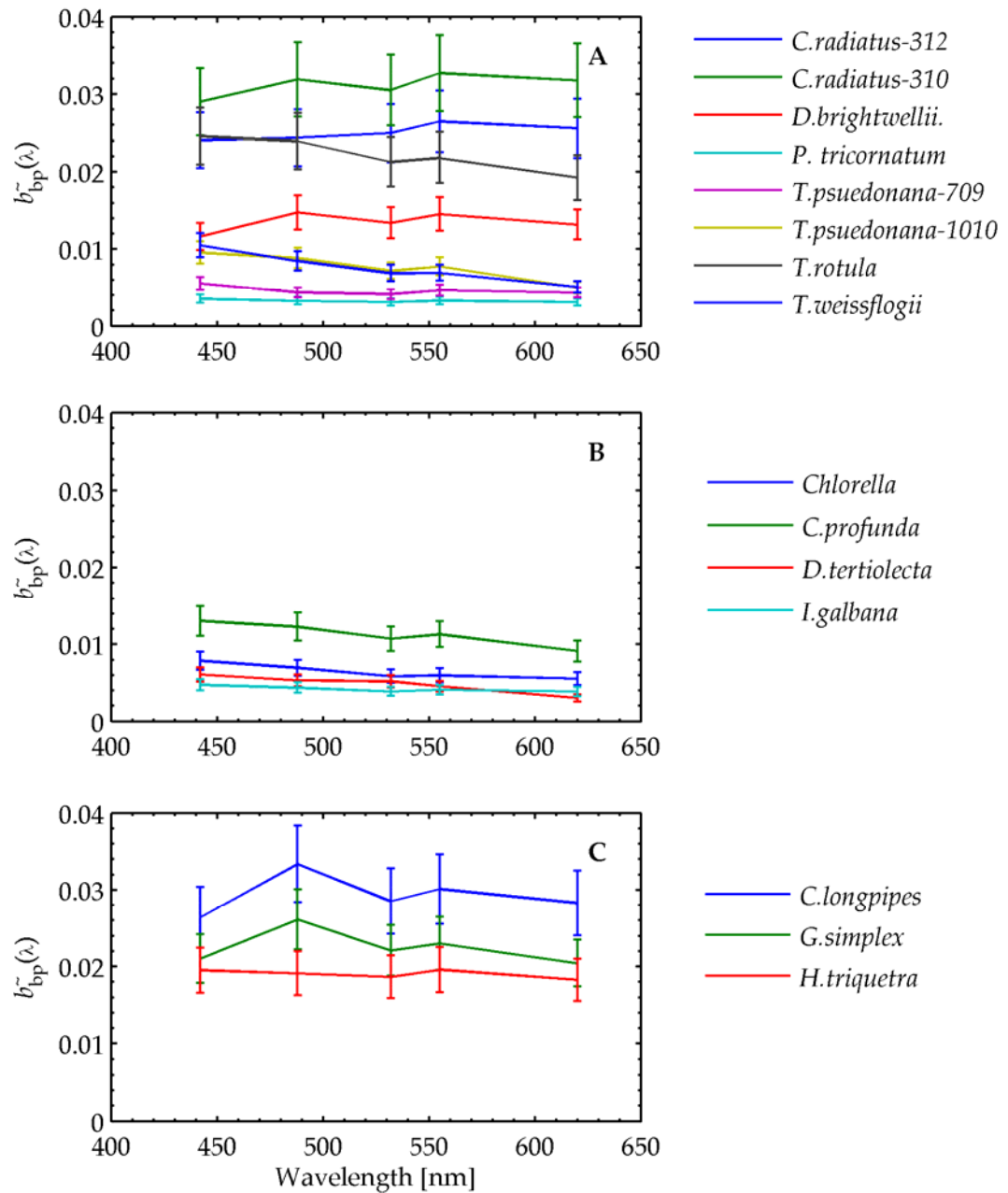
Figure 3.8. Spectral particulate backscattering ratios for fifteen phytoplankton cultures, separated into taxonomic groups. Error bars show 15% of the signal at each wavelength. A) Diatoms. Where more than one species was sampled, the strain number is shown B) Flagellates C) Dinoflagellates.
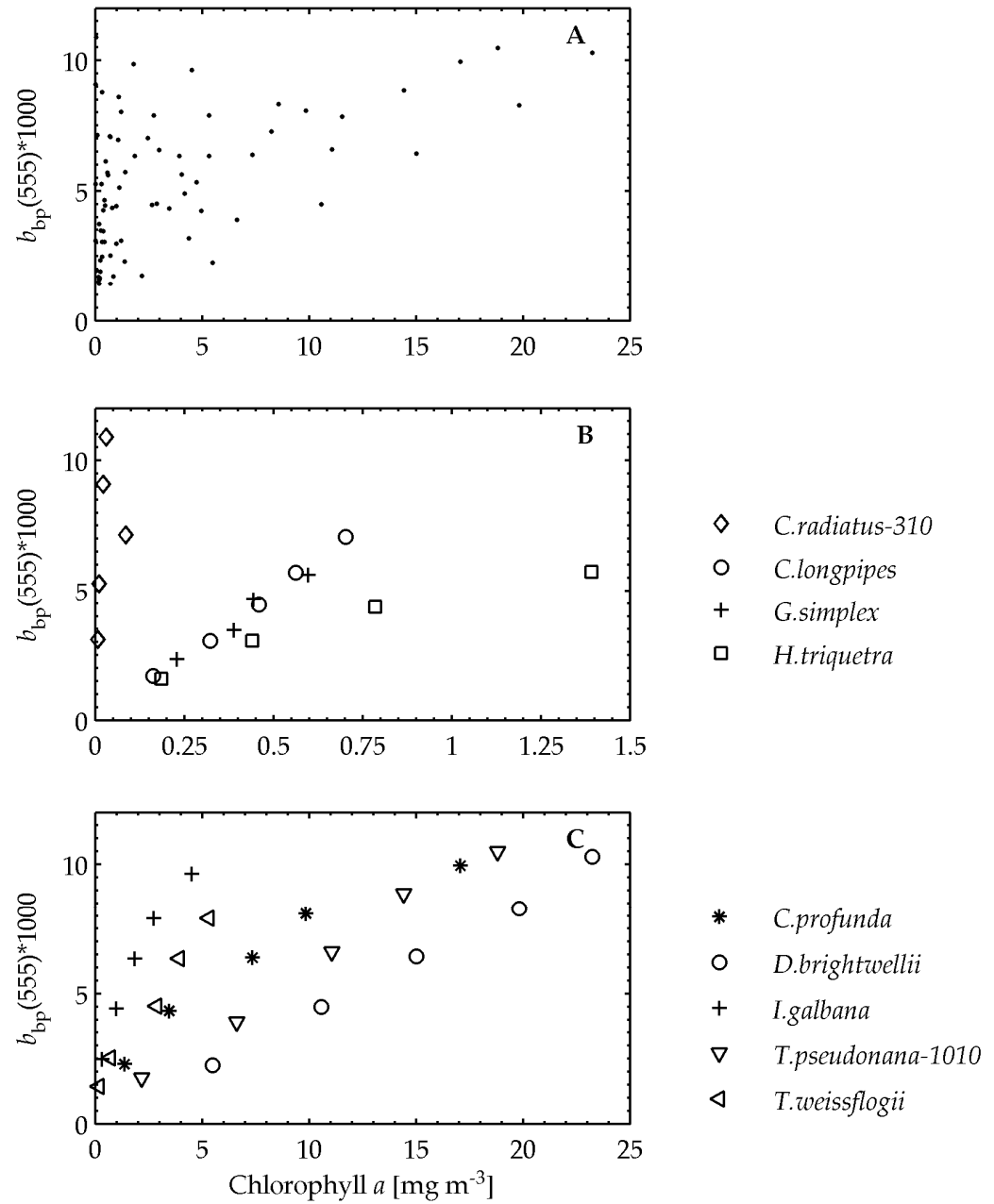
Figure 3.9. The backscattering coefficient at 555 nm * 1000 versus chlorophyll-a concentration. A) data for all cultures B) data for selected cultures with chlorophyll concentrations of less than 1.5 mg m^{-3}) data for selected cultures with chlorophyll conentrations up to 25 mg m^{-3}.
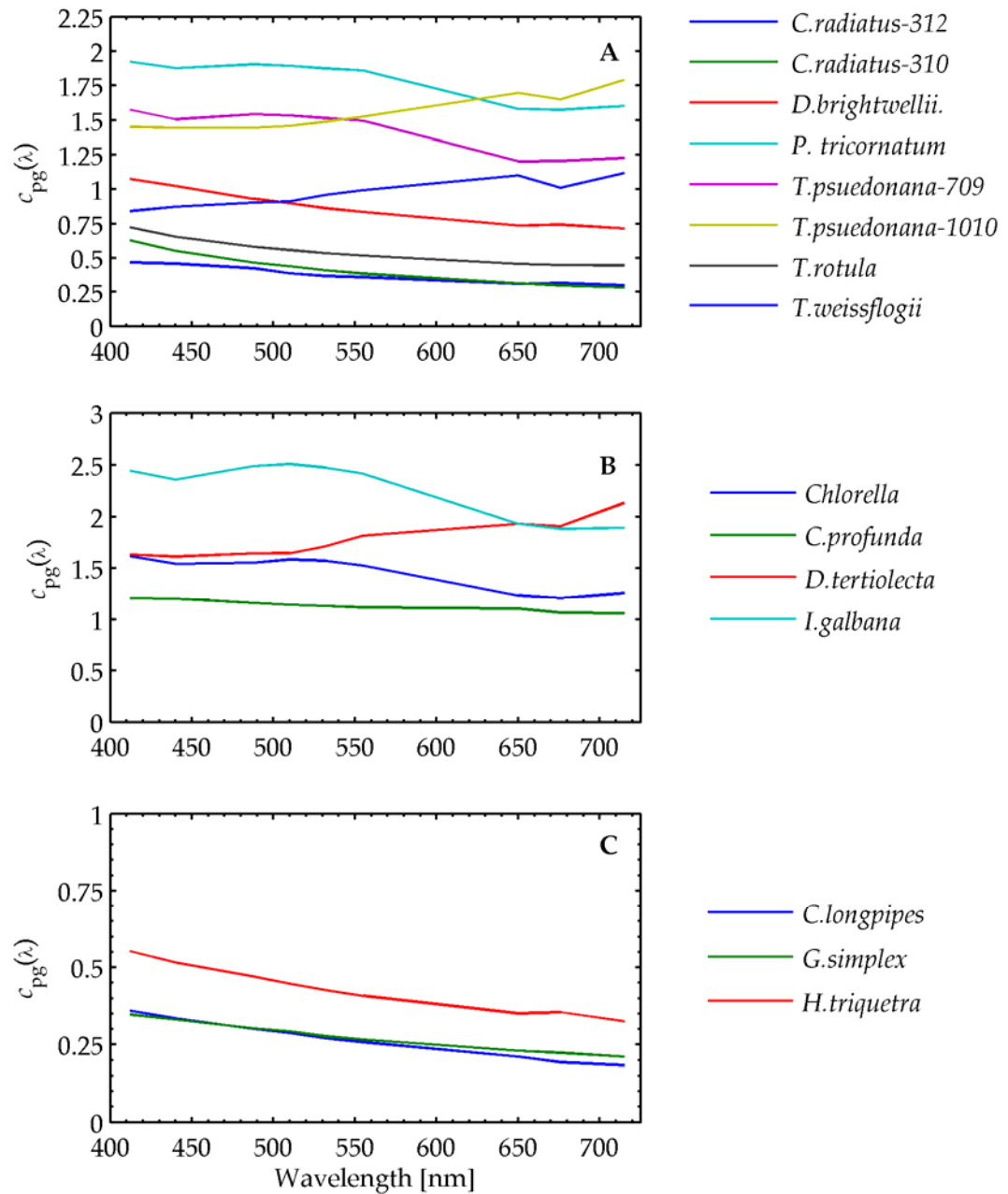
Figure 3.10. Spectral attenuation coefficients for fifteen phytoplankton cultures, separated into taxonomic groups. A) Diatom species sampled. Where more than one strain was sampled, the strain number is shown. B) Flagellates. C) Dinoflagellates.
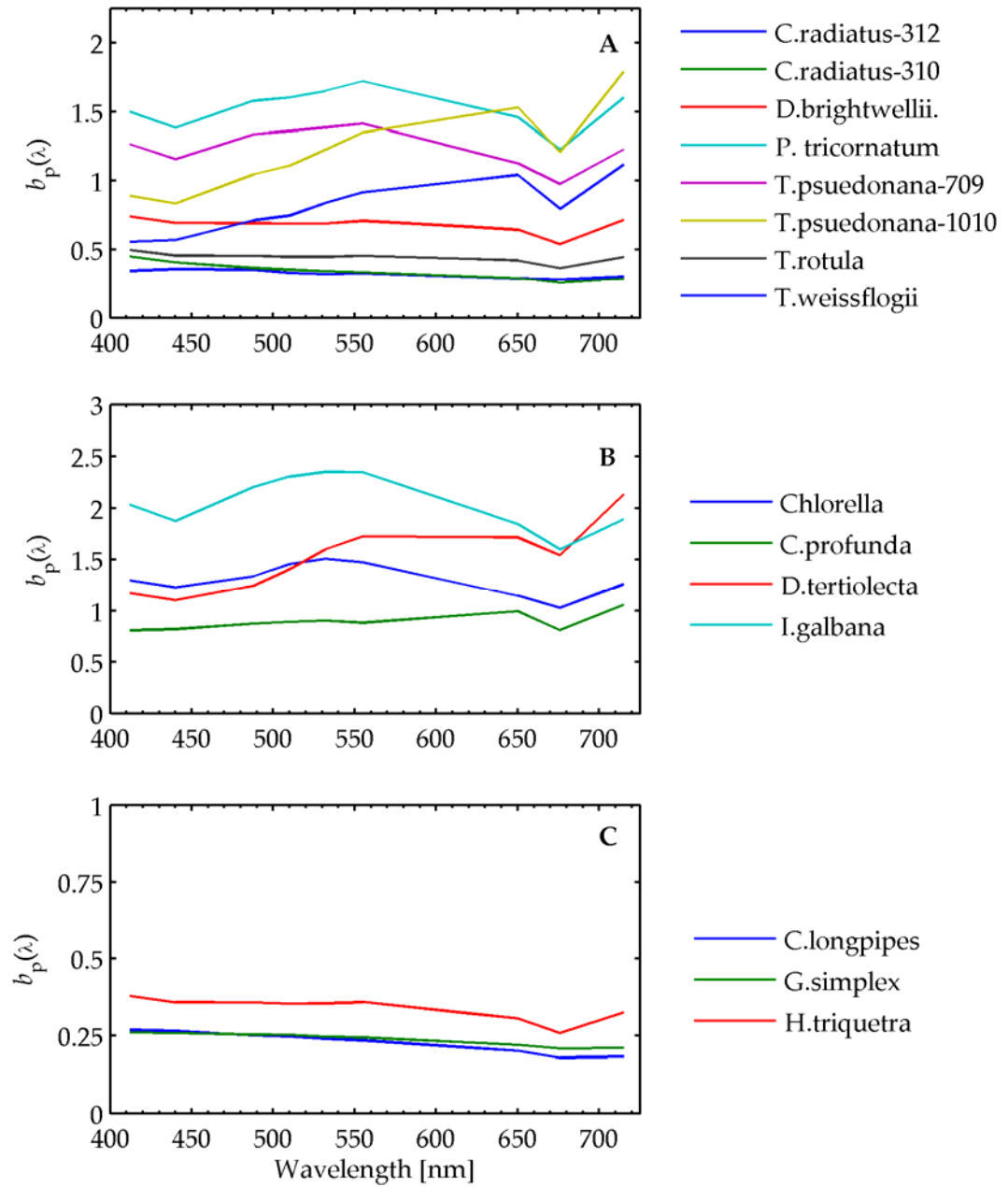
Figure 3.11. Spectral scattering coefficients for fifteen phytoplankton cultures. A) Diatom species sampled. Where more than one strain was sampled, the strain number is shown. B) Flagellates. C) Dinoflagellates.
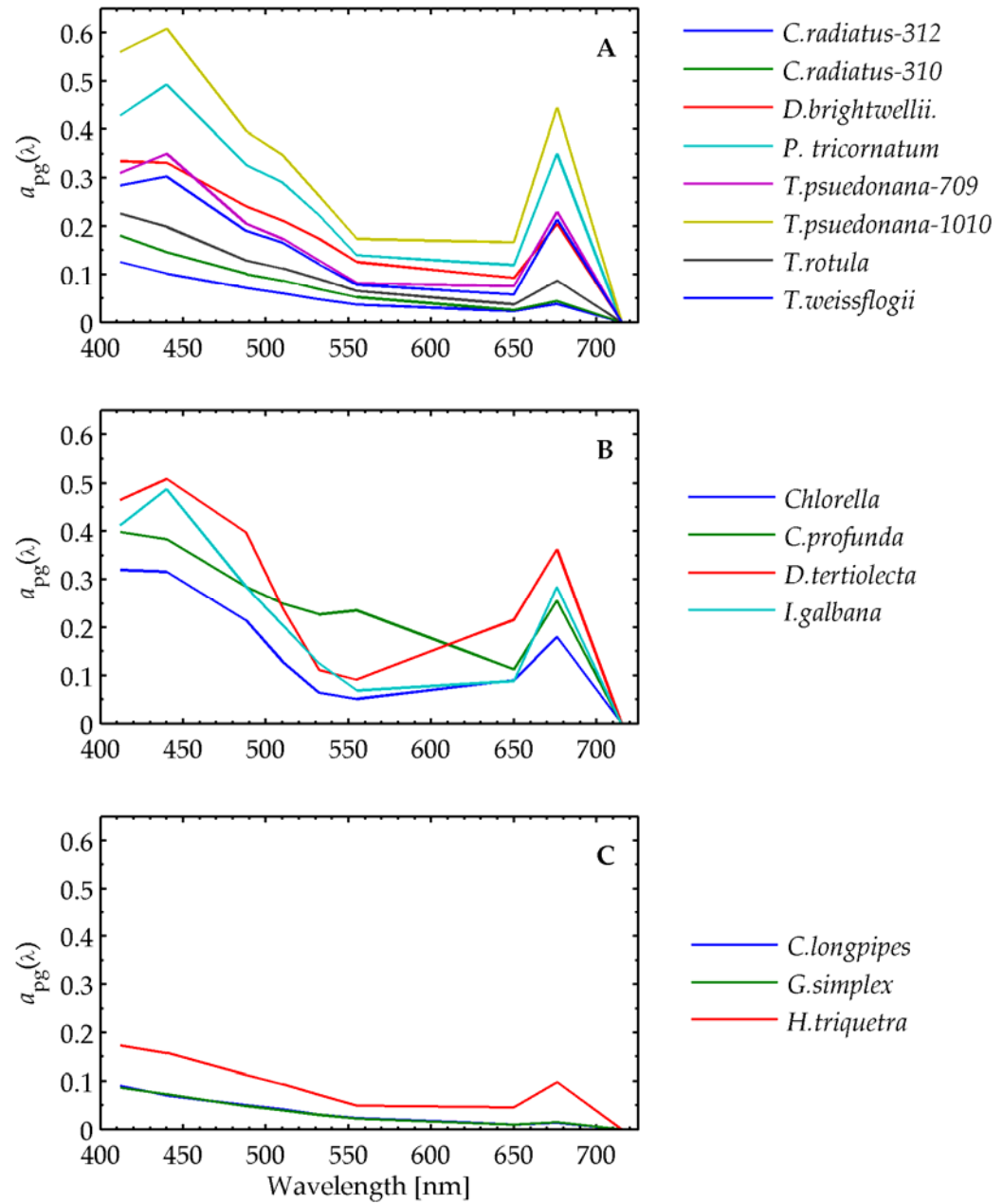
Figure 3.12. Spectral absorption coefficients for fifteen phytoplankton cultures separated into taxonomic groups. A) Diatom species sampled. Where more than one strain was sampled, the strain number is shown. B) Flagellates. C) Dinoflagellates.
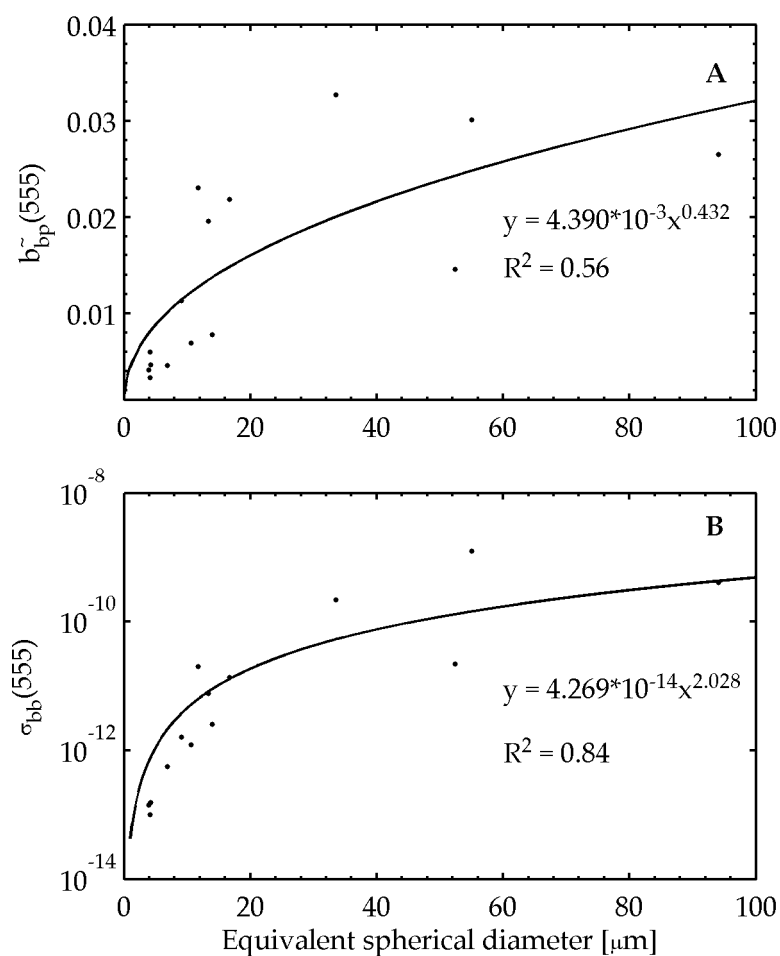
Figure 3.13.A) The particulate backscattering ratio at 555 nm versus the equivalent spherical diameter for phytoplankton cultures measured with a Coulter counter or light microscopy (see Table 3.1). B) The backscattering cross-section at 555 nm versus the equivalent spherical diameter for phytoplankton cultures. The equations for a power law fit and the R^2 of the fits are shown.
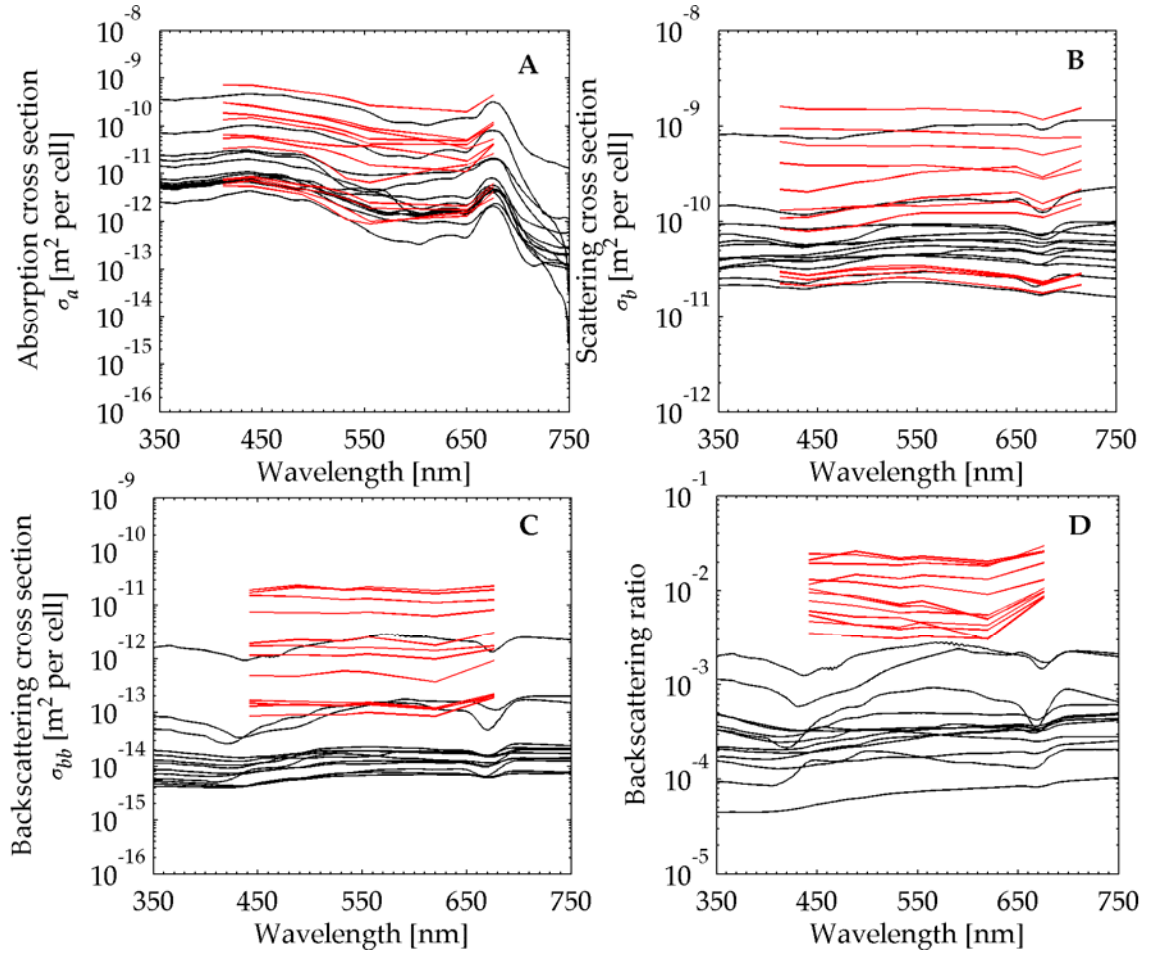
Figure 3.14. Spectral values of IOP cross-sections and backscattering ratios for cultures that were in the same size range as those shown by Stramski et. al. (2001). Red lines are our data, black lines are from Starmski et al. (2001). The absorption (A) and scattering cross-sections (B) from Stamski et. al. (2001) were based on measurements. The backscattering cross-section (C) and backscattering ratio (D) were model results in Stramski et al. (2001), and were measured in our study.

Chapter 4. Temporal changes in nearshore surface optical properties in relation to phytoplankton community structure in the Santa Barbara Channel

A.L. Whitmire, G. Chang, A.H. Barnard, and T.J. Cowles

4.1 Introduction

Under the increasing stresses that result from population growth along our coastlines, the nation's coastal ecosystems are faced with significant pollution, habitat destruction, and their effects. Improved understanding of coastal ocean dynamics and their effects on biology is essential for proper management of these productive areas. Observation and quantification of phytoplankton ecological processes are of particular interest in coastal environments because they form the foundation of the food web. However, research in coastal phytoplankton ecology can be difficult because physical, chemical, and biological processes in the coastal ocean are generally more dynamic and complex than in the open ocean. The temporal and spatial complexity of coastal ecosystems has been difficult to resolve using conventional sampling techniques.

A new generation of optical instrumentation now permits direct, *in situ* measurement of chlorophyll concentration, particle size distribution, particulate and dissolved absorption and attenuation, and several other parameters that were formerly obtained only through laboratory analyses of discrete samples. These measurement approaches are possible because a direct dependence exists between optical properties of natural waters and the concentration and nature of optically significant biogeochemical constituents (Morel and Prieur, 1977; Morel, 1988). These constituents include phytoplankton (Morel and Bricaud, 1981a; Morel and Bricaud 1981b; Stramski et al., 2001) and its co-varying material of biological origin (detritus or non-algal particles and colored dissolved organic material (CDOM); Bricaud et al., 1981; Bricaud and Stramski, 1990; Oubelkheir et al., 2004), lithogenic material from resuspension events, river flow, or Aeolian fallout (Stramski et al., 2004), and heterotrophic bacteria and flagellates (Morel and Bricaud, 1986).

This direct relationship between the optical properties of a water mass and its particle assemblage has fostered interest in the development of optical proxies for the characterization of marine particles. In contrast to recently developed instruments that measure inherent optical properties (IOPs; the absorption and attenuation coefficients, e.g.), chlorophyll fluorescence sensors have been in use for decades. There is now a

large body of literature on the subject of the theoretical relationships between IOPs and the chlorophyll-*a* concentration (Chl; Morel 1988; Stramski and Kiefer, 1991). Using these relationships, Chl has served as a proxy for certain optical properties of a water mass in order to characterize the underwater light environment and predict, for example, the euphotic zone depth (Morel, 1988). Some of the earliest research also focused on characterizing the nature and range of variability in the IOPs of phytoplankton cultures using benchtop equipment, with the aim of being able to identify or distinguish their signal from the bulk optical properties of seawater in discrete samples (water itself, biological and non-biological particles, and dissolved substances; Bricaud et al., 1983). The next logical step in the development of optical proxies for marine phytoplankton is to apply this rich body of theoretical and laboratory-based knowledge to observations obtained with recently developed *in situ* sensors (Sosik, *in press*).

Relationships between characteristics of the bulk oceanic particle population and some IOPs have already been developed. For example, the backscattering properties of the bulk particle population reveal information about particle size and index of refraction (Ulloa et al., 1994; Twardowski et al., 2001; Boss et al., 2004b). This information can be used in conjunction with other optical observations (absorption, attenuation, and fluorescence) to further characterize *in situ* particle populations and track their response to environmental forcing (Bergman et al. 2004). Hyperspectral absorption measurements (greater than 10 nm waveband resolution; Chang et al., 2004) have been used to deconvolve various components of the bulk absorption spectrum in discrete samples (phytoplankton, colored dissolved organic matter, and non-algal particles; Roesler et al., 1989). This same approach has been applied *in situ* with the use of a multi-spectral sensor with some success (Chang and Dickey, 1999; Schofield et al., 2004). In a different approach that utilizes spectral absorption, the combined use of a similarity index and fourth derivative analysis of the hyperspectral absorption coefficient has shown that certain phytoplankton species with a unique pigment (e.g. the dinoflagellate *Karenia brevis* with the pigment gyroxanthin-diester) can be identified in mixed cultures in the laboratory (Mille et al., 1997). It has also been demonstrated that information from combining IOPs and other variables (e.g. chlorophyll) derived from

inversions of remote sensing reflectance can be used to detect changes in phytoplankton community structure in a complex coastal environment (Cannizzaro et al., 2008). The implication from this previous body of research is that the most robust approach to developing optical proxies for phytoplankton groups should combine hyperspectral absorption and attenuation coefficient measurements with data from backscattering and chlorophyll sensors. Also, rather than relying on semi-constrained inversions from remote sensors, as in Cannizzaro et al. (2008), direct *in situ* measurements of IOPs and chlorophyll from observing systems that are already in place could offer a superior interpretation of coastal ocean phytoplankton dynamics in real time. The ultimate goal for this research is to be able to implement real-time IOP data inversion into quantitative descriptions of phytoplankton community structure.

As mentioned above, phytoplankton play a critical role in the functioning of marine ecosystems, and the potential for remote discrimination of dominant phytoplankton groups has profound applications in coastal monitoring. The Southern California coastal system exhibits many of the characteristics that are suited to monitoring with *in situ* observing systems. In particular, the Santa Barbara Channel is a physically and biogeochemically complex area that provides a wide variety of particle and species assemblages that would challenge and enhance optical proxy development. The Santa Barbara Channel (hereafter referred to simply as the Channel) is located off southern California, U.S.A., in the Southern California Bight (Figure 4.1). Sediment plumes are caused by river runoff or resuspension events, and are associated with winter storm activity. More than seventy percent of storm runoff in the Channel flows from the mouths of the Ventura and Santa Clara Rivers (Warrick, 2004). Primary production in the Channel is dependent on nutrients from storm runoff, seasonal upwelling, anthropogenic inputs, aerial fallout, and the relatively long periods of sunlight that are available in southern CA (Dailey et al., 1993). Diatoms and dinoflagellates are the two most abundant types of phytoplankton in the Channel (Hardy, 1993).

Harmful algal blooms (HABs) are also known to occur in the Channel. Bioluminescent red tides, dominated by the dinoflagellate *Lingulodinium polyedrum*, are commonly observed in the southern California coastal region (Sweeney, 1975;

Sournia, 1995). Although not proven toxic, these bioluminescent red tides can have deleterious effects on the local fauna. The senescence and sinking of these HABs in semi-enclosed basins can lead to biomass decay, resulting in hypoxia or anoxia and fish kills (Horner et al., 1997). A massive fish kill, after the decline of a *L. polyedrum* red tide, occurred in Ventura Harbor in October 2004 (Scheibe, 2003). Toxic diatom blooms of *Pseudo-nitzschia australis* are also common in southern California coastal waters, occurring most often during the late spring to early autumn months (May to October) when upwelling ceases or becomes sporadic. *P. australis* blooms oftentimes produce domoic acid and can poison zooplankton, fish, shellfish, seabirds, marine mammals, and humans *(*Price et al., 1991; Horner et al., 1997; Scholin et al., 1997). The increasing prevalence of harmful algal blooms provides even more impetus for establishing reliable methods of remote, real-time detection in coastal systems.

It was the goal of this work to investigate the relationships between particle characteristics and inherent optical properties and derived parameters for important phytoplankton taxa in the Santa Barbara Channel. Our objectives were to combine information from hyperspectral absorption deconvolution with other IOPs and chlorophyll fluorescence to develop indicators for dominant phytoplankton groups in the Santa Barbara Channel. We combine optical and hydrographic data collected from a mooring and from ship-based profiles with discrete samples to identify and monitor phytoplankton populations.

In section two we describe the methods used to collect discrete samples and optical data in the Santa Barbara Channel. In section three we develop the theoretical basis for linking particle characteristics and phytoplankton groups to specific optical properties and inversions of optical coefficients. We also describe in detail the development of the absorption deconvolution approach in conjunction with HPLC data, and how we modified previous approaches to address the specific objectives of this work. In the results section, we begin by establishing relationships between hydrography, chlorophyll, and common bio-optical parameters of absorption, attenuation and backscattering. We look at temporal variability with data from the mooring, and depth variability with data from vertical profiles. With these relationships

established for our research area, we then describe the results of the absorption deconvolution method and derived optical parameters of the particle size distribution slope and the backscattering ratio. In the discussion we highlight specific time periods of mooring data and discuss the relationships between individual components of the particle population and their effects on the bulk bio-optical properties in greater detail.

4.2 Methods

We used mooring and shipboard observations to establish the hydrographic context for our bio-optical characterization of the study area. We measured hyperspectral absorption and attenuation, chlorophyll fluorescence and the volume scattering function at three angles. We measured these parameters in order to derive the following parameters for use in this analysis: the absorption, scattering, attenuation, and backscattering coefficients, the particulate backscattering ratio, the particle size distribution slope, and the chlorophyll concentration. We also used an absorption deconvolution technique to estimate the relative abundances of five major particle populations in the Santa Barbara Channel. In order to assist with our interpretation of the absorption deconvolution, we first compared the results to an independent dataset collected off of the Oregon coast, and then applied the approach to data collected in the Channel. We describe the sampling methods used in Santa Barbara and the Oregon coast below.

4.2.1 In situ sampling – hydrography and optical properties

Hydrographic and optical data were collected from a mooring and a vessel in order to sample at different spatial and temporal scales. Time-series data were collected on the Santa Barbara CHAnnel Re-locatable Mooring (CHARM; Figures 4.1 and 4.2). The location of the CHARM is about 34°21'N, 119°28'W, approximately 1.5 km offshore of La Conchita, CA in 25 m water depth (Figure 4.1). The mooring was first deployed on May 19, 2003; mooring turnarounds are conducted every 3-4 months. Time

series of IOPs and apparent optical properties (AOPs) as well as ancillary physical and chemical data are collected on the CHARM (Chang et al. 2006, 2007). Instruments on the CHARM relevant to this study included: a hyperspectral absorption-attenuation meter (WET Labs, Inc. ac-s; 4 m water depth; ~4 nm resolution between 400 and 730 nm), a spectral backscattering meter (WET Labs, Inc. ECO-BB3; 4 m depth; $\lambda = 470$, 532, and 660 nm), a spectral fluorometer (WET Labs, Inc. ECO-FL3; 4 m depth; excitation and emission wavelengths for chlorophyll, phycoerythrin, and CDOM), and chlorophyll fluorometers (WET Labs, Inc. ECO-FL; at 10 and 22 m depths; Figure 4.1). In addition, data from temperature-conductivity sensors (Sea-Bird; 4, 10, 16, and 22 m water depths), and a bottom-mounted, uplooking acoustic Doppler current profiler (RDI) are available for complementary analyses (Figure 4.2). For most sensors, data were collected for 12 seconds every fifteen minutes, twenty-four hours a day. However, due to data storage limitations, data from the ac-s were collected for 12 seconds (at 8 samples per second) each hour. All mooring results shown in this analysis were based on hourly data.

We collected depth profiles of hydrologic and bio-optical properties from the research vessel R/V Point Sur on February 1 and May 6, 2006 in conjunction with mooring deployments and recoveries. Vertical profiles were collected within 500 meters of the mooring location. Measurements included temperature, salinity, chlorophyll fluorescence, hyperspectral absorption and attenuation, and multi-angle volume scattering (ECO-VSF; one wavelength, three angles). In the February deployment the conductivity sensor on the profiling package failed, so we merged the data from the profiling package with hydrographic data collected with the ship's CTD. The vertical resolution of the CTD data was not as fine as the profiling package, so data were binned to two meter depth bins. Data collected with the vertical profiler on the May 5th cruise were binned to 25 cm depth bins.

4.2.2 Optical methods – data processing

The ac-s on the profiling package was factory calibrated directly prior to the one-day field deployments, so additional clean water calibrations and drift corrections were not necessary. The ac-s on the CHARM was factory calibrated before and after deployment, and any drift was assumed to be linear over the course of the deployment. The data were corrected for temperature and salinity effects (Pegau et al., 1997; Sullivan et al. 2006), and the absorption coefficient was corrected for scattering using the proportional method (Zaneveld et al., 1994).

The particulate backscattering coefficient, b_{bp} at 440 nm, was estimated from the ECO-VSF instrument. We obtained raw values of the volume scattering function (VSF), $\beta(\theta)$, at 100, 125 and 150 degrees. We corrected raw volume scattering for absorption along the path length of the instruments using data obtained with the ac-s (scattering along the pathlength is already accounted for in the calibration of the instruments). We removed pure seawater volume scattering, $\beta_w(\theta)$ from $\beta(\theta)$ to obtain the volume scattering function for particles, $\beta_p(\theta)$, before converting to the backscattering coefficient (Boss and Pegau, 2001). We used estimates for $\beta_w(\theta)$ from Buiteveld et al. (1994) instead of Morel (1974; cf. Twardowski et al. 2007). In brief, Buiteveld used more robust empirical data to define the depolarization ratio of water molecules, which resulted in a more accurate parameterization of scattering by water molecules. Particulate volume scattering data from the ECO-VSF was converted to the backscattering coefficient by converting scattering measurements at three angles in the backward direction to scattering flux by multiplying by $2\pi\sin(\theta)$. Scattering flux at 180 degrees is zero, since $2\pi\sin(180)$ is equal to zero. We then fit a third-order polynomial to the scattering flux at the four angles (100, 125, 150, and 180), and then integrated from $\pi/2$ to π (90 to 180 degrees) to estimate the particulate backscattering coefficient.

4.2.3 Discrete measurements – collection and processing

Two datasets of field data were used in this study, one for development of the absorption deconvolution, and the second for model testing and interpretation. We first describe the independent discrete measurements that were used for model development. HPLC and particulate absorption measurements were collected off of the Oregon coast during August 2001 by Dr. Ricardo Letelier. For a full description of the hydrographic conditions during the sampling period, the reader is referred to Castelao and Barth (2005). Discrete sample collection methods and processing techniques are discussed in Eisner et al. (2005), but are reviewed briefly here. Water samples were collected from a tow-yo sled equipped with a pumping system that delivered water to a bench-top sampling system with in-line bio-optical and CTD sensors. Phytoplankton pigment concentrations were determined with HPLC (Wright and Jeffrey, 1997). Particulate absorption measurements were made using the quantitative filter technique, with subsequent non-algal particle absorption estimates conducted by the Kishino method (Kishino et al., 1985). All filterpad measurements were corrected by first removing the absorption of blank glass fiber filters and then by subtracting absorption at 750nm from all wavelengths. A correction factor for pathlength amplification (β) of 2 was used in this analysis (Roesler, 1998). Phytoplankton absorption ($a_\phi(\lambda)$)was obtained as the difference between particle absorption, $a_p(\lambda)$, and non-algal or detrital absorption, $a_{NAP}(\lambda)$. All particulate absorption spectra were smoothed with a 1-D Loess filter with a 15nm span to remove the effect of instrument noise (Schlax and Chelton, 1992).

The second set of discrete samples were collected as a means to ground-truth optical measurements collected in the Santa Barbara Channel in 2006. Phytoplankton pigments were analyzed at OSU with the same HPLC protocol as the Oregon Coast analyses. The HPLC data were also used as inputs into the CHEMTAX program to obtain estimates of phytoplankton community composition (Mackey et al.,1996). For these samples we used initial pigment ratios (the F_0 matrix) developed specifically for the Santa Barbara Channel (Anderson et al., 2008).

4.3 Inherent optical properties (IOP) theory

In order to obtain insight into particle properties or phytoplankton populations from *in situ* bio-optical data, we must build upon the theory that quantifies the relationship between the optical properties and particle characteristics. In this section we review the inherent optical properties and derived parameters that are relevant to this work. We begin with the beam attenuation coefficient, backscattering coefficient, and the backscattering ratio, and then discuss deconvolution of the hyperspectral absorption coefficient.

4.3.1 Beam attenuation, backscattering and the backscattering ratio

The beam attenuation coefficient describes the loss of photons over a discrete pathlength due to the additive removal processes of scattering and absorption. Beam transmissometers, which measure the beam attenuation coefficient, are now standard equipment on most research vessel CTD frames, as they provide a first-order proxy for the particle concentration *in situ*. Following the introduction of multi-spectral beam attenuation sensors over a decade ago, a robust empirical relationship has been established between the slope of the spectral beam attenuation coefficient and the particle size distribution in oceanic waters (Boss et al. 2001a, 2001b). The theory (Mie) behind this relationship assumes spherical, homogenous particles with a constant index of refraction. However, Boss et al. (2001a) found that absorption and shape effects had only a minor influence on the estimated attenuation slope.

The particulate attenuation spectrum is described by the following equation:

$$c_p(\lambda) = A\lambda^{-\gamma}$$

<div align="right">Eq. 1</div>

where γ is the "attenuation spectral slope" parameter, but is more often referred to as the "c_p slope." Higher γ indicates a steeper slope in the attenuation spectrum. A typical range in γ for oceanic particle assemblages is zero to two. Negative c_p slopes have been observed during blooms of large phytoplankton species (Sullivan et al., 2005). This is

the result of a shift from a power law to a Gaussian size distribution and the large mean size of the particle population relative to the wavelengths of impinging light.

The attenuation slope parameter is usually obtained from the particulate attenuation coefficient, c_p. We did not have measurements of dissolved attenuation, c_g, to remove from the c_{pg} measurements to obtain c_p. Therefore, we used the bulk attenuation coefficient for particulate and dissolved components, c_{pg}, to obtain the attenuation slope for this analysis. Recent work has shown that c_p and c_{pg} are highly correlated in coastal waters, and that the correction for c_g is simply the removal of small a linear offset from c_{pg} (Sullivan et al., 2005). This indicates that the retrieval of the attenuation slope parameter is not affected by the presence of c_g in the c_{pg} signal.

Oceanic particle size distributions (PSD) are commonly described by a differential power-law function:

$$N(D) = N_0 \left(\frac{D}{D_0} \right)^{-\xi}$$

Eq. 2

where ξ is the PSD slope parameter and D is the particle diameter. This relationship assumes a minimum diameter, D_{min}, of 0 microns, and a maximum, D_{max}, of infinity. Boss et al. (2001a) found that $D_{min} < 0.2\mu m$ and $D_{max} > 150$ μm were necessary when modeling the attenuation spectra of typical oceanic populations (i.e. c_p slopes of filtered or truncated size distributions may be erroneous). The attenuation spectral slope (γ) and the PSD slope (ξ) are related through a simple function derived from the application of Mie theory to hypothetical particle populations with varying PSD slopes:

$$\xi = \gamma + 3 - 0.5 \exp(-6\gamma)$$

Eq. 3

Typical oceanic size distributions and particle types produce a PSD slope from 2.5 to 5. Particle assemblages dominated by smaller particles will have a higher PSD slope, and vice versa.

In addition to the beam attenuation slope, the spectral particulate backscattering coefficient, $b_{bp}(\lambda)$, and backscattering ratio, $\tilde{b}_{bp}$, also provide information about particle properties. The backscattering coefficient is sensitive to particles in a smaller size range than the scattering coefficient, and thus provides additional and unique information

about particle properties and distributions (Boss et al., 2004a). There some indication that the backscattering coefficient can aid in the discrimination of phytoplankton taxa in inversions of remote sensing reflectance when it is combined with information on Chl in a well characterized coastal ecosystem (Cannizzaro et al., 2008). The backscattering ratio, the ratio of backward scattering to total scattering, provides a first-order estimation of the "hardness" of particles relative to water, with low observed values (0.005 – 0.01) in areas with high concentrations of phytoplankton (high water content, organic particles) and much higher values (>0.015) in areas with lithogenic particles (Aeolian fallout, resuspended sediments, etc.; Boss et al. 2004b; Whitmire et al., 2007).

4.3.2 The absorption coefficient and deconvolution

Chang et al. (2007) demonstrated that hydrographic and inherent optical properties could be used to distinguish between water masses with unique particle populations in the Santa Barbara Channel over weekly and monthly timescales. We extend this work by developing basic indicators for distinct phytoplankton groups and then combine this information with coincident IOP data to identify and track particle populations, four phytoplankton groups and non-algal particles, *in situ*. We did this by partitioning particulate absorption into absorption by four dominant phytoplankton groups and one non-algal component using the deconvolution technique discussed in Roesler et al. (1989) and Roesler and Perry (1995). Here we review the concepts behind the theory of absorption deconvolution.

The deconvolution technique utilizes non-negative linear least squares regression between total absorption measurements and input basis vectors. Roesler et al. (1989) developed the technique as a way to differentiate absorption by phytoplankton and colored detrital matter (dissolved and detrital fractions taken as a whole) on filterpad samples analyzed with a benchtop spectrophotometer. Chang and Dickey (1999) applied the technique to a moored multi-spectral absorption meter and were able to successfully differentiate between the dissolved and particulate absorption components at nine wavelengths . Schofield et al. (2004) refined the technique by

introducing basis vectors for three phytoplankton groups, and also applied the inversion to *in situ* absorption measurements rather than filterpad data. However, the methods of Chang and Dickey (1999) and Schofield et al. (2004) were constrained by the nine-wavelength absorption meter used in their studies, and Schofield et al. (2004) were ultimately unsuccessful in discriminating phytoplankton groups. We extended this previous work by using the hyperspectral (89 wavelengths) absorption data from the ac-s to test the inversion model in an optically complex coastal area.

The total absorption coefficient $a_t(\lambda)$ can be separated into additive components as follows (all quantities are spectrally dependant, but we omit (λ) for clarity):

$$a_t = a_w + a_\phi + a_{CDM} \qquad \text{Eq. 4}$$

where the subscripts "w", "ϕ", and "CDM" stand for water, phytoplankton, and colored detrital matter respectively. As such, the total absorption can be modeled by a combination of dimensionless basis vectors and wavelength independent optical weights as follows:

$$a_t = w_w \mathbf{a}_w + w_\phi \mathbf{a}_\phi + w_{CDM} \mathbf{a}_{CDM} \qquad \text{Eq. 5a}$$

Because the absorption properties of pure water are well characterized and are accounted for in the calibration of the ac-s instrument, we omit a_w from the model. If we consider the case of discretized phytoplankton groups, the equation becomes:

$$a_t = w_1 \mathbf{a}_{\text{phyto1}} + w_2 \mathbf{a}_{\text{phyto2}} + \ldots + w_n \mathbf{a}_{\text{phyto,n}} + w_{CDM} \mathbf{a}_{CDM} \qquad \text{Eq. 5b}$$

where $\mathbf{a}_{\text{phyto1}}$, $\mathbf{a}_{\text{phyto2}}$, …, $\mathbf{a}_{\text{phyto,n}}$ are the dimensionless absorption basis vectors for different phytoplankton groups, $\mathbf{a}_{CDM}$ is the basis vector for colored detrital matter, and w_1, w_2, … ,w_{CDM} are spectrally independent weighting factors derived from the total absorption deconvolution. The product of the weighting factor (w) and the spectrally dependent basis vector ($\mathbf{a}$) provides the individual component absorption.

Phytoplankton basis vectors are derived from hyperspectral absorption measurements of representative species from different phytoplankton groups, normalized to 676 nm (Figure 4.3). We considered four groups in this analysis. The phytoplankton groups are differentiated by their pigment composition as those

containing chlorophylls *a* and *c*, phycobilin, chlorophylls *a* and *b*, and peridinin respectively. Group 1 roughly corresponds to a broad community of "golden-brown algae" composed of diatoms, dinoflagellates, haptophytes and chrysophytes, and its basis vector is the normalized absorption spectrum from the diatom *Thalassiosira pseudonana*. Group 2 corresponds to cryptophytes (with a basis vector from *Chroomonas fragarioides*), and Group 3 to the "green algae," chlorophytes, prasinophytes, and euglenoids (Jeffrey and Vesk, 1997; basis vector from *Dunaliella bioculata*). The fourth group represents peridinin-containing phytoplankton, the dinoflagellates, and uses a basis vector derived from the absorption spectrum of *Prorocentrum micans*. Previous work used similar basis vectors for three groups of phytoplankton (Schofield et al., 2004), and we discuss the addition of the fourth group in the section 4.3.3.1.

Absorption by colored detrital matter, a_{CDM}, can be further separated into:

$$a_{CDM} = a_{CDOM} + a_{NAP} \qquad \text{Eq. 6}$$

where "*CDOM*" and "*NAP*" stand for colored dissolved organic matter and non-algal particles respectively (e.g. detrital particles and inorganic sediments). Roesler et al. (1989) and Roesler and Perry (1995) used a merged basis vector for $\mathbf{a}_{CDM}$ in their analyses, while Chang and Dickey (1999) and Schofield et al. (2004) used distinct basis vectors for CDOM and NAP. We consider each approach in detail in the next section. Both a_{CDOM} and a_{NAP} can be described by an exponential equation as a function of wavelength with the following form:

$$a_{NAP/CDOM}(\lambda) = Ae^{-S(\lambda-\lambda_o)} \qquad \text{Eq. 7}$$

where A is the absorption at a reference wavelength and S is the slope of the exponential function. S varies as a function of the composition and photo-oxidation state of the dissolved material (fulvics versus humics, e.g.; Bricaud et al. 1981; Twardowski and Donaghay, 2001). For oceanic and coastal waters, S_{CDOM} ranges from 0.011 to 0.019 respectively, and S_{NAP} ranges from 0.006 to 0.014 (Roesler et al, 1989).

4.3.3 Development of absorption deconvolution model

4.3.3.1 Phytoplankton basis vectors

As stated earlier, the most common bloom-forming phytoplankton in the Santa Barbara Channel are diatoms and dinoflagellates (Venrick, 1998). Both of these groups have been responsible for harmful algal blooms in the Channel in recent years (Anderson et al., 2008), so there is ample motivation for developing a technique to distinguish between them in real time. We built upon previous research in absorption deconvolution techniques and tested the effect of adding a fourth basis vector for peridinin-containing phytoplankton, the dinoflagellates (Roesler et al., 1989; Chang and Dickey, 1999; Schofield et al., 2004). We used phytoplankton absorption spectra (a_ϕ, derived from $a_p - a_{NAP}$) from Oregon coastal waters as input for Roesler's deconvolution approach as a 'best case scenario' test. This was the simplest case for testing how well we could deconvolve phytoplankton absorption, a_ϕ, into individual groups because, ideally, most of the non-algal component of absorption was removed by dissolution in hot methanol. To compare between the matching HPLC samples and deconvolution of absorption data, we used a simple scheme of "present or absent." For HPLC samples, any positive (zero) value of peridinin in the samples was considered a "dinoflagellates present (absent)" signal. Likewise, any positive (zero) optical weight, w_4, for Group 4 in the deconvolution results was considered a "dinoflagellates present (absent)." The inversion of bulk phytoplankton absorption identified the presence or absence of dinoflagellates in agreement with HPLC in over 83% of cases (N=109/131). Of the 22 inversion results that did not agree with HPLC, approximately 75% were false negatives, i.e. the inversion failed to identify dinoflagellates when peridinin was present in measurable concentrations by HPLC (N=13/22).

In the less idealized case of retrieving relative phytoplankton abundances from particulate absorption spectra, a_p, deconvolution results agreed with HPLC measurements in over 79% of cases (N=104/131). The inversion failed to identify dinoflagellates in 22 samples in which HPLC found detectable concentrations of perdinin, and falsely identified dinoflagellates in 5 samples when there were none

according to HPLC results. The erroneous retrievals were not correlated with depth, temperature, or salinity, which suggests that the erroneous results were not a consequence of photoadaptation or the physiological state of phytoplankton.

We used the correlation in dinoflagellate detection between absorption deconvolution and HPLC as a justification for adding a fourth basis vector (dinoflagellates) in our analysis of *in situ* hyperspectral absorption data from our profiles and the mooring.

4.3.3.2 Detritus and CDOM basis vectors

Having concluded that four phytoplankton basis vectors provided an improved estimate of phytoplankton group composition, we next investigated whether or not to treat the CDOM and NAP basis vectors as a single entity (CDM) as in Roesler et al. (1989) and Roesler and Perry (1995), or to treat them as distinct components as in Chang and Dickey (1999) and Schofield et al. (2004). Since the filterpad absorption data from Oregon coastal waters did not have coincident CDOM absorption, we used the *in situ* Santa Barbara Channel data to test the outcomes of separating vs. merging the two non-algal components.

We carried out absorption deconvolution on the same dataset for each of the two scenarios, and then estimated the absorption coefficient for each component of the deconvolution according to Equation 4, in which absorption at a given wavelength is the product of the wavelength-independent weighting factor (w_i, from the deconvolution) and the wavelength-dependent basis vector ($\mathbf{a}_{\text{phyto-i}}$, $\mathbf{a}_{\text{CDM}}$, $\mathbf{a}_{\text{NAP}}$, and $\mathbf{a}_{\text{CDOM}}$). We then compared phytoplankton group inversions from the two scenarios against each other by performing robust type-II linear regressions between scenarios for the estimated absorption coefficients from each component.

We first compared the outcomes for each of the four phytoplankton groups (Figure 4.4A-D), and for the sum of all groups (Figure 4.4E). We found that using a single CDM basis vector resulted in slightly lower representation by Group 1 and Group 3 phytoplankton, indicated by a regression slope of less than one (0.77 and 0.70

respectively; Figure 4.4A,C). The opposite case was observed for Group 2 and Group 4, which had regression slopes of 10.02 and 1.18 respectively (Figure 4.4.B,D). Group 2, which is generally in low abundance in these samples, was found in concentrations up to an order of magnitude higher in the inversion using a CDM basis vector compared to using both CDOM and NAP basis vectors, but was still low in concentration relative to the other groups. However, if you add up the absorption from all four groups and compare them between the two methods, the total magnitude of deconvolved phytoplankton absorption is nearly equivalent, with a regression slope of 1.06 (R^2 = 0.996; Figure 4.9E). Likewise, the unexplained errors of the deconvolution results (the model residuals) are equivalent for the NAP/CDOM and CDM inversions (data not shown). With the exception of Group 2, there was little difference in community structure between the two non-algal absorption schemes.

Recall from Equation 6 that the sum of absorption by CDOM and NAP should equal the absorption by CDM. We performed a robust type-II linear least squares regression between the sum of a_{NAP} and a_{CDOM} versus a_{CDM} to check this assumption. The regression had a slope of 1.03 (R^2 = 0.99; Figure 4.5B), therefore we concluded that the total quantity of the components, either the sum of a_{NAP} and a_{CDOM} or a_{CDM} alone, was not affected by the selection of one approach over the other. In other words, whether we used two basis vectors for non-algal components (NAP and CDOM) or a single basis vector (CDM), the estimated contribution of these components to the total absorption was the same.

We also examined how the non-algal absorption was partitioned when using the two basis vector approach, i.e. how much non-algal absorption was attributed to CDOM and how much to NAP. Deconvolution results indicated that a_{NAP} was three times as high as a_{CDOM}, with a regression slope of 0.37 (Figure 4.5A). However, non-algal absorption in the Santa Barbara Channel is generally dominated by CDOM, whereas a_{NAP} only accounts for 10% of total non-algal absorption (Toole and Siegel, 2001; Kostadinov et al. 2007). While it is possible that our shallow sampling site and close proximity to shore increased the percentage of NAP present relative to CDOM in our samples, it is more likely that the similar spectral shape of these two basis vectors, both

exponential functions with similar slopes, were not well distinguished by the inversion. Therefore, we opted for a conservative approach and used a single a_{CDM} basis vector in this analysis.

4.4 Results

4.4.1 Hydrographic and inherent optical property time-series

We have time-series data from two mooring deployments in the Santa Barbara Channel. The first deployment occurred on February 1, 2006. Unfortunately, the data logger failed after 27 hours of deployment, so we only present results from a single day for that deployment (Figure 4.6). Due to this shortened sampling period, we present temperature, salinity, chlorophyll, and backscattering data at their full sampling resolution (every fifteen minutes) instead of restricting analysis to the hourly sampling rate of the ac-s. Over the 24-hour period beginning on the morning of February 1, temperature and salinity displayed variability of only 0.4 degrees and 0.05 respecitvely at the depth of the bio-optical package (4 meters). The hydrography was typical of winter-time conditions in the Channel, with low temperatures (around 13.5 degrees Celsius) and relatively high salinity (>33.35). The water mass was hydrographically similar to what Chang et al. (2006) identify as "Water Mass 1" in CHARM data collected from 12-20 February 2004. The chlorophyll concentration ranged from 1.9 to 5.3 mg m^{-3}. The inherent optical properties were generally low for coastal Channel waters, with beam attenuation at 650 nm ranging from 0.51 to 0.90 m^{-1}, and the particulate backscattering coefficient at 650 nm from 0.0079 to 0.0163 m^{-1} (Chang et al., 2006). While there appeared to be a shift in the nature of the particle population around year day 33.2, as indicated by increased beam attenuation and backscattering, there was no indication in the T/S data that a different water mass had advected into the area (Figure 4.7A). The absorption coefficient at 676 nm, $a_{pg}(676)$, is strongly linked to concentration of chlorophyll-a, since little else absorbs in that region of the spectrum. Chlorophyll-a fluorescence and $a_{pg}(676)$ should significantly co-vary, unless non-photochemical quenching caused by high light levels suppresses chlorophyll

fluorescence. Over the course of the day, $a_{pg}(676)$ was highly correlated to the chlorophyll concentration (r=0.75, p<0.0010), which suggests that phytoplankton populations were not photoinhibited over this time period. Beam attenuation was also correlated to Chl (r=0.57, p=0.0017), but the backscattering coefficient was only weakly correlated with Chl (r=0.39, p=0.0436).

The May 2006 deployment provided approximately eighteen days of data that were not contaminated by biofouling. There is a six-day period, from year day 135 to year day 141, during which the ac-s data were not archived by the data logger. All other data were collected without incident. The sampling period was without measurable precipitation except on May 22 and May 23 (year days 142 and 143), when up to an inch of rain was measured at rain stations throughout the watershed of the Ventura and Santa Clara Rivers (http://www.cnrfc.noaa.gov/). Likewise, river flow into the sampling region was low except for the short period of rain at the end of the time-series.

In the absence of rain, variability in temperature and salinity in the Channel is primarily driven by local forcing (solar heating and evaporation), episodic upwelling, and along-Channel pressure gradients (Otero and Siegel, 2004). The time period before the rain event was characterized by salinity of 33.5 for days 126 through 138. The salinity fluctuates from 33.45 − 33.55 until year day 144. Temperature displayed an increasing trend from 14°C to almost 18°C, marked with higher frequency 1°C excursions, likely due to solar heating and tidal mixing (Figure 4.8A).

Chlorophyll concentrations were mostly below 5 mg m^{-3}, with periods of higher, temporally dynamic values occurring before year day 130 and after year day 138 (Figure 4.8B, green). There were intense, short duration pulses of chlorophyll coincident with low temperature water, high beam attenuation, and high absorption. The backscattering coefficient at 650 nm followed the same general trends as Chl, but often decoupled from the Chl signal at short (hourly) timescales. It ranged from 0.0035 m^{-1} to a maximum of 0.0255 m^{-1}, and was significantly correlated with chlorophyll over the sampling period (r=0.50, p<0.0010). Temporal variability in the backscattering and beam attenuation coefficients were also significantly correlated over the sampling period before the ac-s data stream was interupted (r=0.53, p<0.0010).

On year day 139 we observed a decline in salinity from 33.55 to 33.41 that lasted for approximately 36 hours. As there was no measurable rain during this period, we attribute these changes to advection of a slightly different water mass by the mooring location (Figure 4.7B). The backscattering coefficient and Chl both increased slightly before the advection of this feature, and remained elevated for the duration of this feature at the mooring. Absorption and attenuation data were not available during this period.

In order to interpret these temporal changes in Chl, backscattering, attenuation, and absorption in a more meaningful way, we conducted vertical profiles of hydrographic and bio-optical properties during the mooring deployments in February and May 2006. We also collected discrete samples in order to identify and characterize the particles and pigment characteristics that were driving the changes in *in situ* parameters. We discuss these profiles in the following section.

4.4.2 Hydrographic and inherent optical property vertical profiles

Before interpreting the *in situ* absorption deconvolution results, it is important to characterize the relationships between bulk phytoplankton abundance (Chl), attenuation, and backscattering, and other derived parameters. There was clear co-variability between phytoplankton biomass (Chl) and the bio-optical parameters of beam attenuation (beam-c), backscattering, the backscattering ratio, and the PSD slope in May 2006 (Figure 4.9). There was an increase in particulate backscattering and beam-c associated with a chlorophyll maximum of nearly six mg m^{-3} at a depth of eight meters. There was also a clear decrease in the PSD slope from a background of four to a minimum of three within the chlorophyll maximum. This indicates that the PSD within the peak was skewed to larger particles, while above or below the peak the PSDs reflect assemblages with fewer large cells. The large cells in the chlorophyll maximum may have been dinoflagellates from the genus *Ceratium*, which was identified as the main genus responsible for a large, spatially variable red tide event that occurred throughout the Santa Barbara Channel during early May of 2006 (G. Chang, personal

communication). Concurrent with a decrease in the PSD slope was an increase in the backscattering ratio to almost 0.025, which is high for biological particles (Sullivan et al., 2005). The backscattering ratio had a very different vertical distribution than the backscattering coefficient and beam-c. While b_{bp} and beam-c increased in magnitude within the chlorophyll maximum and in a strong bottom boundary layer, the backscattering ratio slowly increased from 0.015 at the surface to 0.020 at 20 meters, with the exception of the increase in the chlorophyll peak.

Bio-optical properties were not as clearly associated with the chlorophyll signal in the vertical profile obtained in February 2006 (Figure 4.10). Chlorophyll concentrations were lower than in May, with a maximum of approximately 3.5 mg m^{-3} at seven meters and values near 2.5 mg m^{-3} below the 7 m peak, and then decreased below twelve meters. The chlorophyll gradients were located directly above weak but distinct density steps at 7 and 12 meters. The backscattering ratio was higher than in May throughout most of the water column, but in this case the backscattering ratio appeared to be co-varying with beam-c and the backscattering coefficient, and showed no relationship to the chlorophyll signal. It is possible that at the lower chlorophyll concentrations in February, lithogenic and detrital material dominated the scattering-based IOPs (the beam attenuation and backscattering coefficients) and had a strong influence on derived bulk particle properties (e.g., the PSD slope and backscattering ratio).

In order to shed more light on the nature of the particle populations that were driving these optical signals, we next discuss the application of hyperspectral absorption deconvolution to these data sets.

4.4.3 Comparison of optical properties and phytoplankton community structure: vertical profiles

We compared the phytoplankton community structure derived from the deconvolution results from vertical profiles of absorption with the community structure derived from CHEMTAX in an effort to ground-truth the deconvolution. As output

CHEMTAX provides, among other choices, the absolute concentration of chlorophyll-*a* attributable to each group in the model that, when summed, add up to the total chlorophyll-*a* signal. We used the chlorophyll-*a* associated with diatoms, cryptophytes, chlorophytes, and dinoflagellates to compare with the optical weights of Groups 1 through 4 respectively from the absorption deconvolution. To facilitate direct comparisons between CHEMTAX and deconvolution results, we calculated the percent contribution of each group to the sum of all groups for each method as follows:

$$\%Group_i = \frac{Group_i}{Group_1 + Group_2 + Group_3 + Group_4} * 100 \qquad \text{Eq.8}$$

where $Group_i$ was either the optical weight, w_i, or the chlorophyll-*a* concentration from CHEMTAX, for a Groups 1 through 4.

The sampling depths of the discrete measurements were limited to coincide with the depths of the moored sensors on CHARM, so we did not capture discrete samples from chlorophyll maxima that occurred between those sampling depths. For the February cruise, the discrete samples at four meters and 19.5 meters were both collected in low chlorophyll water (< 1.5 mg m^{-3}). The 10 meter sample was collected in water with a chlorophyll concentration of approximately 2.5 mg m^{-3}. The CHEMTAX results did not show any significant changes with depth in the relative abundances of the four phytoplankton groups (Figure 4.11, right panel). The absorption deconvolution results did not show the same community composition as the CHEMTAX results, especially at the lower chlorophyll concentrations (depths 4 and 19.5 meters; Figure 4.11, left panel). The comparison was somewhat better for the discrete samples and deconvolution results at 10 meters, with both showing Group 4 as most abundant (60% and 80% respectively), with smaller contributions from Groups 1 and 3 (16% and 4% for CHEMTAX, 13% and 8% for the deconvolution for Groups 1 and 3 respectively). The absorption deconvolution did not identify the presence of Group 2 phytoplankton, whereas the CHEMTAX results indicated that they were the second most abundant group (21% of total chlorophyll-*a*).

The deconvolution performed better for the May 2006 data (Figure 4.12). At the 10 meter sampling depth, the deconvolution results indicated a phytoplankton

community dominated by Group 1 and Group 4 taxa (30% and 50% respectively), which agrees well with HPLC results (28% and 60% respectively). The absorption deconvolution indicated that Groups 2 and 3 were 4% and 17% of the community population, while the CHEMTAX results found that they were 11% and 1% at this depth. At 20 meters, Groups 1 and 4 represented 34% and 66% of the total phytoplankton absorption in the deconvolution results, and 30% and 58% in the CEMTAX model. The deconvolution did not detect the presence of any Group 2 or 3 phytoplankton, while CHEMTAX designated 11% and 1% of the chlorophyll-*a* to them at this depth.

The comparisons between the CHEMTAX and absorption deconvolution interpretations of community structure indicate that hyperspectral absorption can be used as a basic indicator of diagnostic groups in the Santa Barbara Channel. Although more comparisons between the deconvolution and HPLC are necessary, these initial results indicate that we can combine information from the absorption data with other inherent optical properties and optical parameters (Chl, PSD slope and the backscattering ratio) to build a better understanding of temporal phytoplankton community dynamics at the CHARM location. We discuss these results in the next section.

4.4.4 Temporal shifts in optical properties and phytoplankton community structure

To interpret temporal shifts in the absorption deconvolution data in relation to the other optical data, we converted the derived optical weights for each group into estimated absorption according to Equation 5. We inferred a community composition by estimating a percent absorption at 440 nm, $\%a_{\text{t-w}}(440)$, (see Equation 8). In this case, however, we included a_{CDM} in our calculation so that the sum of Groups 1 through 4 plus a_{CDM} yielded a full accounting of the absorbing materials that were present, according to the deconvolution. The resulting distribution of absorption enabled us to infer which of our basis vector constituents was dominating the absorption at any given time. We chose 440 nm as a reference wavelength because phytoplankton and CDM

both absorb strongly in the blue, which facilitates a comparison of their relative influence in this region of the spectrum. In order to determine whether shifts in % absorption were due to changes in one or many groups, we also examined the absolute magnitudes of absorption at 440 nm.

Despite the short time period of observations in February, there were interesting features in the data that indicate a diel cycle of growth and grazing. Over the 27 hours of observations, we observed a nighttime decline and subsequent daytime elevation in Chl, beam attenuation, and absorption (Figure 4.6). Absorption inversion results indicated that the phytoplankton population was dominated by dinoflagellates (Group 4, between 35 and 55% of absorption at 440 nm) followed by diatoms (Group 1, 0 to 10% of $a_{t-w}(440)$) and very minor populations of Group 2 and Group 3 algae (Figure 4.13B). The general trend in chlorophyll and beam attenuation was also observed in the Group 4 absorption at 440 nm (Figure 4.13B, red line). Absorption by CDM at 440 nm was high throughout the sampling period, with a slow increasing trend from 0.11 m^{-1} to 0.14 m^{-1}. Group 4 absorption at 440 nm fluctuated around the magnitude of CDM absorption. It was lowest in the middle of the night, with higher levels at midday. The same trend was observed in Group 3, albeit at lower concentrations (Figure 4.13C). The opposite trend, high values at night and low during the daylight hours, was observed in the particle size distribution slope. Throughout the observations we found that the PSD slope was sensitive to fluctuations in particle composition (Figure 4.13A, green line). Higher relative CDM absorption, as indicated by higher % absorption, was directly reflected in higher PSD slopes, which is in agreement with the theory that a population of smaller particles will produce a steeper size distribution slope. It is worth emphasizing that these shifts in particle characteristics were detected by independent measurements of absorption and attenuation.

The backscattering ratio did not respond as noticeably to changes in the particle population that were implied by concurrent changes in the PSD slope, absorption deconvolution, and IOP's (Figure 4.13A, blue line). For much of the sampling period the backscattering ratio went through minor oscillations that were not related to variability in other parameters. There is an exception however, in the final few hours of

available data. In the time period following year day 33.4 we observed the highest values of Group 4 (dinoflagellates) absorption, low values in CDM, and minimums in PSD slope and the backscattering ratio. We also observed the highest chlorophyll concentrations for the time period in these final few hours.

The May deployment of CHARM provided approximately 18 days of high quality hydrographic and bio-optical measurements (Figure 4.14). Several features in this time series concur with those observed in the February time-series. Group 4, the dinoflagellates, continued to dominate the phytoplankton community composition at the mooring location. CDM concentrations were also high throughout the sampling period. We found that, just as in February, fluctuations in absorption by dinoflagellates resulted in shifts between a particle population dominated by CDM absorption or by phytoplankton absorption.

Other optical parameters varied over the same time scales, and coincide with the observed shifts in dominance from CDM to phytoplankton and back again. For example, at year day 128 we observed an influx of cold water to the mooring with concurrent increases in backscattering, absorption, attenuation, and chlorophyll (Figure 4.15). At the same time we also observed a steep decline in the PSD slope, a decline in the relative importance of CDM absorption, and a sharp increase in Group 4 absorption. Interestingly, the diel pattern in the accumulation of biomass during the daylight hours and a decline at night was not observed over the time period shown in Figure 4.15, year days 125.5 though 128.5. Also, prior to day 128 there was no strong relationship between Chl or any of the optical parameters.

We observed the opposite scenario for year days 141.5 through 144 (Figure 4.16). During this time period we observed clear diel patterns in Chl, backscattering, the PSD slope, and fluctuations in the contribution of Group 4 to total absorption at 440 nm. Given the relatively invariant absorption of CDM during this segment of the time series ($0.15 - 0.18$ m^{-1}), the fluctuations in Group 4 display a striking diel pattern. We observed that night-time hours exhibited a steeper PSD slope, low total absorption and attenuation, and low chlorophyll and backscattering. The opposite was true for daylight hours. During this time period, as opposed to the February time-series and year days

125.5 through 128.5, the backscattering coefficient tracked changes in chlorophyll. The backscattering ratio did not show any diel patterns of variability, and fluctuated between 0.01 and 0.02.

Less salient daily transitions were observed during the middle of the time series, from year day 131 through 138 (or 135 for the ac-s-based data). Here we found that the contribution of Group 4 to total absorption varied between 30 and 40%, CDM between 50 and 60%, Group 2 around 10%, and Group 3 around 5% of the community. This less dynamic time period also had stable levels of total absorption, attenuation and Chl, and more aperiodic variability in temperature.

4.5 Discussion

4.5.1 Relationships between particle characteristics and optical properties

The overall trends that we observed in the absorption deconvolution tracked changes in other optical properties. For example, the effect of the relative abundance of phytoplankton versus CDM on the PSD slope is in line our understanding about how small particles affect the slope of spectral beam attenuation. More small particles, i.e. more CDM, should cause the slope of the attenuation to increase. This is because the maximum volume-specific attenuation for small particles occurs at shorter wavelengths than for larger particles, so an abundance of small particles will preferentially increase attenuation in the blue (Boss et al., 2001b). Likewise, when larger particles are numerous, attenuation increases at longer wavelengths and results in a flatter beam attenuation spectrum. During monospecific blooms of very large phytoplankton, positive beam attenuation slopes have been observed (Sullivan et al., 2005). We observed nearly flat beam attenuation spectra that may have been associated with a red tide event around year day 128.

Fluctuations in the backscattering coefficient and backscattering ratio were occasionally decoupled from phytoplankton absorption. This is not surprising, however, because lithogenic particles have the strongest influence on the backscattering signal, are only weakly absorbing, and cannot be properly resolved in the deconvolution. It is

also possible that the concentrations of lithogenic and detrital particles vary on different timescales than does the phytoplankton population. The strong response of the backscattering coefficient to particles other than phytoplankton can provide additional context for and verification of the absorption deconvolution results. For example, an increase in backscattering or the backscattering ratio with no observable shift in absorption or attenuation would indicate an increased contribution of CDM to the bulk particle composition. We observed this scenario many times over the deployment period in the Channel. The backscattering ratio at the mooring was consistently between 0.01 and 0.02, which indicates a strong lithogenic influence on the bulk backscattering signal throughout the sampling period (Boss et al, 2004). But, even under these circumstances, we observed shifts in the relative dominance of CDM absorption that were reflected in the backscattering ratio.

As mentioned previously, we would expect high concentrations of phytoplankton cells to cause a decrease in the backscattering ratio compared to cases when lithogenic materials dominate the optical properties of the particle population. There was at least one occasion, however, when we observed an increase in the backscattering ratio in a phytoplankton layer (Figure 4.9). This would imply that either there was an increase in the proportion of very small particles or an increase in the refractive index of the particles relative to the water column directly above and below the layer, or both. At the time of this vertical profile there was a red tide event in the Channel, although it was highly spatially variable. Discrete samples collected by the Plumes and Blooms project (see: http://www.icess.ucsb.edu/PnB/PnB.html) identified the bloom as being mostly dinoflagellates from the genus *Ceratium* (G. Chang, personal communication). *Ceratium* are large dinoflagellates, and although they have higher backscattering ratios than most phytoplankton groups, they are still not likely to produce a higher backscattering ratio than lithogenic particles in the bottom boundary layer (previous chapter). It is possible that the large size of *Ceratium* influenced the attenuation measurement in such a way that, when it was propagated to the backscattering ratio, actually lead to the opposite and spurious conclusion that small, hard particles were present. Large particles disproportionately scatter light in the

forward direction via diffraction. High levels of forward scattered light would cause an underestimate of the attenuation coefficient due to excess light reaching the detector (Roesler and Boss, 2008). When the attenuation coefficient is underestimated, the scattering coefficient derived from the measurement would also be underestimated. When the scattering coefficient is underestimated, the backscattering ratio would then be overestimated. This effect would be observable during a phytoplankton bloom of large algae and we hypothesize that it was responsible for the increased backscattering ratio in the chlorophyll maximum of the May 5 profile.

Our absorption deconvolutions lead to the conclusion that Group 4 dominated the phytoplankton. Observations in the Southern California Bight and in the Santa Barbara Channel reveal that it is common for one group to dominate the assemblage (Venrick, 1998; Anderson et al., 2008). With the exception of the large chlorophyll signal at the beginning of the time series that may have been due to a red tide event, the chlorophyll concentration was generally around 5 mg m^{-3}. It is reasonable to hypothesize that the sampling period occurred prior to the primary spring upwelling and bloom events in the Channel. In low nutrient, non-upwelling conditions, dinoflagellates are commonly found in high abundance at nearshore stations in the Santa Barbara Channel (Anderson et al., 2008). Considering this information, it is not suprising that we observed such a strong signal in the Group 4 phytoplankton while other Groups vary between 15 and 5% of the community composition. This was also reflected in the HPLC samples collected on the 5th of May, in which Group 4 represented 60% of the observed Chlorophyll-*a*.

The largest source of uncertainty in our work, in terms of lack of validation by discrete samples, is the proportion of absorption by CDM. It was somewhat surprising that deconvolution results from both of the cruises and from the mooring data regularly attributed fifty to ninety-five percent of the total absorption optical weight to CDM. When using discrete basis vectors for CDOM and NAP, G. Chang found that a disproportionately large percentage of non-algal absorption is attributed to NAP rather than CDOM, which conflicts with previous findings from stations further offshore and to the west in the Channel (G. Chang, unpublished data, 2007; Kostadinov et al., 2007).

While it is possible that the shallow, nearshore mooring location was substantially influenced by the presence of detrital particles relative to dissolved matter, it is more likely that the CDM portion of the deconvolution model needs to be further constrained.

As stated earlier, the deconvolution approach that we used requires a fixed a_{CDM} slope as input. To test the effects of the magnitude of the a_{CDM} slope on the quality of the absorption deconvolution results, we conducted a sensitivity analysis on a range of a_{CDM} slopes. Following Equation 5b, we used values of S_{CDM}, from -0.008 to -0.016 in increments of 0.002. To compare deconvolution results between phytoplankton groups for different input S_{CDM} values, we calculated the percent of phytoplankton absorption for each group at 676 nm (% $a_\phi(676)$) as follows:

$$\%a_\phi(676) = \frac{a_{phyto-i}(676)}{a_{phyto1}(676) + a_{phyto2}(676) + a_{phyto3}(676) + a_{phyto4}(676)} * 100 \quad \text{Eq.9}$$

S_{CDM} had a strong effect on the concentrations of all of the phytoplankton groups (Figure 4.16). Small changes in the slope parameter had a significant effect on the absorption attributed to each group. For example, using a value of S_{CDM} of -0.010 instead of -0.012 results in a switch from a Group 1 dominated community to a Group 4 dominated community. This sensitivity to the CDM slope implies a greater need to describe the variable absorption characteristics of the dissolved and detrital matter at time scales relevant to the system. One way to get at this problem would be to utilize an additional spectral absorption meter with an attached pre-filter to exclude particles. This would enable us to determine S_{CDOM} directly and therefore reduce the uncertainty in assuming an S_{NAP}.

4.6 Conclusions

There is a direct dependence between the optical properties of a water mass and the concentration and nature of its dissolved and particulate components. Likewise, the characteristics of the particles themselves, their size, shape, and composition, are what determine their optical properties. In the case of the inherent optical properties, the

contributions of individual particulate and dissolved components combine linearly to form the ensemble or bulk optical properties of the water mass. Therefore, if the optical properties of the individual components were well known, and those optical properties could be measured with enough certainty, one should be able to determine with accuracy the individual particles that determine the optical properties of a water mass. In reality, only some of the optical properties of marine particles are well constrained. The absorption coefficient, for example, has been measured routinely for many phytoplankton and marine microbial species under various environmental conditions. The backscattering properties of marine particles are less well understood, but general ideas about their backscattering efficiency and limited spectral characteristics are under investigation. Due to the difficulty in physically separating detrital particles from phytoplankton cells, either in culture or *in situ*, we understand very little about the nature and optical properties of these particles. However, given these limitations, we found that combining information from multiple measurements, including chlorophyll concentration, hyperspectral absorption and attenuation, and backscattering, enabled us to discriminate and track phytoplankton groups and colored detrital matter in an optically complex, nearshore environment. While there are still areas where we need to constrain the uncertainty in our absorption inversion, this work is a significant step in the direction of remote, real-time monitoring of phytoplankton community composition.
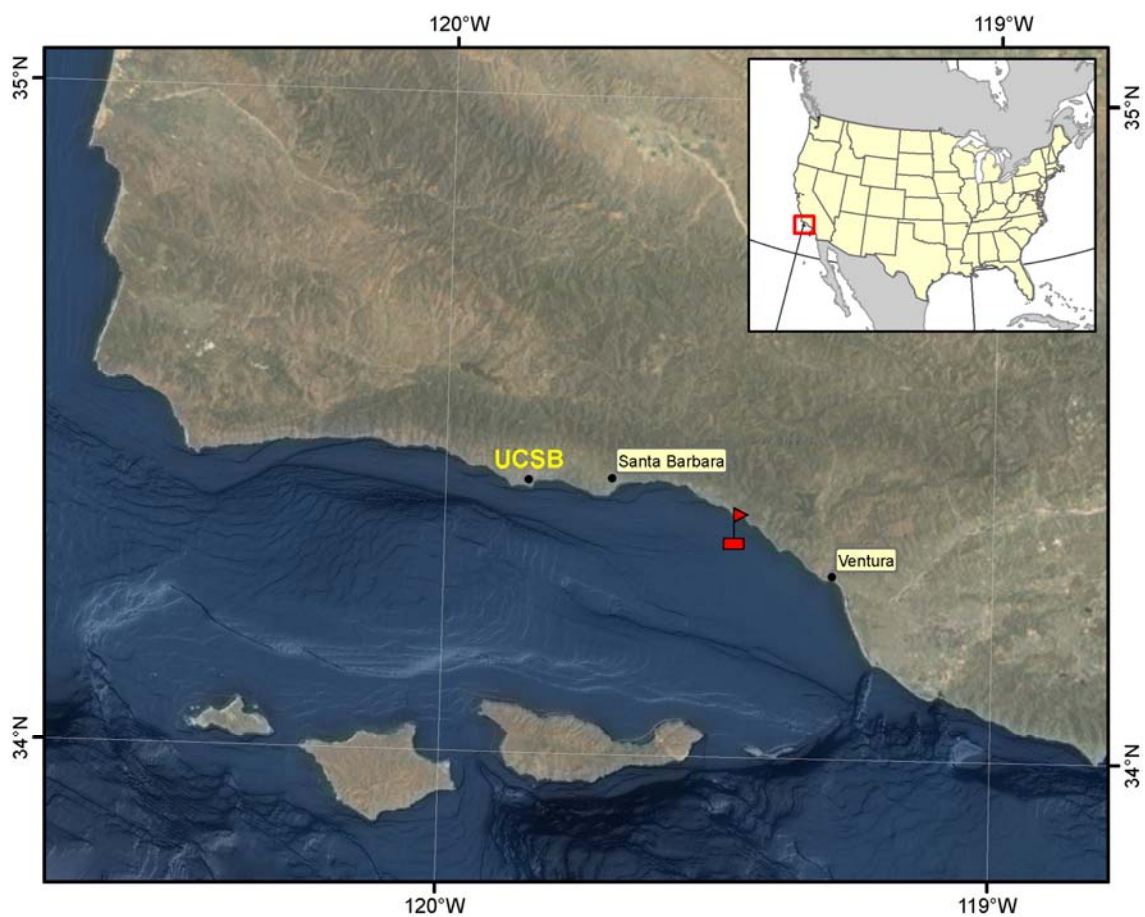
Figure 4.1. Mooring and sampling location in the Santa Barbara Channel, off Southern California, U.S.A. Image courtesy of C. Whitmire.
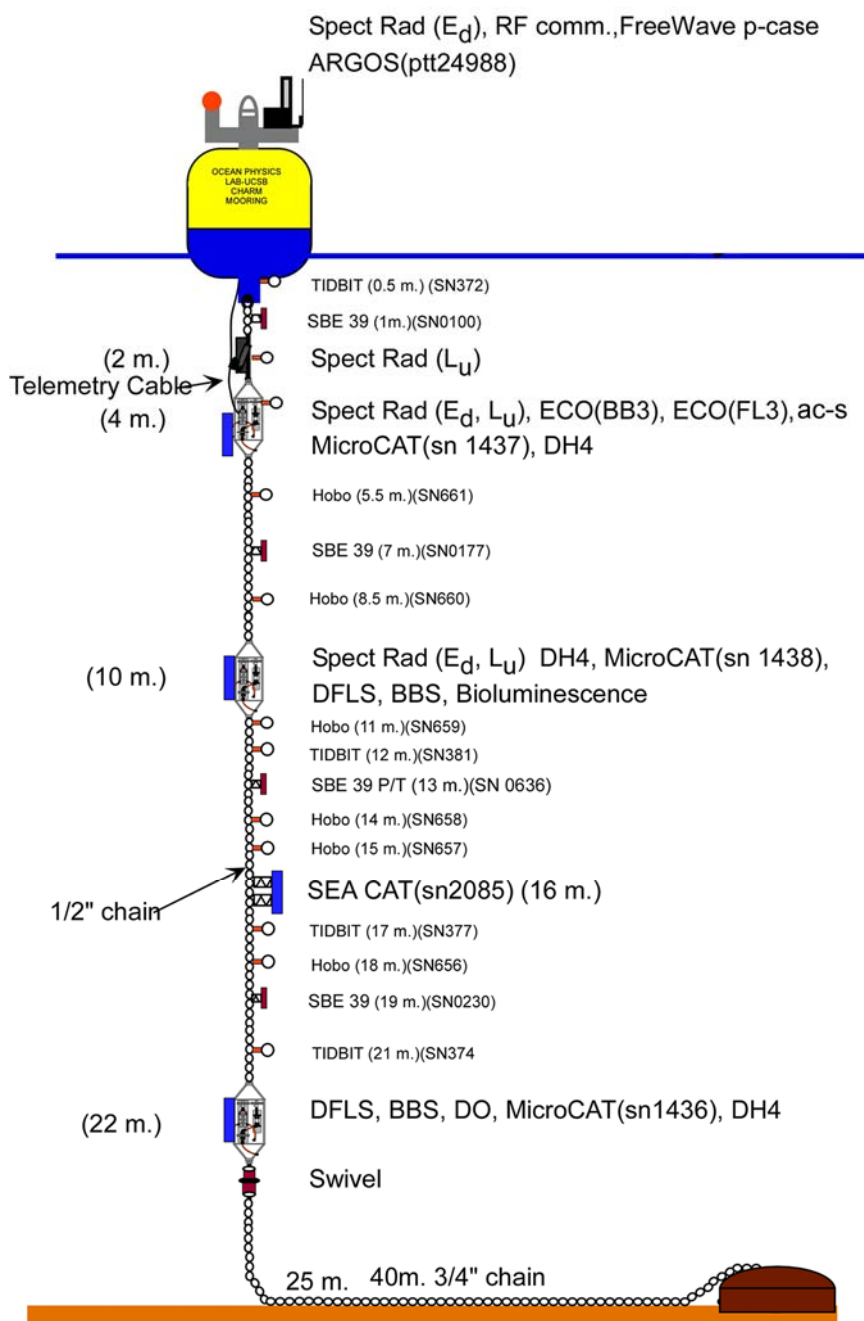
Figure 4.2. Schematic diagram of the CHARM. Locations of instruments are labeled. ac-s = hyperspectral absorption-attenuation meter, ECObbx = spectral backscattering meter (x = number of wavelengths), ECOfl3 = spectral fluorometer, Fluor = chlorophyll fluorometer, Temp & Sal = temperature and conductivity meter, Temp = temperature sensor, ADCP = acoustic Doppler current profiler, RF = radio frequency. Image courtesy of Frank Spada; see http://www.opl.ucsb.edu/mosean.
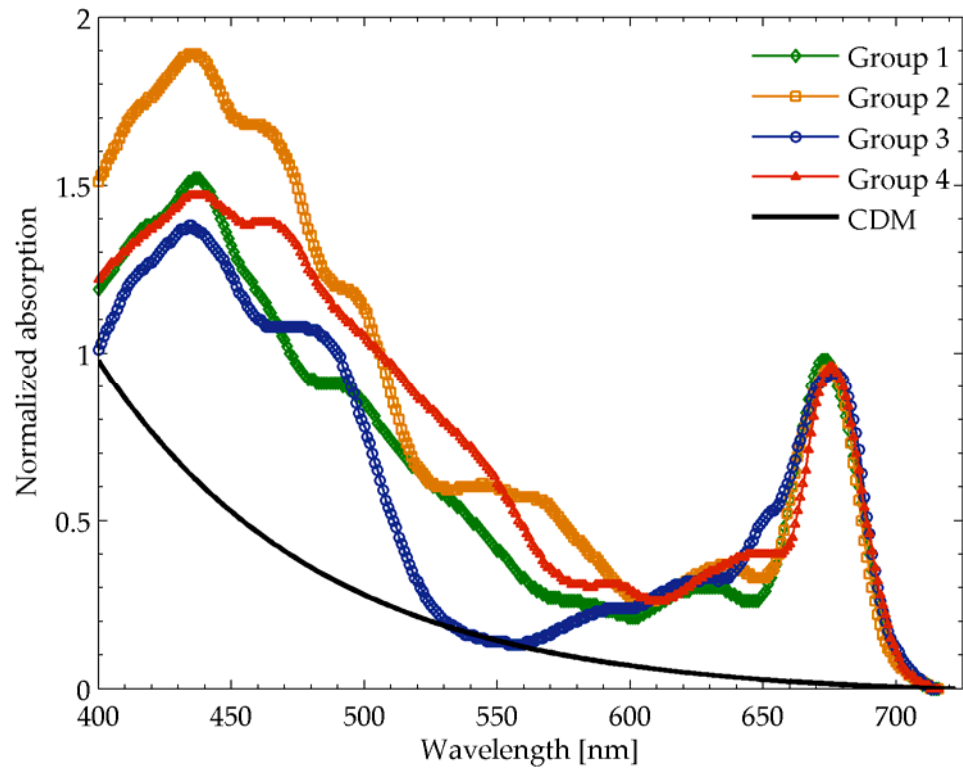
Figure 4.3. Dimensionless basis vectors for phytoplankton absorption, Groups one through 4 as defined in the text, non-algal particles, and colored dissolved organic matter. The spectral slope of colored detrital matter, S_{CDM} = -0.012.
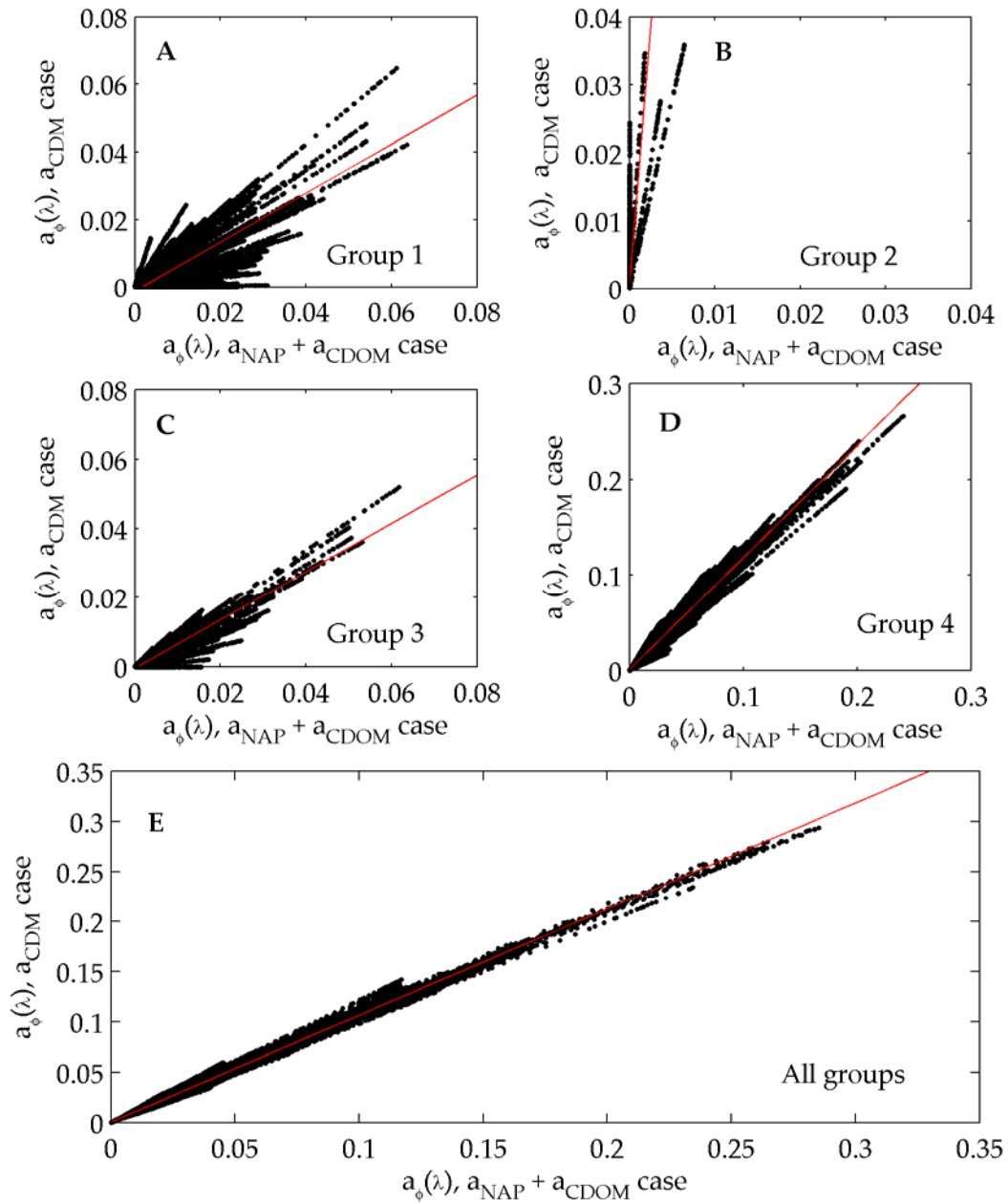
Figure 4.4. Phytoplankton group absorption derived from deconvolution for the case of separate CDOM and NAP basis vectors versus the case with a merged CDM basis vector. Red lines are the robust, type-II linear least squares regression results for each group. A-D) Absorption for individual groups at all wavelengths. E) The sum of absorption from all phytoplankton groups, all wavelengths are shown.
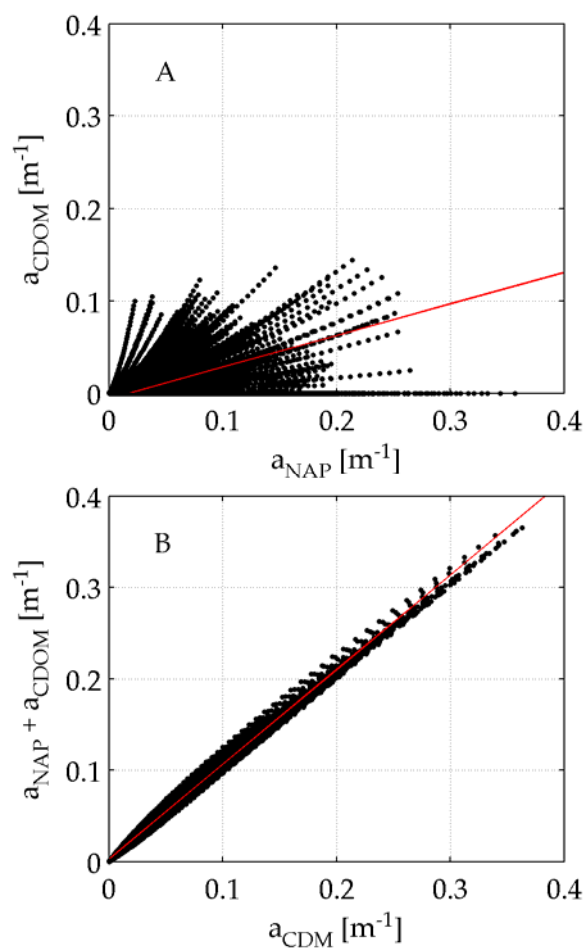
Figure 4.5. Absorption deconvolution results from using two non-algal components, CDOM and NAP and from using a single component, CDM. Robust model-II linear least squares regression lines are shown in red. A) Absorption by NAP versus absorption by CDOM when individual basis vectors are used for each. B) Absorption by colored detrital material versus the sum of absorption by CDOM and NAP.
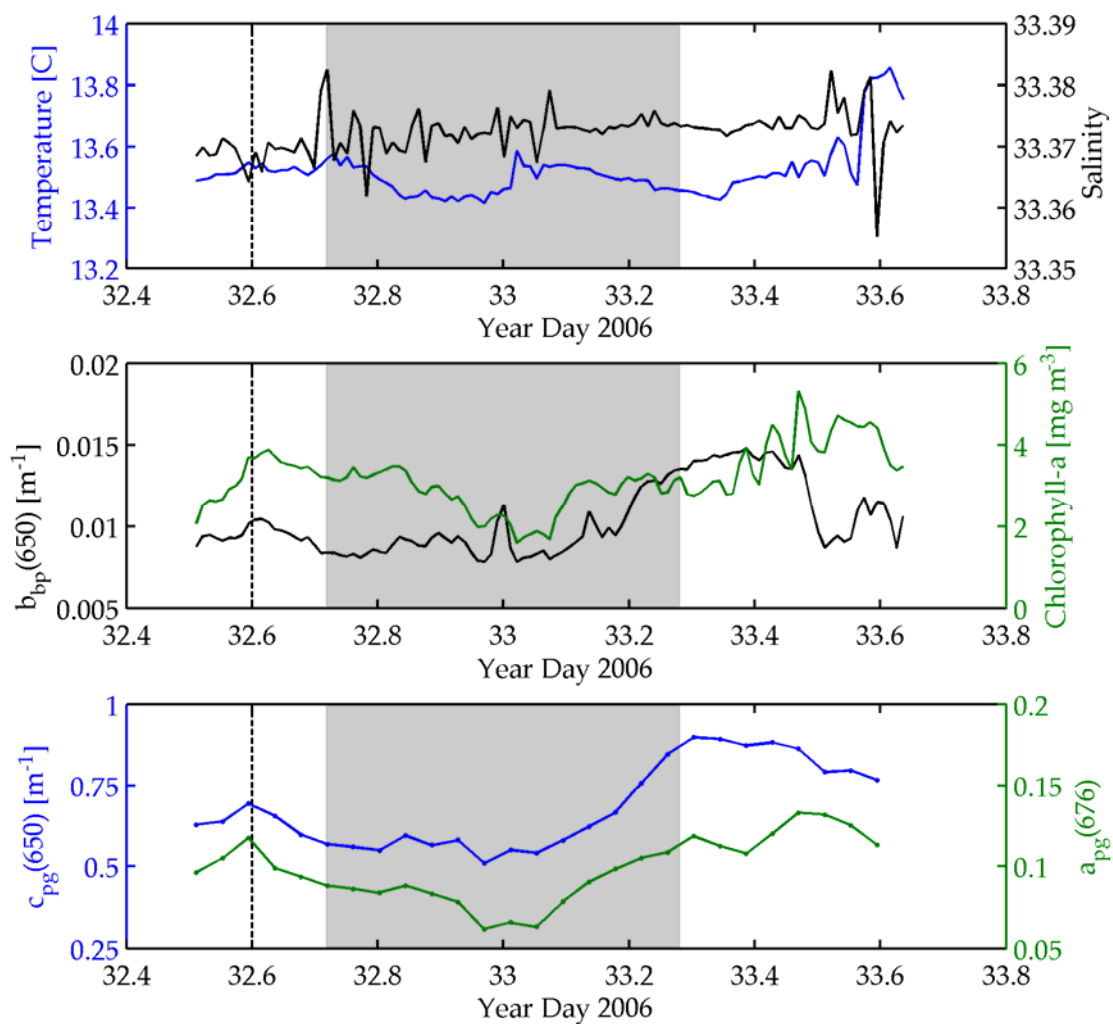
Figure 4.6. Time series data from SB CHARM for deployment beginning at 1200 hours (local) on February 1, 2006. Dashed vertical line indicates time of sampling. Grey boxes indicate hours between sunset and sunrise. A) Temperature (blue) and salinity (black) B) The particulate backscattering coefficient at 650 nm (black) and chlorophyll-a concentration (green) C) the attenuation coefficient at 650 nm (blue) and the absorption coefficient at 412 nm (green).
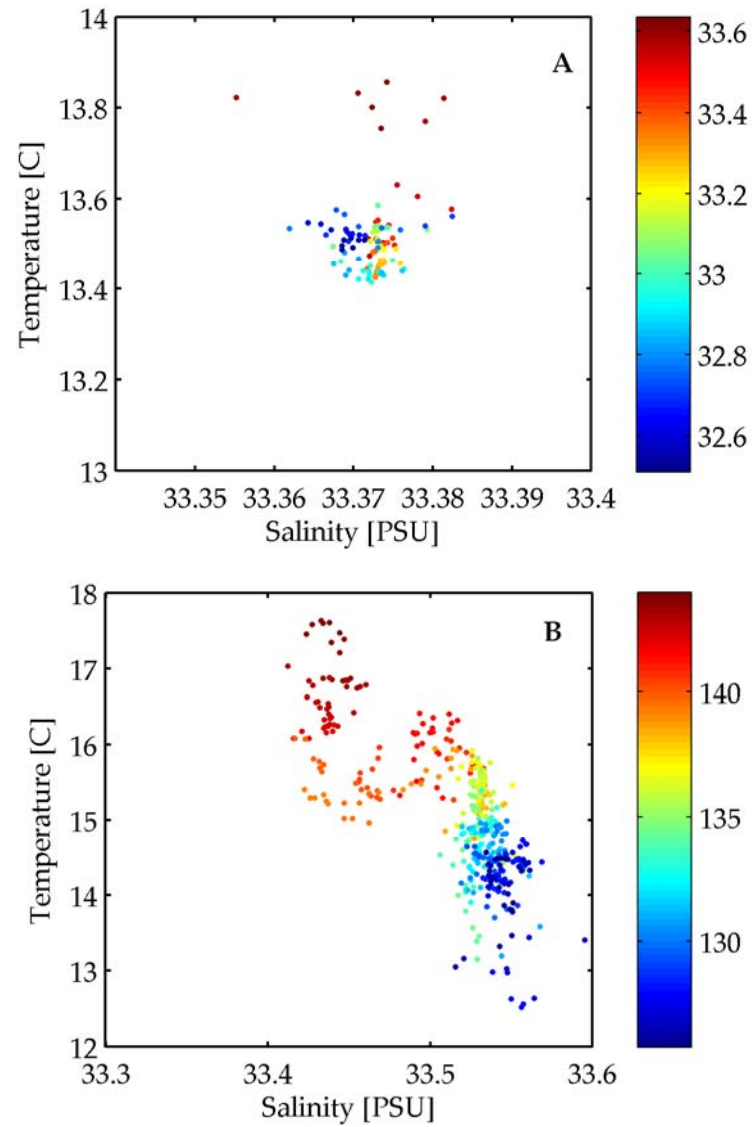
Figure 4.7. A) Temperature-salinity diagram for February 2006 deployment. B) Temperature-salinity diagram for May 2006 deployment. Colorbar is year day of 2006.

Figure 4.8. Time series data from SB CHARM for deployment beginning on May 5, 2006. The vertical line indicates the date of ship-based discrete sampling. Shaded regions indicate the hours between sunset and sunrise. A) Temperature (blue) and salinity (black) B) The particulate backscattering coefficient at 650 nm (black) and chlorophyll-a concentration (green) C) the attenuation coefficient at 650 nm (blue) and the absorption coefficient at 412 nm (green).
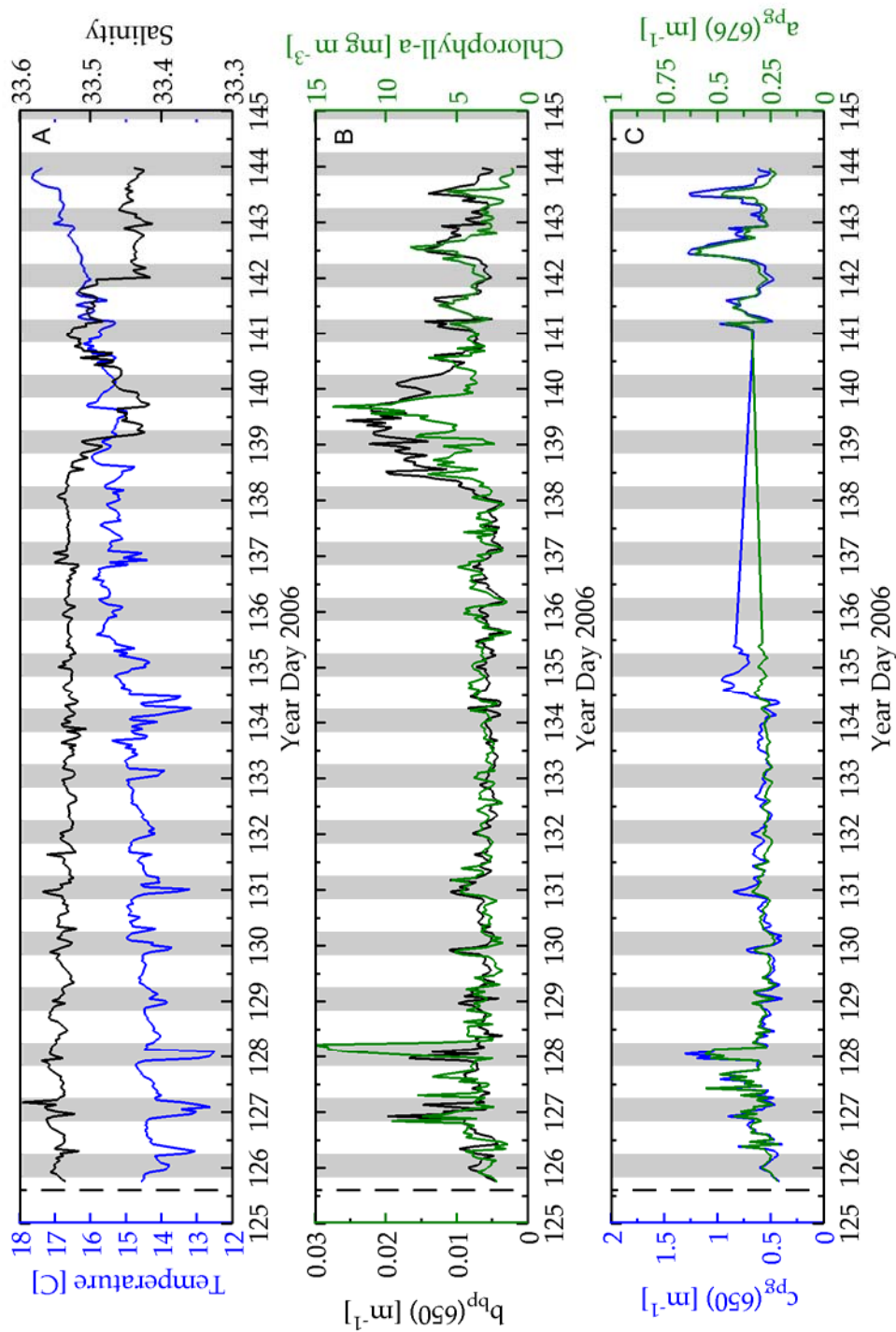
Figure 4.9. Hydrographic and bio-optical profiles collected near the Santa Barbara Channel Relocatable Mooring (CHARM) in May 2006. Dashed lines indicate depths of discrete samples, which coincide with depths of moored instruments on CHARM.
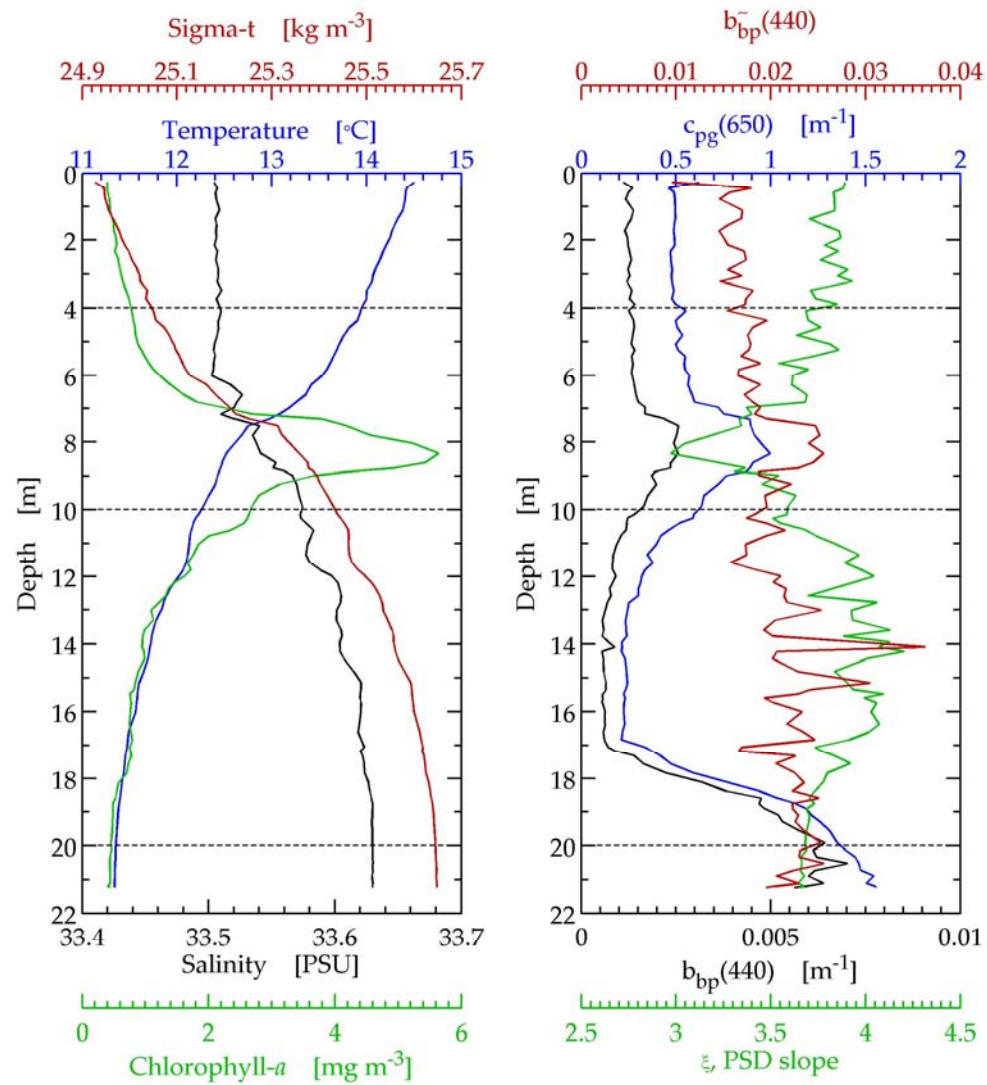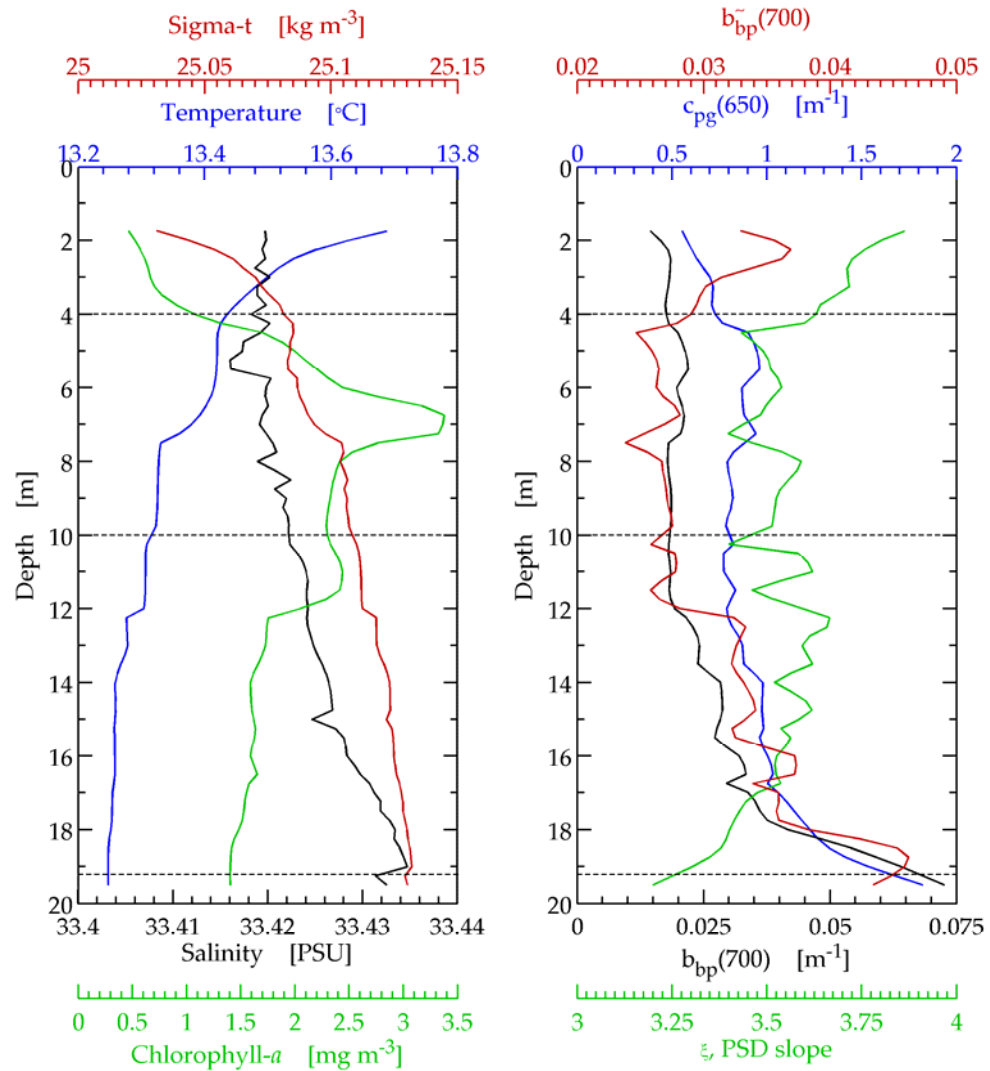
Figure 4.10. Hydrographic and bio-optical profiles collected near the Santa Barbara Channel Relocatable Mooring (CHARM) in February 2006. Dashed lines indicate depths of discrete samples, which coincide with depths of moored instruments on CHARM. Data are binned to 0.25 meter depth resolution.

Figure 4.11. Comparison of absorption deconvolution (left) and HPLC/CHEMTAX (right) at depths of 4 meters (top), 10 meters (middle) and 20 meters (bottom) in the Santa Barbara Channel in February 2006. Deconvolution results shown are group optical weight, w_i, as a percentage of total phytoplankton group weights (sum of all phytoplankton weights). HPLC results are class abundances as fraction of a chlorophyll *a*.

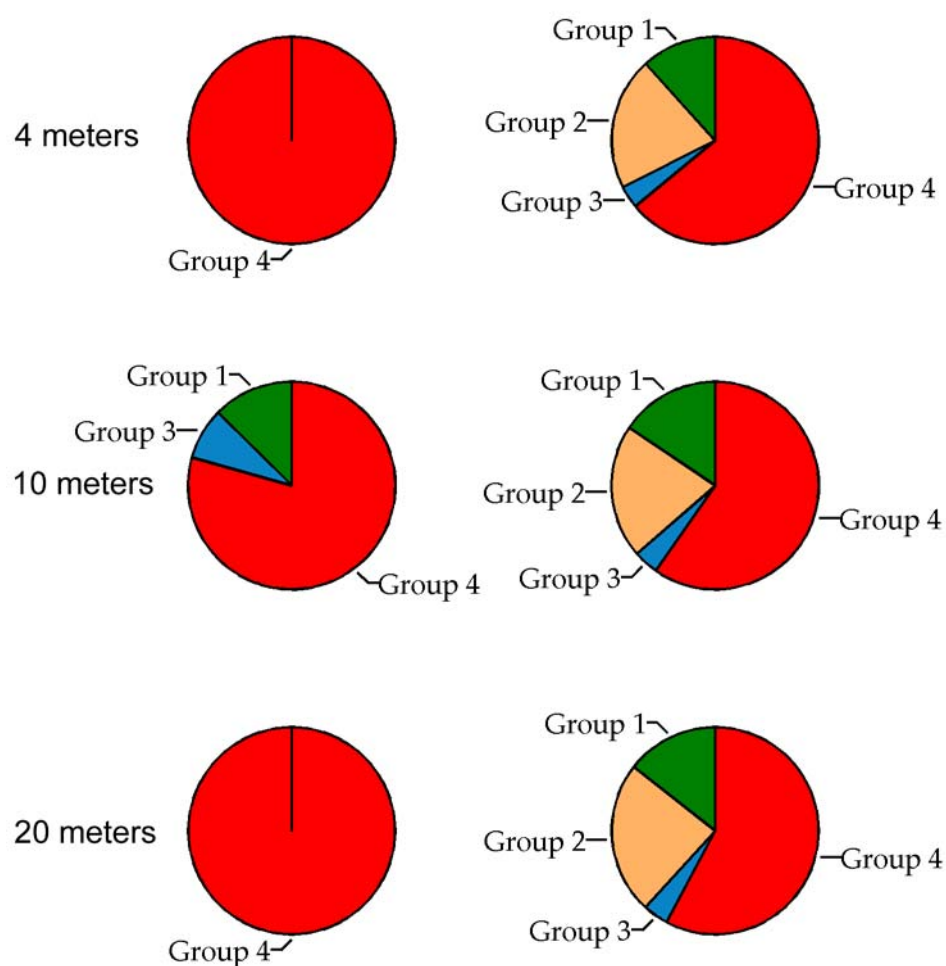Figure 4.12. Comparison of absorption deconvolution (left) and HPLC/CHEMTAX (right) at depths of 4 meters (top), 10 meters (middle) and 20 meters (bottom) in the Santa Barbara Channel in May 2006. Deconvolution results shown are group optical weight, w_i, as a percentage of total phytoplankton group weights (sum of all phytoplankton weights). HPLC results are class abundances as fraction of a chlorophyll *a*.
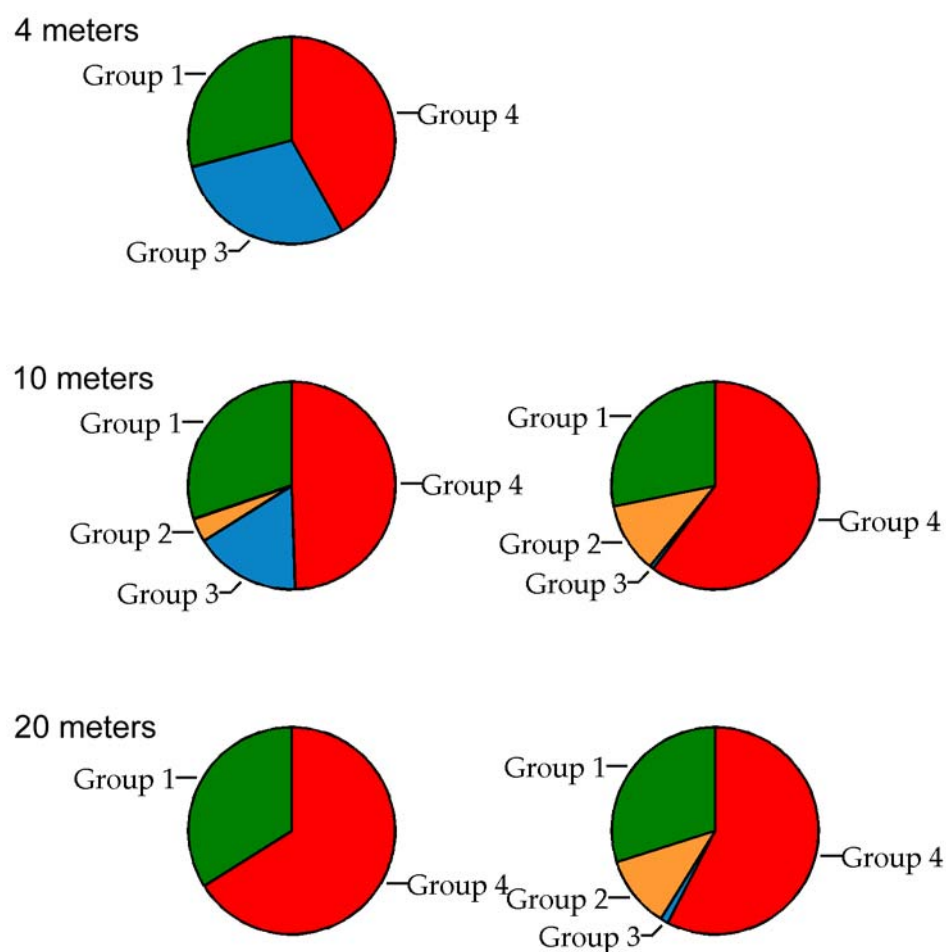
Figure 4.13. CHARM Time-series data from February, 2006. The vertical line indicates the date of ship-based discrete sampling. The shaded region indicates hours between sunset and sunrise. Top panel shows the particulate backscattering ratio at 650 nm (blue) and the particle size distribution slope (green). The middle and bottom panels show results from the absorption deconvolution. In the middle panel, each component, either a phytoplankton group or colored detrital matter, CDM, are shown as a percent of the summed absorption from all components at 440 nm. In the bottom panel, the magnitude of the estimated absorption at 440 nm for each component is shown.

Figure 4.14. CHARM Time-series data from May, 2006. The vertical line indicates the date of ship-based discrete sampling. Shaded regions indicate hours between sunset and sunrise. A) The particulate backscattering ratio at 650 nm (blue) and the particle size distribution slope (green). results from the absorption deconvolution. B) Results from the absorption deconvolution where each component, either a phytoplankton group or colored detrital matter, CDM, are shown as a percent of the summed absorption from all components at 440 nm. C) Results from the absorption deconvolution where the magnitude of the estimated absorption at 440 nm for each component is shown.
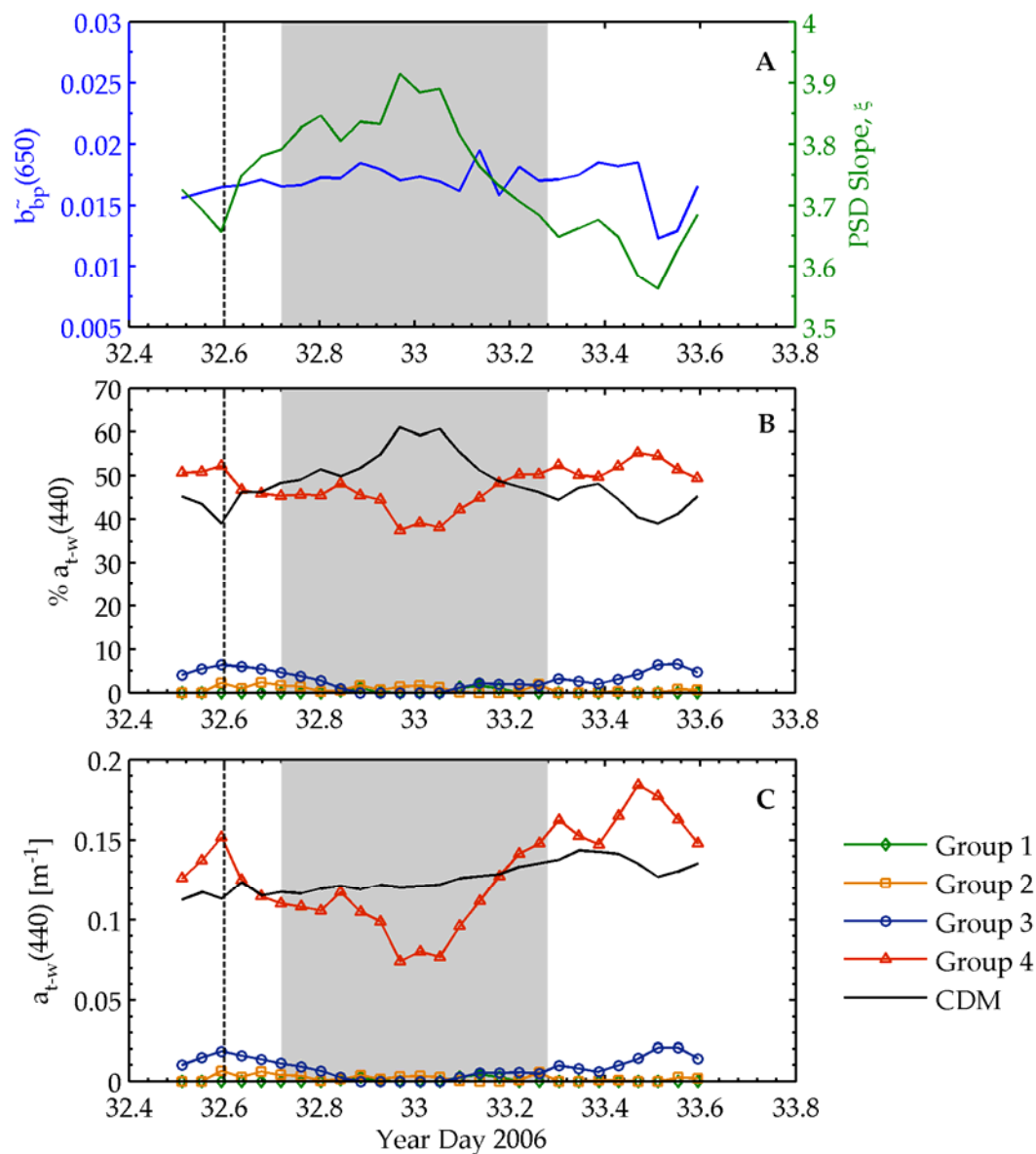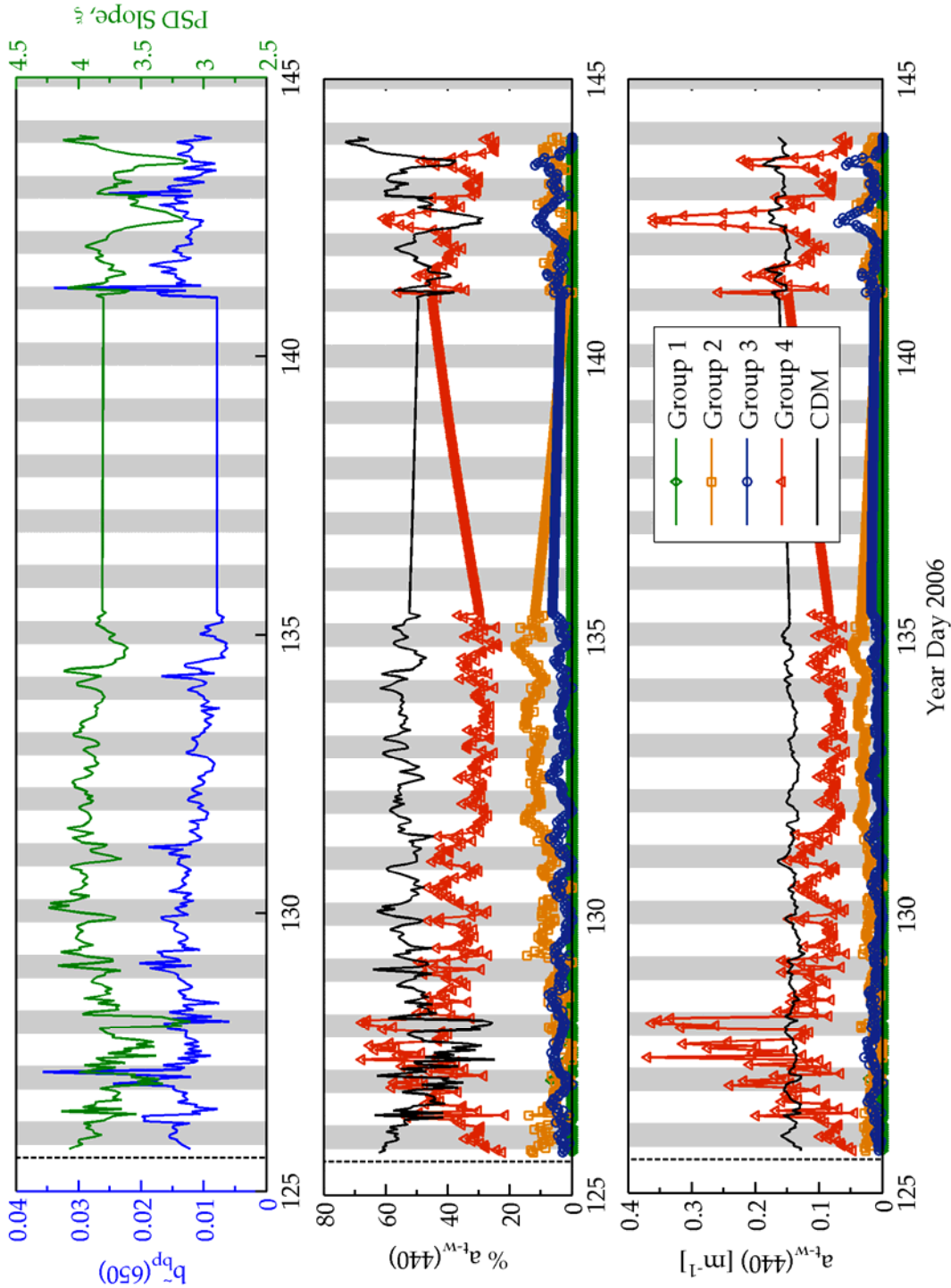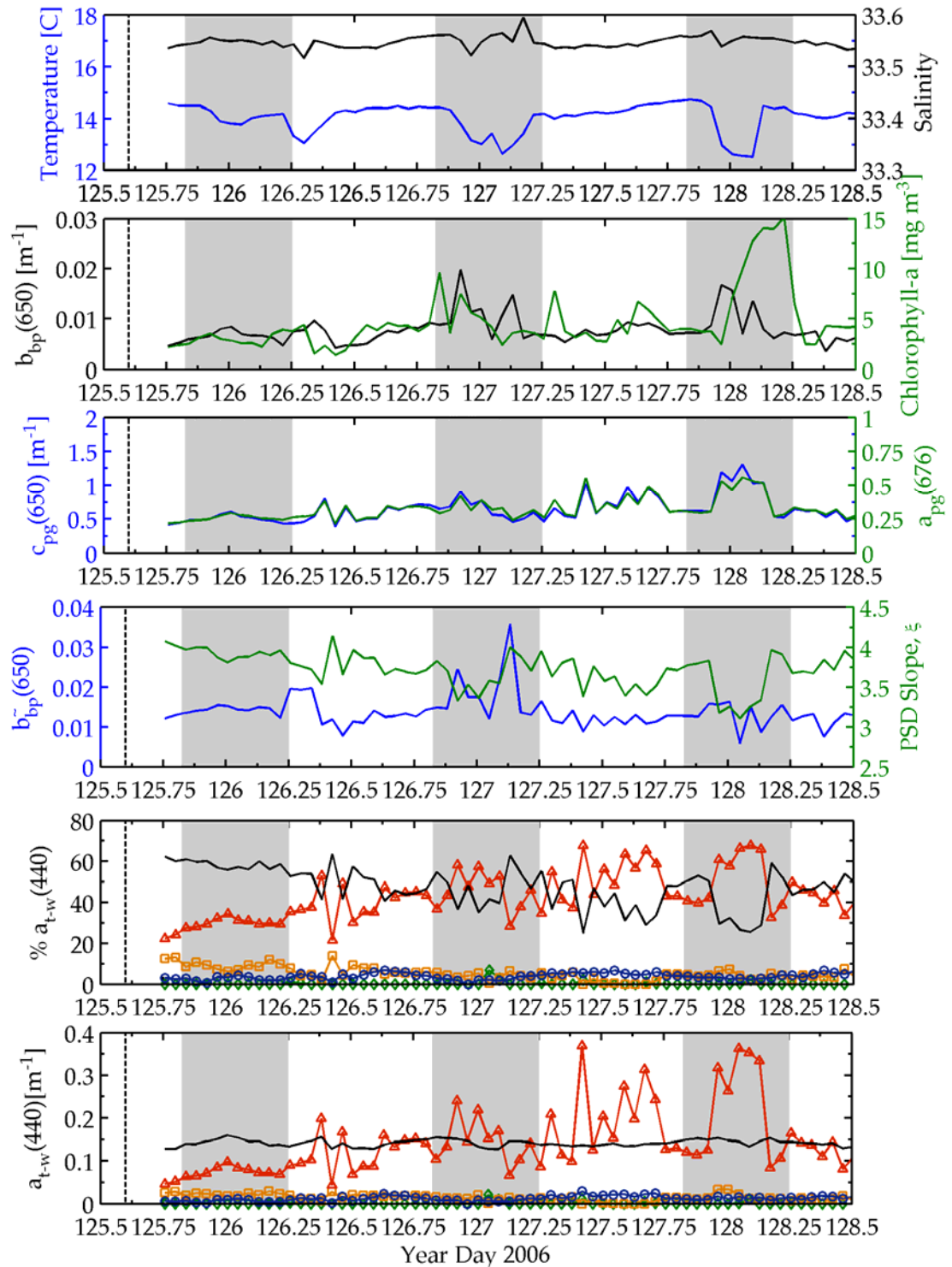
Figure 4.15. Selected CHARM time-series data from May, 2006. The vertical line indicates the date of ship-based discrete sampling. Shaded regions indicate hours between sunset and sunrise. Symbols and colors for absorption deconvolution components are the same as in Figure 4.14.
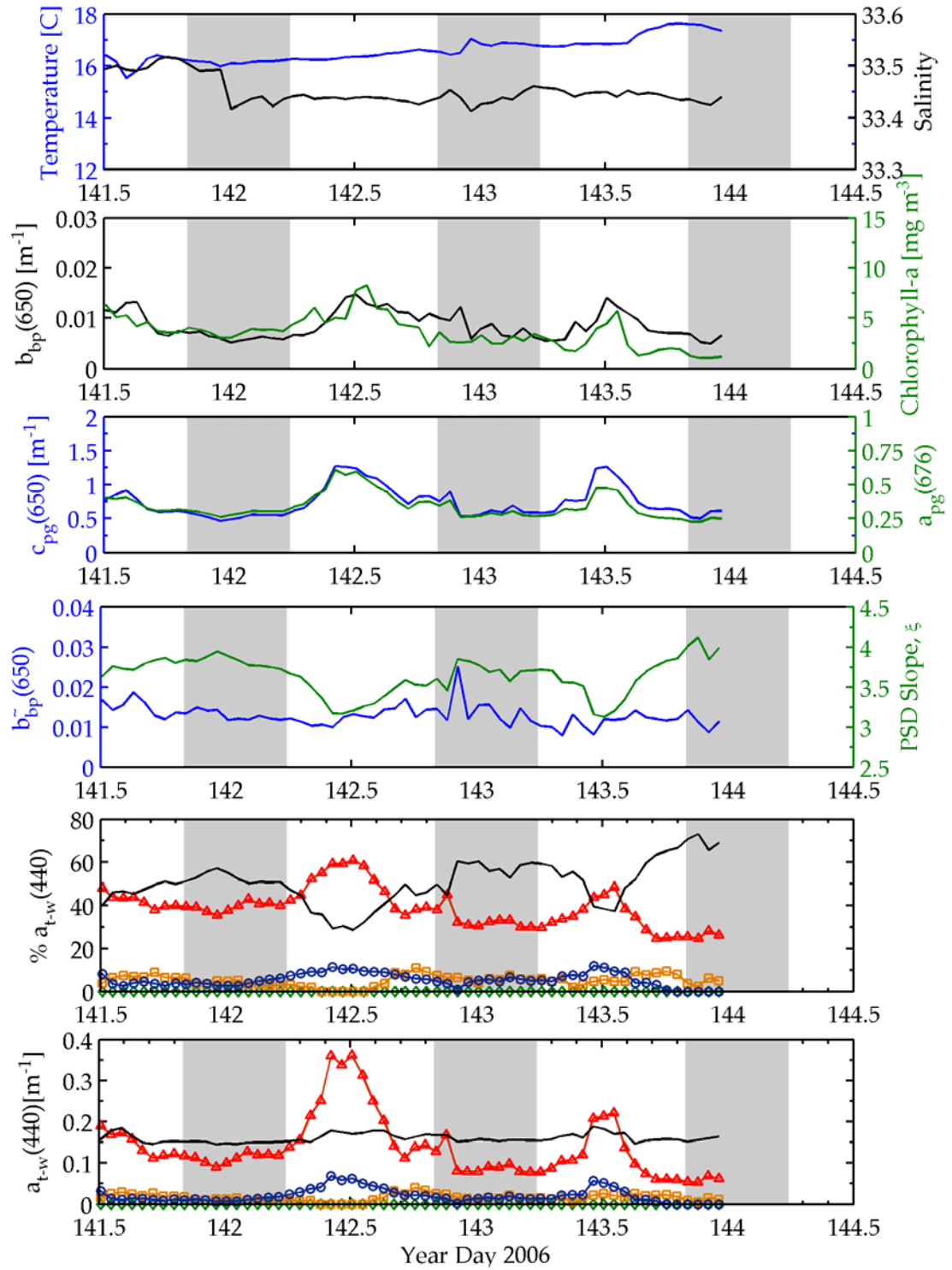
Figure 4.16. Selected CHARM time-series data from May, 2006. Shaded regions indicate hours between sunset and sunrise. Symbols and colors for absorption deconvolution components are the same as in Figure 4.14.
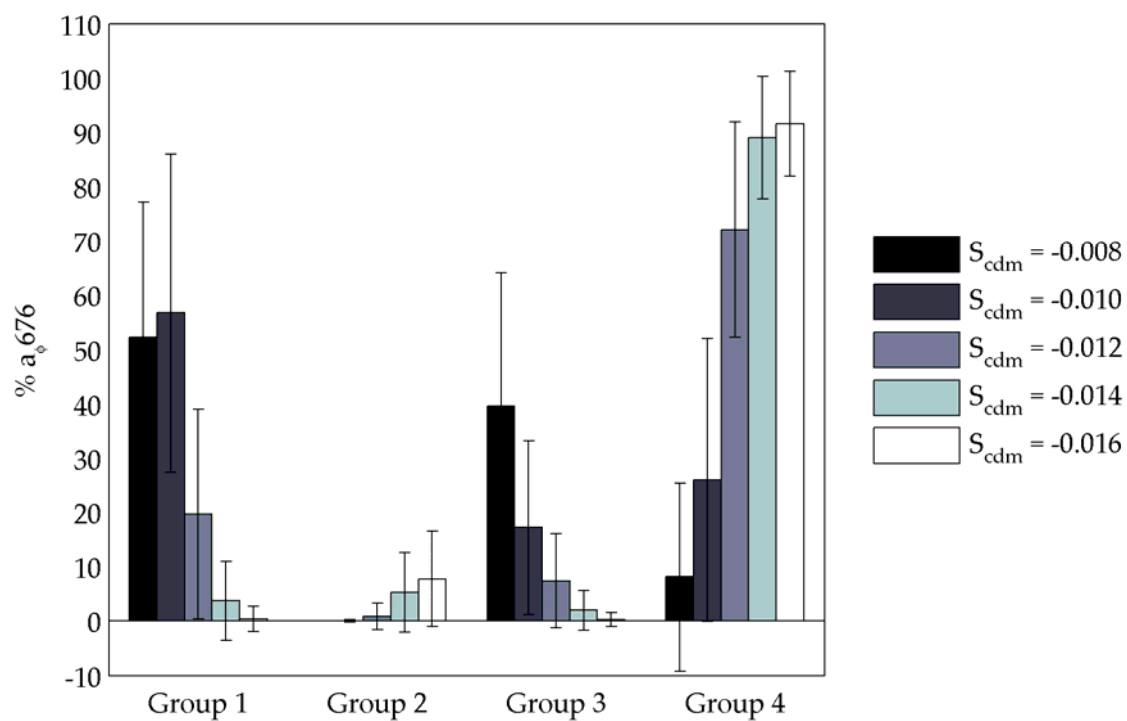
Figure 4.17. Percent of total absorption by phytoplankton at 676 nm for four phytoplankton groups (average of all depths) for five values of the detrital absorption slope, S_{cdm}. Error bars indicate one standard deviation of the mean.

Chapter 5. General Conclusions

It was the objective of this dissertation to examine relationships between the physical characteristics of marine particles and their spectral backscattering properties. This subject was examined from three perspectives: global relationships for the bulk particle assemblage (Chapter 2), the mean particle properties of marine phytoplankton cultures (Chapter 3), and the discrimination of specific particle populations from bulk measurements in a coastal environment (Chapter 4). In the first chapter we concluded that there was no spectral variability in the particulate backscattering ratio within our measurement capabilities, and that the magnitude of the backscattering ratio was linked to characteristics of the particle population. In the second chapter, we examined the spectral backscattering characteristics of individual phytoplankton species and found that features in the spectral backscattering coefficient were not easily related to particle characteristics or other inherent optical properties. We also found that the backscattering ratio for phytoplankton cells was spectrally flat, and that it was related to cell size and composition. Our results showed that phytoplankton have significantly higher backscattering signals than previous model results suggest. Finally, in the last data chapter, we examined how information from the backscattering coefficient and backscattering ratio could be combined with information from attenuation and inversions of hyperspectral absorption to make qualitative interpretations of the phytoplankton community composition over space and time in an optically complex coastal ecosystem.

The conclusions reached in Chapter 2 regarding the spectral nature of the backscattering ratio and its magnitude range in various oceanic environments has wide-ranging applicability in the fields of optical remote sensing and modeling of the underwater light field. Many remote sensing algorithms rely on a single value of the backscattering ratio, 0.0183, obtained from volume scattering measurements collected over 35 years ago (Petzold, 1972). Due to a severe shortage of estimates of the backscattering ratio from *in situ* data, most previous work in light field modeling used a spectrally flat ratio because models of light scattering for "characteristic" oceanic

particle populations predicted it. However, the most commonly used framework for modeling the optical properties of particles is the Mie model, which assumes spherical, homogeneous particles. The complex nature of most marine particles provided strong impetus for empirical validation of these model results. While we did find significant spectral variation in the backscattering ratio that was associated with rare occurrences of particles that deviate strongly from theoretical assumptions, we ultimately found that a spectrally neutral backscattering ratio can be assumed in most cases. Recent work in the extremely clear waters of the eastern South Pacific Ocean has reached the same conclusion (Huot et al., 2008).

Measurements of the spectral backscattering properties of marine phytoplankton are extremely rare. Prior to starting this work, I could find only one published research paper with spectral backscattering measurements in it, but the study lacked complementary measurements of other important optical properties (e.g. the absorption, attenuation, and scattering coefficients; Vaillancourt et al., 2004). The work done in Chapter 3 makes a significant contribution to our understanding of how the characteristics of phytoplankton cells influence their backscattering properties. We observed significant spectral variability in the backscattering coefficient between phytoplankton cultures, not just between taxonomic groups, but within them as well. We found that there were species-specific relationships between chlorophyll and the backscattering coefficient that varied widely for the 15 cultures that we studied. This finding provides some explanation for the apparently confusing and common observation that backscattering and chlorophyll are not always well correlated *in situ*, even in phytoplankton dominated waters.

Perhaps the most significant finding in Chapter 3 was that phytoplankton have significantly higher backscattering ratios than was previously believed on the basis of model results. There is a longstanding discussion among members of the ocean optics community concerning the perceived gap between measurements of light leaving the ocean and models that try to account for the light scattering budget for particles in open ocean waters. It appeared that although a large portion of the total scattering budget could be attributed to phytoplankton cells, only a few percent of the backscattering

budget could be attributed to these same particles (Stramski et al., 2004). The common perception was that phytoplankton were very weak backscatterers, and that the "missing" backscattering must be attributed to some portion of the particle population that could not be individually quantified, i.e. submicron colloidal particles. The weaknesses in this line of reasoning are two-fold. First, in order for non-phytoplankton particles to be responsible for the majority of backscattering in open-ocean waters, these particles have to co-vary over the exact same temporal and spatial scales as phytoplankton. Second, the basis for the argument that phytoplankton are weak backscatterers is rooted in the pervasive use of a model that is recognized to underestimate backscattering for phytoplankton cells by up to an order of magnitude. The measurements in our work suggest that the "missing" backscattering was never missing at all, and that we don't have to invoke the presence of unidentifiable particles whose optical properties are even less well understood than phytoplankton cells to close a light budget for the surface ocean.

The final chapter of my dissertation was an effort to improve our ability to discriminate major phytoplankton groups from bulk optical measurements. The ability to remotely discriminate between phytoplankton groups has profound applications in coastal monitoring. The ability to follow qualitative changes in community composition in real time, using *in situ* or satellite-based sensors, would enable tracking of phytoplankton blooms and species succession, which represent key ecological processes in ocean environments. While there is still more work required to test and validate our conclusions, we believe that the results shown in Chapter 4 demonstrate an incremental improvement in our ability to interpret bio-optical data in an ecological context. We found that the relative abundances of phytoplankton taxa and colored detrital matter obtained from the deconvolution of hyperspectral absorption data showed significant co-variation with chlorophyll, backscattering, and changes in the bulk particle size distribution. Constraining the uncertainty in the basis vectors used in this approach will improve model retrievals and strengthen the conclusions drawn from applying it in optically complex coastal regions where monitoring for harmful algal blooms and other relevant ecological processes are of critical importance to human health.

Perhaps even more exciting than our conclusions, however, are the additional questions that this research prompted, and the prospect of finding approaches to address them. First, what spectral resolution would be necessary to definitively link aspects of phytoplankton cells, such as size, shape, morphology, composition, or internal structures, with their backscattering characteristics? It is likely that our inability to link specific characteristics of phytoplankton cells with the spectral backscattering coefficient was related to the wide spectral bands and limited wavelengths sampled. In this same vein, I wonder if detailed measurements of the volume scattering functions for phytoplankton cells over the entire angular range (0-180 degrees) might be a more fruitful endeavor. Are certain angular ranges more sensitive than others to the presence or absence of specific organelles like vacuoles, or to cell wall thickness? Will particular combinations of angular and spectral measurements of phytoplankton scattering be necessary for the development of robust optical proxies that can be applied in real time to remote sensors? Could there be a "sweet spot" of measurement angle and wavelength that could be adapted to a small sensor and used on remote and autonomous platforms that are already operational, e.g. gliders and profiling floats?

Optical methods now allow us to sample the marine environment at unprecedented time and space scales. We know that the optical properties of the ocean are directly linked to the particulate and dissolved substances found there, and that the characteristics of these substances, their size, shape, and composition, drive their optical properties. Establishing firm relationships between the physical properties of ecologically important marine particles, especially marine phytoplankton, and their optical properties would vastly expand our ability to monitor ecological processes like phytoplankton blooms. It is this prospect that motivates my interest in studying the bio-optical properties of marine particles, now and in the future.

APPENDIX

Appendix A. Modeling the IOPs of unspecified non-algal particles

Non-phytoplankton particles are an unavoidable component of most laboratory monocultures. Phytoplankton 'monocultures' are often a combination of the target culture, resident heterotrophic bacteria, organic, non-living particles composed of dead cells or sloughed cell fragments, and various flocs containing all of the above. These non-target particles pose a considerable problem when trying to characterize the optical properties of phytoplankton cells.

Contamination by small, non-algal particles (including bacteria and detritus, hereafter called simply NAP) is easily observed in the Coulter counter data of affected cultures (Figure 1). A very high signal in the lowest size bins indicates the presence of bacteria or other NAP that could significantly influence the measured optical properties of the cultures. The backscattering coefficient, b_{bp}, is especially sensitive to this kind of contamination because of the high backscattering efficiency of small particles (< 3 microns). However, backscattering data alone are not sufficient to indicate contamination because it may not be clear if a high backscattering signal is due to the cells themselves or to the presence of NAP. The backscattering ratio (the ratio of backscattering to total scattering) is a much better indicator of potential contamination, again because of the differential effect of small particles on backscattering relative to total scattering. In our study of fifteen cultures, nine had indications of contaminated by NAP. All of the contaminated cultures, except one, had a particulate backscattering ratio above 0.010 m^{-1} at 442 nm. The single exception, *Thalassiosira pseudonana*, had a b_{bp} ratio of 0.0096, which is arguably within the range of error of 0.010. Of the six non-contaminated cultures, only one had a backscattering ratio above 0.010. *Thalassiosira weissflogii*, a centric diatom, had a backscattering ratio of 0.0105.

We discovered the presence of NAP in the post-processing stages of this experiment. We attempted to apply a correction factor to the measured optical data after the fact. Our approach was to model the contribution of NAP to the bulk optical properties and retrieve the phytoplankton optical properties by difference. In order to use the Mie model to estimate the optical properties of NAP (backscattering, scattering,

absorption, and attenuation coefficients), the particle size distribution (PSD) and the real and imaginary indexes of refraction of the NAP component of each culture must be determined. We retrieved PSD information from the Coulter counts by fitting a power function to the NAP portion of the Coulter counts (Figure 1, dotted line). We started with a real refractive index (*n*) of 1.04 at all wavelengths, and an imaginary index of refraction varying with wavelength as $n'(\lambda) = 0.010658e^{-0.007186\lambda}$ (Stramski et al., 2004). We set the limits of the particle size distribution from 0.2 – 100 microns in 35 size classes.

An *n* of 1.04 was used for the NAP associated with *C. profunda* and *D. tertiolecta*. Unfortunately, the estimated IOP's for NAP exceeded the bulk measurements in six of the remaining eight affected cultures. We attempted to obtain more satisfactory results by systematically "nudging" the real index of refraction downward. In this manner we determined an *n* of 1.03 for NAP associated with *C. radiatus*, *T. pseudonana*, and *T. rotula*, an *n* of 1.02 for *G. simplex* and *H. profunda*, and an *n* of 1.015 for *D. brightwellii*. We selected acceptable *n* values as those in which the modeled NAP IOP were lower than the measured IOP (Figure 2). Once modeling of NAP was complete, we removed the modeled absorption, attenuation, and backscattering coefficients from the bulk culture measurements. The scattering coefficient was obtained by difference using the corrected attenuation and absorption values.

To quantify the impact of removing the modeled NAP signature from the bulk measurements we calculated the percent change in each IOP as follows:

$$\frac{X_{corr} - X_{meas}}{X_{meas}} * 100$$

The largest decreases in bulk coefficients occurred in the blue for absorption, attenuation, and scattering (Figure 3). The opposite trend was observed for the backscattering coefficient. Interestingly, the scattering coefficient was most strongly affected by the removal of the non-algal signal, sometimes being reduced by as much as 94% at 412 nm (Figure 3). The average reduction in the scattering coefficient ranged from 59% to 27% of its uncorrected value from the blue to red wavelengths. The

absorption coefficient was reduced by a maximum of 40% in the blue to only 1% at 676 nm, with the average ranging from 18% to 1.5%. The backscattering coefficient was generally reduced by 25% or less, with one exception. The average reduction of the backscattering coefficient was 14% of its measured value at 442 nm and increased to 21% at 620 nm. The attenuation coefficient was reduced by up to 63% at 412 nm and 41% at 715 nm after the removal of the NAP attenuation signal.

The primary effect of removing the IOP signal of non-algal particles from the culture measurements was to reduce the magnitude (Figure 4). Changes in the spectral shape of the IOP's were relatively minor. Upon initial inspection, the proposed "correction" to the culture measurements with modeled IOP's of NAP did not seem unreasonable. Previous work has hypothesized that scattering, and backscattering in particular, by detrital particles could be significant (Morel and Maritorena, 2001; Stramski et al., 2004). The suggestion remains a hypothesis because detrital particles are impossible to isolate from phytoplankton, marine bacteria, and other non-algal particles that coexist in the rich assemblage of oceanic particles. Corrections that resulted in large reductions in the scattering and backscattering of the cultured phytoplankton in this study could have been justified. However, the effects of these adjustments on the backscattering ratio reveal a more complicated scenario. We see in Figure 4E that the differential effect of removing a very large portion of the scattering coefficient and only a minor portion of the backscattering coefficient resulted in unrealistic backscattering ratios for the phytoplankton cells. The unadjusted backscattering ratios were high for phytoplankton, in the 0.01 to 0.035 range, but could still be justified by the hypothesized effects of internal structure and cell covering on the backscattering efficiency of cells. However, a backscattering ratio above 5 percent is outside the range of all previous observations. Given the large uncertainties in the modeling effort (we must assume spherical, homogeneous particles, neither of which is likely true for detrital particles), we ultimately rejected the NAP model results and did not apply any correction factors to the measured optical properties of the phytoplankton cultures.
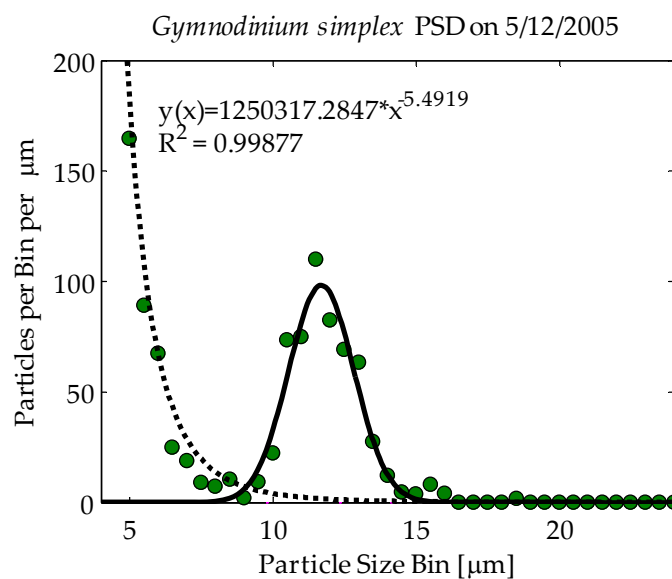
Figure A.1. Particle size distribution (PSD) measured on a Coulter counter for the dinoflagellate *Gymnodinium simplex*. Green dots are Coulter measurements binned to 0.5 microns. Solid line is Gaussian fit to the culture PSD. Dotted line is the power fit to the non-algal particles.
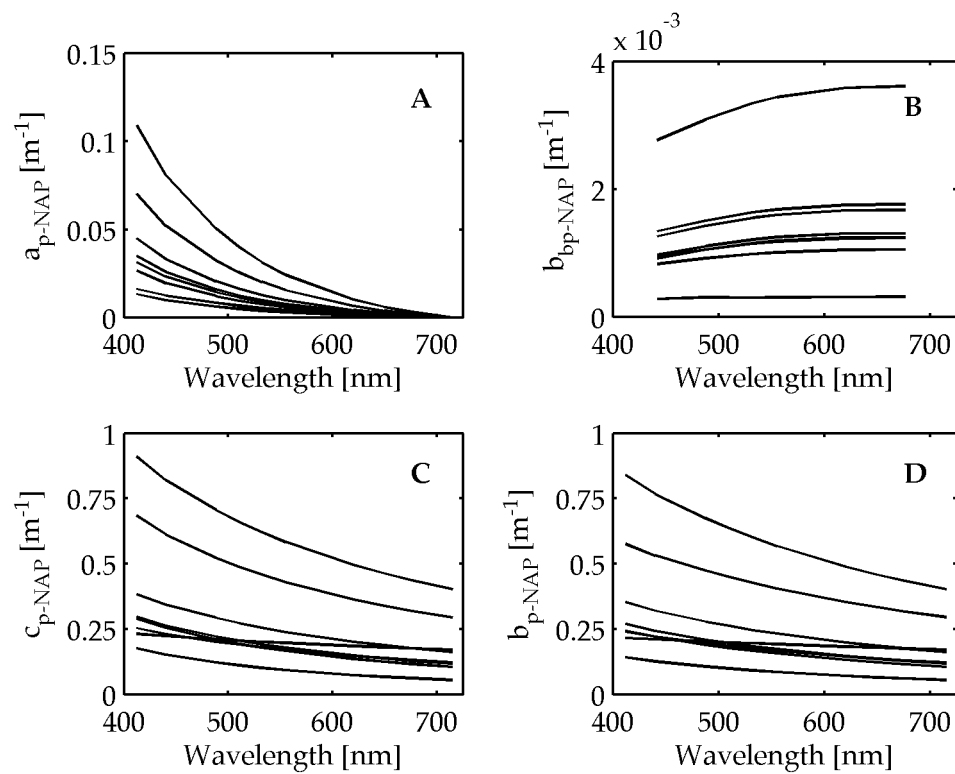
Figure A.2. Modeled inherent optical properties of non-algal particles associated with marine phytoplankton cultures. A) absorption coefficient B) backscattering coefficient C) attenuation coefficient D) scattering coefficient.
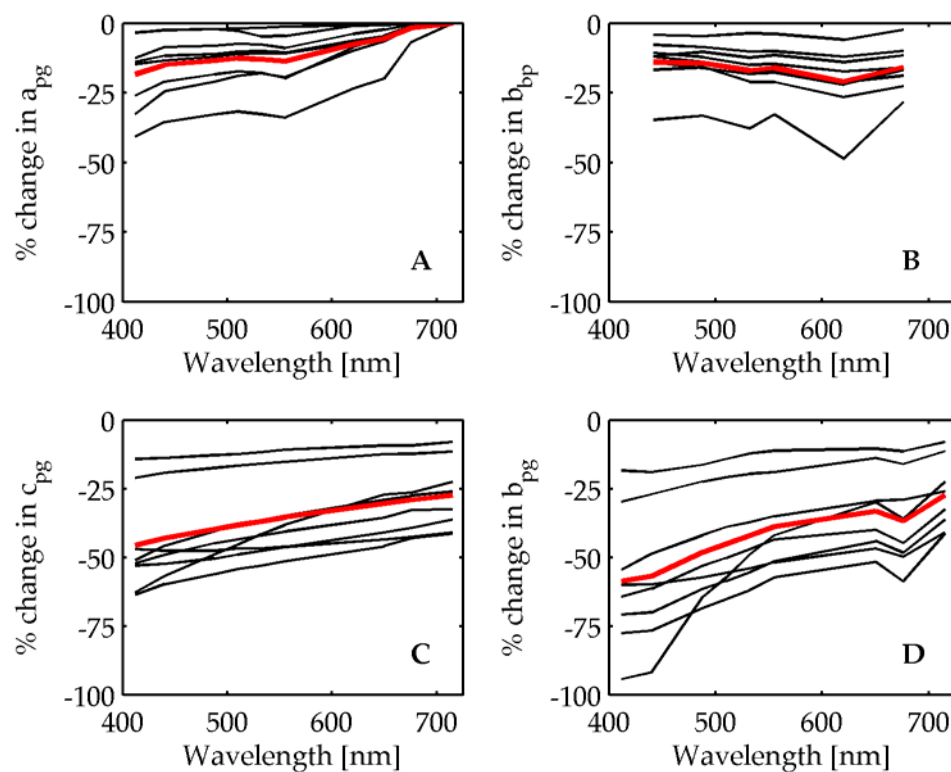
Figure A.3. Percent change in the particulate inherent optical properties of
phytoplankton cultures after correcting for influence of modeled non-algal particles.
Mean value of the percent change for each IOP is shown in red. A) absorption
coefficient B) backscattering coefficient C) attenuation coefficient D) scattering
coefficient.

Figure A.4. Inherent optical properties for marine phytoplankton cultures before (black) and after (red) the subtraction of the non-algal particle signal. A) absorption coefficient B) backscattering coefficient C) attenuation coefficient D) scattering coefficient E) backscattering ratio.

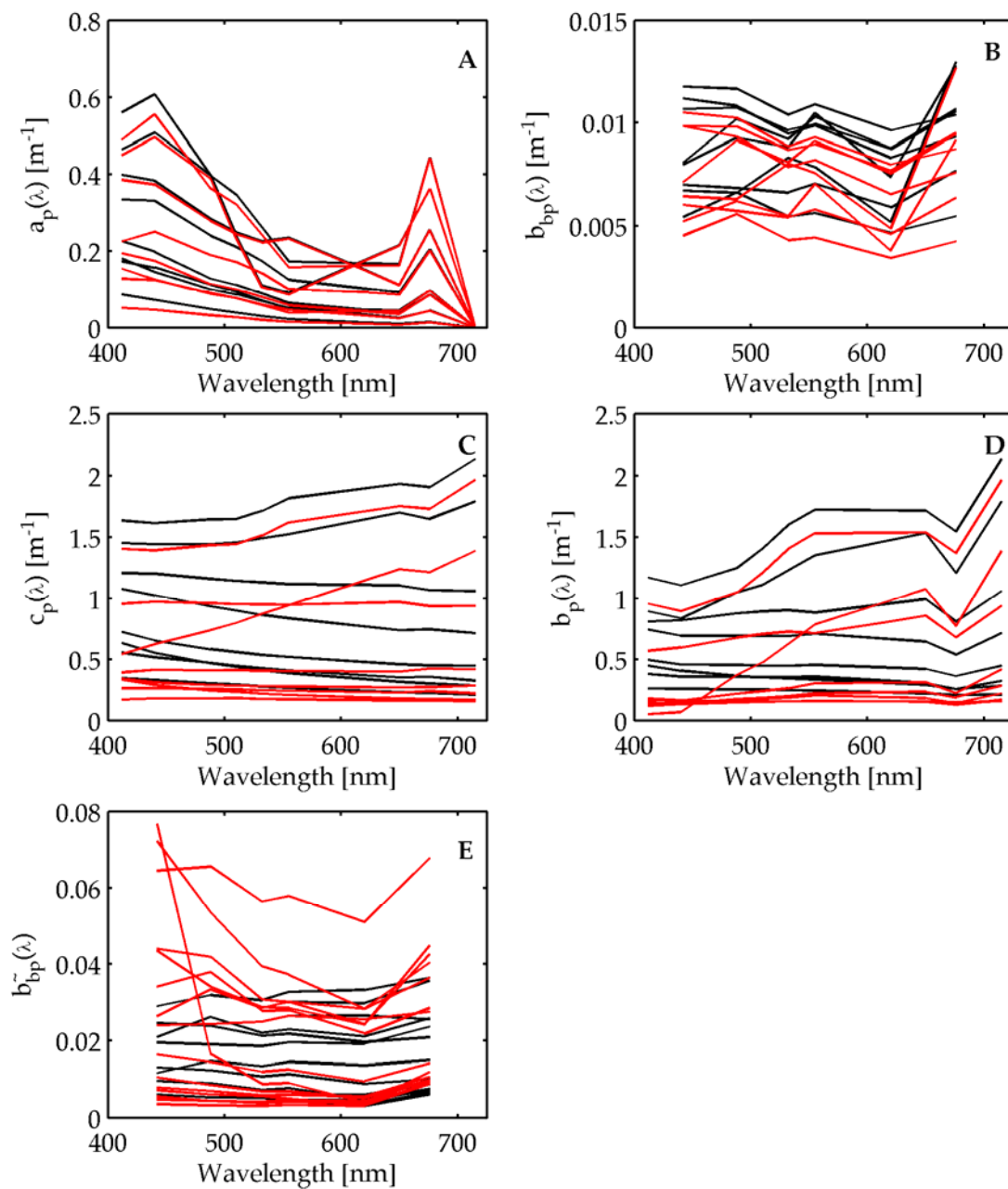# Bibliography

Aas, E., 1996. "Refractive index of phytoplankton derived from its metabolite composition," J. Plankt. Res. 18, 2223-2249.

Ahn, Y-H., A. Bricaud, and A. Morel, 1992. "Light backscattering efficiency and related properties of some phytoplankters," Deep Sea Res., 39(11/12), 1835-1855.

Anderson C. R., D. A. Siegel, M. A. Brzezinski, N. Guillocheau, 2008. "Controls on temporal patterns in phytoplankton community structure in the Santa Barbara Channel, California," J. Geophys. Res., 113, C04038, doi:10.1029/2007JC004321.

Balch, W. M., D. T. Drapeau, T. L. Cucci, R. D. Vaillancourt, K. A. Kilpatrick, and J. J. Fritz, 1999. "Optical backscattering by calcifying algae: Separating the contribution of particulate inorganic and organic carbon fractions," J. Geophys. Res., 104(C1), 1541–1558.

Barnard, A.H., W.S. Pegau, and J.R.V. Zaneveld, 1998. "Global relationships in the inherent optical properties of the oceans," J. Geophys. Res., 103:24,955–24,968.

Beardsley,G.F. Jr. and J. R. V. Zaneveld, 1969. "Theoretical Dependence of the Near-Asymptotic Apparent Optical Properties on the Inherent Optical Properties of Sea Water," J. Opt. Soc. Am. 59, 373.

Bohren, C. F. and Huffman, D. R., 1983. <u>Absorption and Scattering of Light by Small Particles</u>, New York: John Wiley & Sons.

Boss E. and W. Scott Pegau, 2001. "The relationship of light scattering at an angle in the backward direction to the backscattering coefficient," Appl. Opt., 40, 5503-5507.

Boss, E., D. Stramski, T. Bergmann, W.S. Pegau, and M. Lewis, 2004a. "Why Should We Measure the Optical Backscattering Coefficient?" Oceanography 17(2), 44-49.

Boss E., W. S. Pegau, M. Lee, M. S. Twardowski, E. Shybanov, G. Korotaev, and F. Baratange, 2004b. "The particulate backscattering ratio at LEO-15 and its use to study particle composition and distribution." J. Geophys. Res., 109, C1, C0101410.1029/2002JC001514.

Boss, E., M. S. Twardowski, and S. Herring, 2001a. "Shape of the particulate beam attenuation spectrum and its inversion to obtain the shape of the particulate size distribution," Appl. Opt. 40, 4885-4893.

Boss, E., R. Collier, G. Larson, K. Fennel, and W. S. Pegau, 2007. "Measurements of spectral optical properties and their relation to biogeochemical variables and processes in Crater Lake National Park, OR," Hydrobiologia, 574, 149-159.

Boss, E., W. S. Pegau,W. D. Gardner, J. R. V. Zaneveld, A. H. Barnard., M. S. Twardowski, G. C. Chang and T. D. Dickey, 2001b. "The spectral particulate attenuation and particle size distribution in the bottom boundary layer of a continental shelf," J. Geophys. Res., 106, 9509-9516.

Boss, E., MJ Perry, D. Swift, L. Taylor, P. Brickley, J.R. Zaneveld, and S. Riser, 2008. "Three Years of Ocean Data from a Bio-optical Profiling Float." EOS, Vol. 88, No. 23, June 3.

Bricaud, A. and A. Morel, 1986. "Light attenuation and scattering by phytoplanktonic cells: a theoretical modeling," Appl. Opt., 25, 571-580.

Bricaud, A., A. Morel and L. Prieur, 1983. "Optical efficiency factors of some phytoplankters," Limnol. Oceanogr., 28(5), 816-832.

Bricaud, A., Morel, A. and L. Prieur, 1981. "Absorption by dissolved organic matter of the sea (yellow substance) in the UV and visible domains," Limnol. Oceanogr., 26, 43-53.

Bricaud, A., Roesler, C., and J.R.V. Zaneveld, 1995. "In situ methods for measuring the inherent optical properties of ocean waters," Limnol. Oceanogr. 40, 393-410.

Briggs, A.L., W.S. Pegau, L. Karp-Boss and L. Azevedo, 2004. "Backscattering characteristics of marine phytoplankton taxa," Ocean Optics XVII, Fremantle, Australia, October 2004.

Briggs-Whitmire, A.L., T. J. Cowles, and W.S. Pegau, 2004. "Chlorophyll and the spectral backscatter spectrum in Case 1 waters," ASLO Ocean Res. Conf., poster.

Campbell, J.W., 1995. "The lognormal distribution as a model for bio-optical variability in the sea," J. Geophys. Res. 100, 13237-13254.

Cannizzaro, J.P., Carder, K.L., Chen, F.R., Heil, C.A., and Vargo, G.A., 2008. "A novel technique for detection of the toxic dinoflagellate, *Karenia brevis*, in the Gulf of Mexico from remotely sensed ocean color data," Continental Shelf Res., 28,137–158.

Carder, K. L., P. R. Betzer, and D. W. Eggimann, 1974. "Physical, chemical, and optical measures of suspended particle concentrations: Their intercomparison and application to the west African shelf," in Suspended Solids in Water, R. J. Gibbs (ed), pp. 173– 193, Plenum, New York, 1974.

Castelao, R. M. and J. A. Barth, 2005. "Coastal ocean response in a region of alongshore bottom topography variations off Oregon during summer upwelling," J. Geophys. Res., 110(C10), C10S04, doi:10.1029/2004JC002409.

Chami, M., E. B. Shybanov, T. Y. Churilova, G. A. Khomenko, M. E.-G. Lee, O. V. Martynov, G. A. Berseneva, and G. K. Korotaev, 2005. "Optical properties of the particles in the Crimea coastal waters (Black Sea)," J. Geophys. Res. 110, doi:10.1029/2005JC003008.

Chami, M., E. Marken, J. J. Stamnes, G. Khomenko, and G. Korotaev, 2006. "Variability of the relationship between the particulate backscattering coefficient and the volume scattering function measured at fixed angles," J. Geophys. Res. 111, doi:10.1029/2005JC003230.

Chang G. C. and T. D. Dickey, 2001. "Optical and physical variability on timescales from minutes to the seasonal cycle on the New England shelf: July 1996 to June 1997," J. Geophys. Res.,106(C5), 9435–9453.

Chang, G. C., A. H. Barnard, S. McLean, P. J. Egli, C. Moore, J. R. V. Zaneveld, T. D. Dickey, and A. Hanson, 2006. "In situ optical variability and relationships in the Santa Barbara Channel: implications for remote sensing," Appl. Opt., 45(15), 3593-3604.

Chang, G. C., T. D. Dickey, O. M. Schofield, A. D. Weidemann, E. Boss, W. S. Pegau, M. A. Moline, and S. M. Glenn, 2002. "Nearshore physical forcing of bio-optical properties in the New York Bight," J. Geophys. Res., 107, 3133, doi:10.1029/2001JC001018.

Chang, G., A. H. Barnard, and J. R. V. Zaneveld, 2007. "Optical closure in a complex coastal environment: Particle effects," Appl. Opt., 46(31), 7679-7692.

Dailey, M. D., J. W. Anderson, D. J. Reish, and D. S. Gorsline, 1993. "The Southern California Bight: Background and setting," in: Ecology of the Southern California Bight, edited by M. D. Dailey, D. J. Reish, and J. W. Anderson, University of California Press, Berkeley, CA, pp. 1-18.

Davis, R. F., C.C. Moore, J.R.V. Zaneveld, and J.M. Napp, 1997. "Reducing the effects of fouling on chlorophyll estimates derived from long-term deployments of optical instruments," J. Geophys. Res., 102, 5851-5855.

Dickey, T. D., 1991. "The emergence of concurrent high-resolution physical and bio-optical measurements in the upper ocean and their applications," Rev. of Geophys. 29: 383-413.

Dickey, T., M. Lewis, and G. Chang, 2006. "Optical oceanography: Recent advances and future directions using global remote sensing and in situ observations," Rev. Geophys., 44, RG1001, doi:10.1029/2003RG000148.

Eisner, L. B., and T. J. Cowles, 2005. "Spatial variations in phytoplankton pigment ratios, optical properties, and environmental gradients in Oregon coast surface waters," J. Geophys. Res., 110, C10S14, doi:10.1029/2004JC002614.

Gordon, H. R., O. B. Brown, R. H. Evans, J. W. Brown, R. C. Smith, K. S. Baker, and D. K. Clarks, 1988. "A semianalytic radiance model of ocean color," J. Geophys. Res. 93, 10,909-10,924.

Gordon, H.R., 2006. "Backscattering of light from disklike particles: is fine-scale structure or gross morphology more important?" Appl. Opt. 45, 7166-7173.

Gordon, H.R. and A. Morel, 1983. "Remote Assessment of Ocean Color for Interpretation of Satellite Visible Imagery: A Review," R. T. Barber, C. N. K. Mooers, M. J. Bowman, and B. Zeitzschel, eds. Springer-Verlag, New York.

Hardy, J. T., 1993 "Phytoplankton," in: <u>Ecology of the Southern California Bight</u>, edited by M. D. Dailey, D. J. Reish, and J. W. Anderson, University of California Press, Berkeley, CA, pp. 233-265.

Horner, R. A, D. L. Garrison, and F. G. Plumley, 1997. "Harmful algal blooms and red tide problems on the U.S. west coast," Limnol. Oceanogr., 42, 1076-1088.

Huot, Y., A. Morel, M. S. Twardowski, D. Stramski, and R. A. Reynolds, 2008. "Particle optical backscattering along a chlorophyll gradient in the upper layer of the eastern South Pacific Ocean," Biogeosciences, 5, 495–507.

IOCCG Report 1, 1998. "Minimum requirements for an operational, ocean-colour sensor for the open ocean. Report Number 1 of the International Ocean Colour Coordinating Group," ed. A. Morel, IOCCG, P.O. Box 1006, Dartmouth, Nova Scotia, Canada, 50pp.

IOCCG Report 2, 1999. "Status and Plans for Satellite Ocean-Colour Missions: Considerations for Complementary Missions. Report Number 2 of the International Ocean Colour Coordinating Group," ed. J. Yoder, IOCCG, P.O. Box 1006, Dartmouth, Nova Scotia, Canada, 43 pp.

IOCCG Report 3, 2000. "Remote Sensing of Ocean Colour in Coastal, and Other Optically-Complex, Waters, Report Number3 of the International Ocean Colour Coordinating Group," Edited by: S. Sathyendranath, IOCCG, P.O. Box 1006, Dartmouth, Nova Scotia, Canada, 140pp.

Kirkpatrick, G. J., D. F. Millie, M. A. Moline, and O. Schofield, 2000. "Optical discrimination of a phytoplankton species in natural mixed populations," Limnol. Oceanogr., 45, 467-471.

Kishino, M., Takahashi, M., Okami, N., Ichimura, S., 1985. "Estimation of the spectral absorption coefficients of phytoplankton in the sea," Bulletin of Marine Science, Vol. 37, no. 2.

Kitchen, J.C. and J.R.V. Zaneveld, 1992. "A three-layered sphere model of the optical properties of phytoplankton," Limnol. Oceanogr., 37(8), 1680-1690.

Kostadinov, T. S., Siegel, D.A., Maritorena, S. and Guillocheau, N., 2007. "Ocean color observations and modeling for an optically complex site: Santa Barbara Channel, California, USA," J. Geophys. Res., 112, C07011, doi:10.1029/2006JC003526.

Laws, Edward, 1997. <u>Mathematical Methods for Oceanographers</u>, John Wiley and Sons, New York, 1997.

Macdonald, J.B., M.S. Twardowski, W.S. Pegau, A.H. Barnard, E. Boss, and J.R.V.Zaneveld, 2000. "Characterization of spectral backscattering in the Gulf of California," EOS Trans. AGU, 80(49), Ocean Sci. Mett. Suppl., OS22E-12.

Mackey, M. D., Mackey, D. J., Higgins, H. W., Wright, S. W., 1996. "CHEMTAX- A program for estimating class abundances from chemical markers: application to

HPLC measurements of phytoplankton pigments," Mar. Ecol. Progr. Ser., 144, 265-283.

Maffione, R.A. and D.R. Dana, 1997. "Instruments and methods for measuring the backward-scattering coefficient of ocean waters," Appl. Opt., 36, 6057-6067.

McKee, D, and A. Cunningham, 2005. "Evidence for wavelength dependence of the scattering phase function and its implication for modeling radiance transfer in shelf seas," Appl. Opt., 44, 126-135.

Millie, D.F., O.M. Schofield, G.J. Kirkpatrick, G. Johnsen, P.A. Tester, and B.T. Vinvard, 1997. "Detection of harmful algal blooms using photopigments and absorption signatures: A case study of the Florida red tide dinoflagellate, *Gymnodinium breve*," Limnol. Oceanogr., 42,1240-l 251.

Mobley, C.D., L.K. Sundman, and E. Boss, 2002. "Phase function effects on oceanic light fields," Appl. Opt., 41, 1035-1050.

Morel, A., 1973. "The scattering of light by seawater, experimental results and theoretical approach," (translated from French), in AGARD Lect. Ser., pp. 3.1.1.-3.1.76.

Morel, A., 1988. "Optical modeling of the upper ocean in relation to its biogenous matter content (Case I waters)," J. Geophys. Res., 93, 10,749 – 10,768.

Morel, A., and S. Maritorena, 2001. "Bio-optical properties of oceanic waters: A reappraisal," J. Geophys. Res., 106, 7763-7780.

Morel, A., and Y.H. Ahn, 1990. "Optical efficiency factors of free-living marine bacteria: Influence of bacterioplankton upon the optical properties and particulate organic carbon in oceanic waters," Journal of Marine Research, 48, 145-175.

Morel, A., and Y.-H. Ahn, 1991. "Optics of heterotrophic nanoflagellates and ciliates: A tentative assessment of their scattering role in oceanic waters compared to those of bacterial and algal cells," Journal of Marine Research, 49, 177-202.

Oishi, T., 1990. "Significant relationship between the backward scattering coefficient of sea water and the scatterance at 120º," Appl. Opt., 29, 4658-4665.

Oliver, M. J., O. Schofield, T. Bergmann, S. Glenn, C. Orrico, and M. Moline, 2004. "Deriving in situ phytoplankton absorption for bio-optical productivity models in turbid waters," J. Geophys. Res., 109 C07S11, doi:10.1029/2002JC001627.

Otero, M.P., and D.A. Siegel, 2004. "Spatial and temporal characteristics of sediment plumes and phytoplankton blooms in the Santa Barbara Channel," Deep Sea Res., 51, 1129-1149.

Pegau, W. S., D. Gray, and J. R. V. Zaneveld, 1997. "Absorption and attenuation of visible and near-infrared light in the water: Dependence on temperature and salinity," Appl. Opt. 36, 6035-6046.

Pegau, W. S., J. R. V. Zaneveld, and K. J. Voss, 1995. "Toward closure of the inherent optical properties of natural waters," J. Geophys. Res., 100, 13,193–13,199.

Pegau, W.S., J.R.V. Zaneveld, A.H. Barnard, H. Maske, S. Alvarez-Borrego, R. Lara-Lara, R. Cervantes-Duarte, 1999. "Inherent optical properties in the Gulf of California," Ciencias Marinas, 25, 469–485.

Peltzer, E. T., "Matlab® shell-scripts for linear regression analysis," http://www.mbari.org/staff/etp3/regressindex.htm (9/18/2006).

Petzold T. J., 1972. "Volume scattering functions for selected ocean waters," SIO Ref. 72-78, Scripps Institution of Oceanography.

Prentice, J., A.D. Weidemann, W.S. Pegau, K.J. Voss, M. Lee, E. Shybanov, O. Martynov, A. Laux, A.L. Briggs, G. Chang, 2002. "Laboratory comparisons of optical scattering instrumentation," Ocean Optics XVI, Santa Fe, NM, November.

Price, D.W., Kizer, K.W., and Hansgen, K.H., 1991. "California's paralytic shellfish poisoning prevention program 1927-89," J. Shellfish Res., 10(1): 119-145.

Roesler C. S. and E. Boss, 2003. "A novel ocean color inversion model: retrieval of beam attenuation and particle size distribution,"Geophys. Res. Let., 30(9), 10.1029/2002GL016366.

Roesler, C. S. and M. J. Perry, 1995. "In situ phytoplankton absorption, fluorescence emission, and particulate backscattering spectra determined from reflectance," J. Geophys. Res. 100(C7): 13,279-13,294.

Roesler, C. S., M. J. Perry, and K. L. Carder, 1989. "Modeling in situ phytoplankton absorption from total absorption spectra," Limnol. Oceanogr. 34: 1512-1525.

Roesler, C.S., and Boss, E., *in press*, "In situ measurement of inherent optical properties and potential for harmful algal bloom detection and coastal ecosystem observations," in Real-time coastal observing systems for marine ecosystem dynamics and harmful algal blooms: theory, instrumentation, and modeling, Babin M., Roesler, C.S., and Cullen, J.J., eds.

Scheibe, J., 2003. "Worst may be over in huge fish die-off: Severe red tide leaves harbor reeling," Ventura County Star, p. A01, 2 October.

Schlax, M.G. and D.B. Chelton, 1992. "Frequency Domain Diagnostics for Linear Smoothers," J. of the American Statistical Association, 87(420), 1070-1081.

Schofield, O., T. Bergmann, M. J. Oliver, A. Irwin, G. Kirkpatrick, W. P. Bissett, M. A. Moline, and C. Orrico, 2004. "Inversion of spectral absorption in the optically complex coastal waters of the Mid-Atlantic Bight," J. Geophys. Res., 109, C12S04, doi:10.1029/2003JC002071.

Schofield, O., T. Bergmann, W.P. Bissett, F. Grassle, D. Haidvogel, J. Kohut, M. Moline, M., and S. Glenn, 2002. "Linking regional coastal observatories to provide the foundation for a national ocean observation network," J. Ocean. Eng. 27(2): 146-154.

Scholin, C.A., P.E. Miller, K.R. Buck, F.P. Chavez, P. Harris, P. Haydock, J. Howard and G. Cangelosi, 1997. "Detection and quantification of Pseudo-nitzschia australis in cultured and natural populations using LSU rRNA-targeted probes," Limnol. Oceanogr. 42, 1265–1272.

Slade, W.H. and E. Boss, 2008. "Is the Spectral Shape of Particle Backscattering a Good Indicator of Particle Size?" Ocean Sciences Meeting, Orlando, FL, March 2-7.

Smith, R.C., and K.S. Baker, 1981. "Optical properties of the clearest natural waters," Appl. Opt., 20, 177-184.

Sokal, R.R, and F.J. Rohlf, 1995. Biometry, W.H. Freeman and Company, New York.

Sosik, H. M. and B. G. Mitchell, 1995. "Light absorption by phytoplankton, photosynthetic pigments and detritus in the California Current System," Deep Sea-Res. 42, 1717-1748.

Sosik, H.M., *in press*, "Characterizing seawater constituents from optical properties," in Real-time coastal observing systems for marine ecosystem dynamics and harmful algal blooms: theory, instrumentation, and modeling, Babin M., Roesler, C.S., and Cullen, J.J., eds.

Sournia, A., 1995. "Red tide and toxic marine phytoplankton of the world ocean: An inquiry into biodiversity," in Harmful Marine Algal Blooms. Proc. 6th Int. Conf. on Toxic Marine Phytoplankton, Lassus, P., G. Arzul, E. Erard, P. Gentien & C. Marcaillou (eds), France, Lavoisier: 103–112.

Stramski, D, and R.A. Reynolds, 1993. "Diel variations in the optical properties of a marine diatom," Limnol. Oceanogr., 38(7), 1347-1364.

Stramski, D., 1999. "Refractive index of planktonic cells as a measure of intracellular carbon and chlorophyll a content," Deep-Sea Res., 46, 335-351.

Stramski, D. and D. A. Kiefer, 1991. "Light scattering by microorganisms in the open ocean," Prog. Oceanogr., 28, 343–383.

Stramski, D., A. Bricaud, and A. Morel, 2001. "Modeling the inherent optical properties of the ocean based on the detailed composition of planktonic community," Appl. Opt., 40, 2929-2945.

Stramski, D., A. Sciandra, and H. Claustre, 2002. "Effects of temperature, nitrogen, and light limitation on the optical properties of the marine diatom *Thalassiosira pseudonana*," Limnol. Oceanogr., 47, 392-403.

Stramski, D., A. Shalapyonok, and R. A. Reynolds, 1995. "Optical characterization of the oceanic unicellular cyanobacterium *Synechococcus* grown under a day-night cycle in natural irradiance," J. Geophys. Res., 100 (C7), 13295-13307.

Stramski, D., and C. D. Mobley, 1997. "Effects of microbial particles on oceanic optics: A database of single-particle optical properties," Limnol. Oceanogr. 42, 538-549.

Stramski, D., E. Boss, D. Bogucki, K. J. Voss, 2004. "The role of seawater constituents in light backscattering in the ocean," Prog. Oceanogr., 61, 27–56.

Stramski, D., S. B. Wozniak, and P. J. Flatau, 2004. "Optical properties of Asian mineral dust suspended in seawater," Limnol. Oceanogr. 49, 749–755.

Sullivan, J.M., M.S. Twardowski, P.L. Donaghay, and S.A. Freeman, 2005. "Use of optical scattering to discriminate particle types in coastal waters," Appl. Opt. 44, 1667-1680.

Sweeney, BM. 1975. "Red tides I have known," in Proceedings of the First International Conference on Toxic Dinoflagellate Blooms, 225-234.

Toole, D. A., and D. A. Siegel, 2001. "Modes and mechanisms of ocean color variability in the Santa Barbara Channel," J. Geophys. Res., 106(C11), 26,985–27,000.

Twardowski, M. S., E. Boss, J. B. Macdonald, W. S. Pegau, A. H. Barnard, J. R. V. Zaneveld, 2001. "A model for estimating bulk refractive index from the optical backscattering ratio and the implications for understanding particle composition in case I and case II waters," J. Geophys. Res., 106(C7), 14,129-14,142, doi:10.1029/2000JC000404.

Ulloa, O., S. Sathyendranath, and T. Platt, 1994. "Effect of the particle size-distribution on the backscattering ratio in seawater," Appl. Opt., 33, 7070-7077.

Vaillancourt, R.D., C.W. Brown, R.R.L. Guillard, and W. M. Balch, 2004. "Light backscattering properties of marine phytoplankton: relationships to cell size, chemical composition, and taxonomy" J. Plank. Res., 26(2), 191-212.

Van de Hulst, H. C. 1957. Light scattering by small particles. Wiley. New-York.

Venrick, E.L., 1998. "Spring in the California Current: the distribution of phytoplankton species, April 1993 and April 1995," Mar. Ecol. Prog. Ser., 167, 73-88.

Volten, H., J. F. de Haan, J. W. Hovenier, R. Schreurs, W. Vassen, A. G. Dekker, H. J. Hoogenboom, F. Charlton and R. Wouts, 1998. "Laboratory Measurements of Angular Distributions of Light Scattered by Phytoplankton and Silt," Limnol. Oceanogr., 43(6), 1180-1197.

Voss, K. J., & Fry, E. S.,1984. "Measurement of the Mueller matrix for ocean water," Appl. Opt., 23, 4427-4439.

Warrick, J.A., Mertes LAK, Wasburn L, Siegel DA., 2004. "A conceptual model for river water and sediment dispersal in the Santa Barbara Channel, California," Continental Shelf Res., 24(17), 2029-2043.

Whitmire, A.L., E. Boss, T. J. Cowles, and W. S. Pegau, 2007. "Spectral variability of the particulate backscattering ratio," Opt. Express, 15, 7019-7031.

Yentsch, C. S., & Menzel, D. W., 1963. "A method for the determination of phytoplankton chlorophyll and phaeophytin by fluorescence," Deep-Sea Res., 10: 221-31.

Zaneveld, J.R.V., J.C. Kitchen, and C.C. Moore, 1994. "Scattering error correction of reflecting tube absorption meter," Ocean Optics XII, Proceedings of the Society of Photo-Optical Instrumentation Engineers (SPIE) 2258, 44-55.

Zaneveld, JRV, J.C. Kitchen, 1995. "The variation in the inherent optical properties of phytoplankton near an absorption peak as determined by various models of cell structure," J. Geophys. Res., 100(C7) pp. 13,309-13,320.